Chapter 4: Result and Discussions

This chapter deals with the results and discussion section. This section is categorized into two subsections. First sections deals with the result and discussion analysis pertaining to the numerical and modelling analysis part and then second subsection describes the result and discussion of the experimental investigations.

First four subsection of the result and discussion part deals with the numerical modelling and analysis of the complete gasification process. In the numerical simulation part first section deals with the Modelling and Multi-objective optimization of variable air gasification performance parameters using Syzygium cumini biomass by integrating ASPEN Plus with response surface methodology (RSM) whereas second subsection incorporate process modelling and thermodynamic performance optimization of biomass air gasification fuelled with waste poultry litter pellet by integrating Aspen plus with RSM. After done with the air gasification, focus has been shifted to steam gasification in order to increase the concentration of hydrogen in the producer gas composition. Therby, third subsection deals with the Process modeling and multi-objective optimization of low-density polyethylene waste gasification for hydrogen-enriched syngas production. Fourth subsection models the advance technique of gasification i.e. plasma gasification.

Next four subsection (fifth to eighth) of the result and discussion part deals with the results obtained from the experimental investigation part. First subsection of the experimental work employs performance and emission Optimization of CI engine fueled with Coconut shell-based Producer Gas and Diesel by using response surface methodology. Second subsection deals with the performance and emission Analysis of triple fuelled CI engine utilizing producer gas, biodiesel and diesel: An optimization study using response surface methodology. Third subsection in the experimental section analyses the coal gasification.

4.1. Numerical simulation-Gasification of Syzygium cumini biomass

The present chapter developed a robust method for the modeling and optimization of variable air gasification parameters using the ASPEN Plus simulator and Response surface methodology (RSM). A comprehensive thermochemical equilibrium based model of downdraft gasifier was developed by minimizing Gibbs free energy. Model validation was done by comparing the simulated result with the experimental result of four different feedstocks from the literature and, a good agreement was attained. The Complete modeling of the air gasification process was segregated into four phases viz. biomass drayng, biomass decomposition, biomass gasification, and producer gas filtration. Drying operation and yield distribution during pyrolysis were computed by incorporating FORTRAN sub-routine statement. Sensitivity analysis was performed to obtain syngas composition using Syzygium cumini biomass fuel and different gasification performances like gas yield (GY), cold gas efficiency (CGE), and higher heating value (HHV) using gasification temperature (600-900)^{0}C and equivalence ratio (ER) (0.2-0.6). Furthermore, RSM has been employed for the multi-objective optimizations of the variable gasification parameter. Central composite design (CCD) is adopted. Two independent parameters viz. temperature and equivalence ratio have opted as decision parameters for estimating the optimum performance parameters i.e., hydrogen concentrations, CGE, and HHV. Regression models created from the ANOVA results are found to be highly accurate in predicting output response variables Proximate and ultimate analysis of Syzygium cumini is depicted in table 4.1.

It is evident from table 4.2 and the literature review that modeling (prediction) and multi-objective optimization of the variable air gasification performance parameters by integrating ASPEN Plus with Response surface methodology (RSM) using Syzygium cumini biomass fuel is scarce. Which offers another scope for the present investigation And, there is lack of work in respect to the integration of ASPEN PLUS with RSM for the production and optimization.

Therefore, this study addresses the research gap by incorporating an optimization strategy coupled with thermochemical equilibrium based robust model ASPEN Plus and multi-objective optimization technique RSM to achieve the optimal conditions. Both variable gasification parameters like temperature, equivalence ratio, and gasification performances like hydrogen yield, cold gas efficiency, and HHV are optimized and optimal working range has been obtained for the gasifier to deliver the best possible output.

Major contributions of the present study are listed below

- Development of a kinetic free thermochemical equilibrium based robust model for downdraft biomass gasification by decreasing Gibbs free energy to its minimum point into ASPEN PLUS.
- Model validation using four different biomass from the literature and sensitivity analysis using Syzygium cumini biomass fuel from the proposed model is performed.
- RSM has been employed for the multi-objective optimizations of the decision variables i.e. temperature and equivalence ratio, which manifests a value addition in the domain of energy conversion.
- A highly accurate robust regression model has been developed from the ANOVA tool for estimating hydrogen concentration, cold gas efficiency, and higher heating value.
- The influences of major decision parameters on the gasification performance parameters like H_2, CGE, and HHV are investigated to attain an optimal state.

Table 4.1. Proximate and Ultimate analysis of Syzygium cumini.[89]

Proximate analysis on % dry ash-free basis	
Volatile matters	78.98
Fixed carbon	21.02
Ash content	2.09±0.08[90]
Ultimate analysis in % dry ash-free basis	
Carbon	44.50
Nitrogen	0.77
Hydrogen	4.98
Oxygen	49.54
Sulfur	0.22

Table 4.2. Previous investigation vs. Present study

Gasification Process	Modeling		Modeling technique	Optimization		Optimization technique	Fuel	Ref
	Yes	No		Yes	No			
Previous investigation								
Entrained flow	✓	×	CFD	✓	×	Pareto	Rice husks	[91]
Downdraft	✓	×	Aspen plus	×	✓	---	Wood chips	[92]
Bubbling Fluidized bed	✓	×	CBP	✓	×	RSM	Forest residues	[93]
Bubbling Fluidized bed	✓	×	Aspen plus	✓	×	Mathematica	Wood residues	[94]
Entrained flow	✓	×	ANN	✓	×	Pareto	Pet cokes	[95]
Downdraft	✓	×	Aspen Hysys	×	✓	---	Date palm wastes	[96]
Present study								
Downdraft	✓	×	Aspen plus	✓	×	RSM	Syzygium cumini	

4.1.1 Model Validation

The model has been validated with the experimental results using four biomasses from the literature named Hardwood chip (HC), Poultry litter Pellets (PP), Softwood Pellets (SP), and Rapestraw Pellets (RS). The chemical properties of all the feedstocks used for validation are depicted in table 4.3. The experimental result of Wei et al. [97] and Stringes et.al. [43] was considered for the validation of the present model. Validation was performed based on the syngas compositions at fixed temperature and ER. Error analysis was also performed by finding the standard mean error. The predicted syngas compositions from the present model were in good agreement with the experimental syngas compositions. However, the magnitude of CH_4 was underpredicted in the present model, which was a general bug in equilibrium modelings [92, 98, 99]. This under-prediction is attributed to the assumption presumed in the equilibrium model that char, tar, and heavy hydrocarbon are not considered in the syngas compositions, which is usually existing in the syngas produced from real air gasification unit.

Table. 4.3. Chemical properties of different biomass

Ultimate analysis (wt. %)	Hardwood chip [97]	Poultry litter pellets [43]	Softwood pellets [43]	Rape straw pellets [43]
Carbon	49.81	43.98	49.20	39.60
Hydrogen	5.55	5.16	6.20	5.60
Nitrogen.	0.07	4.63	0.08	0.78
Oxygen	43.42	31.98	44.06	48.54
Sulfur	0.005	0.75	0.06	0.08
Proximate analysis (wt. %)				
Volatile matter	79.85	63.60	79.20	62.50
Fixed carbon	19.03	15.30	15.20	17.20
Moisture	25.00	7.60	5.20	14.90

Ash	1.11	13.50	0.40	5.40

Comparative analysis between simulated and experimental results on the variation of syngas composition with temperature was depicted in Fig 4.1. The experimental result was obtained by Wei et al. [97]. The simulated and experimental results, both acquired using a similar condition, feed, and Parameters. ER 0.2, airflow rate 35.244 Nm^3/h, biomass feed rate 31.60 kg/h, temperature 775^oC using woodchip. . The accuracy of the simulated results was assessed using the sum square deviations method [100].

$$RSS = \sum_{i=1}^{N}((Yie - Yip)/Yie)^2 \quad (6)$$

$$MRSS = \frac{RSS}{N} \quad (7)$$

$$Mean\ error = \sqrt{MRSS} \quad (8)$$

Where RSS and MRSS are ranked set samplings and median set samplings y_{ie} and y_{ip} are experimental and simulated syngas composition. The temperature and ER were kept constant at 800^{0}C and 0.2 respectively. It is fixed for all the biomasses which were used for the validation process. A comparison of simulated results with the experimental result for the validation of the model is depicted in table 4.4.

Table. 4.4. Experimental result versus Model Prediction

	HC		**PP**		**SP**		**RP**	
Gas Composition (mole %)	Exp.	Sim.	Exp.	Sim.	Exp.	Sim.	Exp.	Sim.
CO	22.16	22.3	17.42	17.05	24.27	24.20	14.59	14.56
H_2	17.5	17.9	14.55	14.47	14.01	14.17	14.43	14.82
CO_2	11.89	12.3	13.51	10.156	10.26	12.43	11.8	11.09

CH_4[a]	3.09	0.17	1.29	0.0024	4.12	0.00322	4.06	0.00143
N_2	44.79	48.78	53.09	48.16	47.07	40.14	54.96	45.21
Mean Error		0.049		0.132				

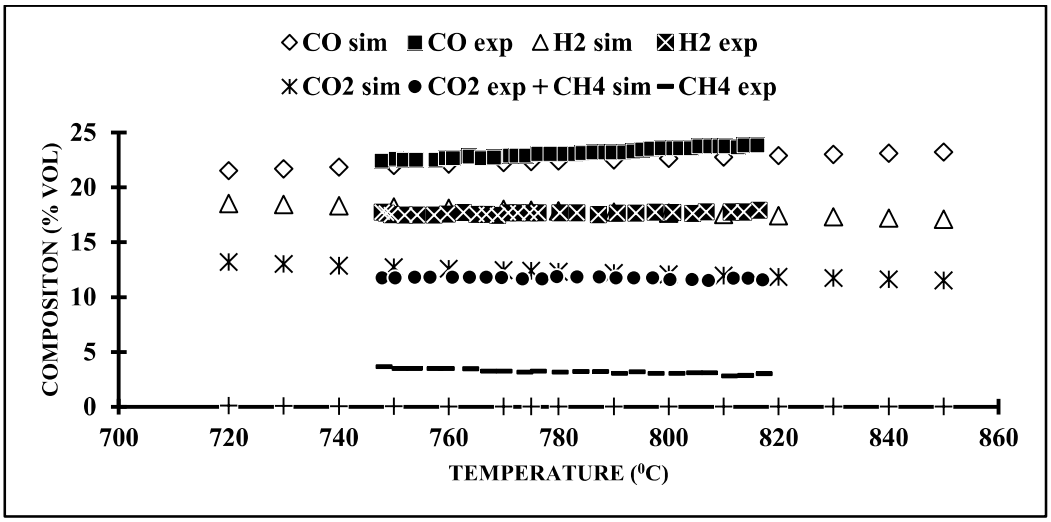

Fig. 4.1 Comparison of experimental and theoretical result on the syngas composition

4.1.2 Sensitivity analysis

The developed model for the downdraft gasifier has been used to execute sensitivity analysis. The reaction temperature and equivalence ratio (ER) are the highly influential parameters that affect the syngas compositions and various gasification characteristics. Therefore, the influence of variable gasifier temperatures (600-900)^{0}C with step size of 100 and variable equivalence ratios (0.2-1) with a step size of 0.2 on the syngas compositions, cold gas efficiencies (CGE), and higher heating value (HHV) has been investigated. Lower heating value of biomass is 14.59 MJ/kg whereas feedstock particle size adopted in the present study is in the range of (3.3-5.5) cm in chip form.

Gas yield (GY) was computed by using the following co-relation [101]

$$GY = \frac{Gas\ volume\ per\ hour}{weight\ of\ biomass\ consumption\ per\ hour} \quad (9)$$

Cold gas efficiency (%) was computed by using the following equation. [40]

$$CGE(\%) = \frac{LHV(PG)}{LHV(BIOMASS)} \times Y \times 100 \quad (10)$$

Where Y is a PG (producer gas) yield and Lower heating value (LHV) of biomass and PG in MJ/kg can be calculated by using the following co-relation. [40]

$$LHV(BIOMASS) = (0.339 \times C + 1.029 \times H + 0.109 \times S - 0.112 \times O - 0.025 \times W) \quad (11)$$

Where C, H, S, O, and W are the constituent of biomass and it can be generated by the chemical analysis of biomass. The lower heating value of PG can be obtained by the following co-relation (8) [40]

$$LHV(PG) = (0.126 \times CO + 0.108 \times H2 + 0.358 \times CH4) \quad (12)$$

Where, CO, H_2, and CH_4 are the component of PG.

The higher heating value (HHV) of PG in (kJ/Nm^3) can be calculated by using the following co-relation [102]

$$HHV(PG) = \left((CO\% \times 3018 + H2\% \times 3052 + CH4\% \times 9500) \times 0.01 \times 4.1858\right) \quad (13)$$

4.1.3 Effect of temperature

The gasification temperatures were varied from 600^0C to 900^0C. The influence of gasification temperatures on the syngas compositions, CGE, and HHV is depicted in fig.4.2 and fig 4.3 respectively

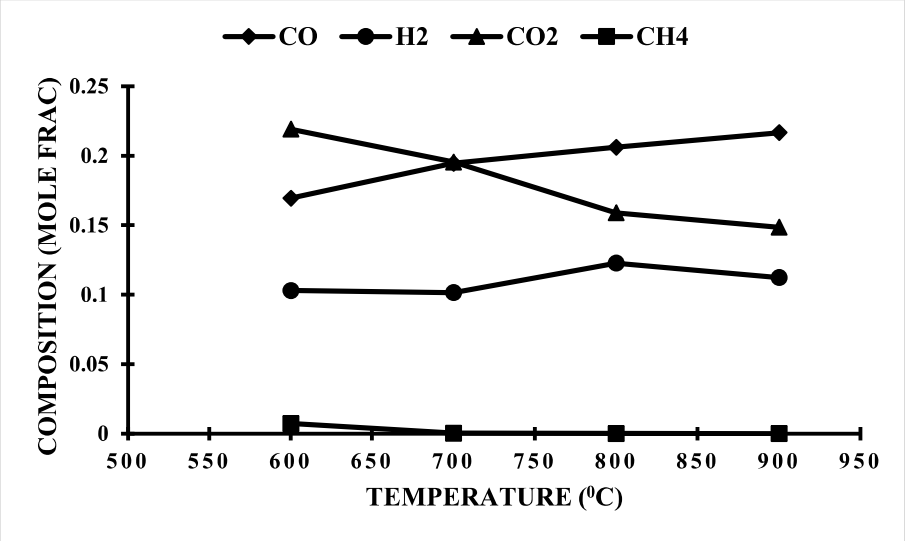

Fig. 4.2. Effect of temperature on gas compositions with ER 0.2 and biomass MC 5 wt%.

Initially, when the temperature is low inside the reactor compositions of PG mainly consist of CO_2, CH_4, and un-burnt carbons. As the temperature rises, the carbon is likely to respond to oxygen and get transformed into carbon monoxide (CO) by the partial oxidation reaction (R4). The mechanism of this reaction is depicted in another investigation [98]. As the temperature further increases, the magnitude of CO content in the syngas composition further increases while CO_2 decreases which are due to Boudouard Reaction. This is an extremely endothermic reaction. Eventually, it increases the HHV of producer gas. Fig. 4.2 depicts that CO and H_2 both rise as the temperatures rise. This rise is mainly indorsed to the water-gas reaction (R7). These reactions also contributed to the enhancement of the calorific value of PG. It is inferred from fig.4.2, the magnitude of CO rises unceasingly with a rise in the variable temperature from 600^0C to 900^0C. This trend is following the outcomes obtained in other research [98, 103, 104]. During the reaction, methane (R9) reacts with the steams that existed inside the biomass and is transformed into hydrogen (R9). This indicates that elevated reaction temperatures favor steam reforming and cracking of CH_4 [105]. It can be concluded from the fig.4.2 that with an intensification in the reactor temperatures, the magnitude of CO and H_2 upsurges while CO_2

and CH_4 declines. A similar trend was obtained wherein the influence of gasification temperature on the magnitude of PG generated from olive kernel and olive trees cutting was investigated in a fixed bed gasifier. They reported that with rising temperatures, the magnitude of CO and H_2 rises while CO_2 and CH_4 decrease [106]. A similar trend of syngas compositions with temperature was cited by Dang et al.[94]. Begum et al. investigated the syngas generated from Municipal Solid Wastes (MSW) in a fixed bed biomass gasifier and reported a similar trend of the gas compositions with increasing temperatures [103]. Nikoo et al. [100] obtained the same trend by simulating the biomass gasification process in a fluidized bed reactor.

The influence of gasification temperatures on the CGE and HHV for Syzygium cumini biomass is depicted in fig 4.3. The CGE is directly proportional to the gasification temperatures. This may be due to the continuous increment in the magnitude of CO and H_2 in the syngas composition. The magnitude of CGE acquired for Syzygium cumini biomass varied in the range of (35-41)%. Fig 4.3 depicts the variation of HHV with temperature. HHV depicts a direct relationship with temperature. This may be due to the increment of H_2 and CO magnitude in the syngas composition as the temperature rises. It is already discussed earlier. Similar results for HHV was reported by Lahijani et al. [107]

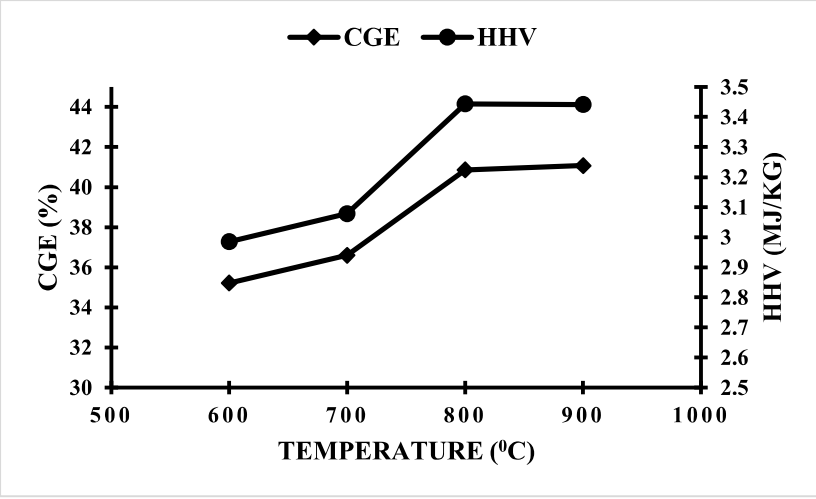

Fig. 4.3. Effect of temperature on CGE and HHV

4.1.4 Effect of equivalence ratio

The equivalence ratio is specified as the ratio of the actual air-fuel ratio to the stoichiometric air-fuel ratio [108]. It is the most influential parameter that influences syngas compositions and gasification performances. ER in the present study was varied from (0.2-1) by changing the airflow rate keeping the temperature constant at 800^0C. Variation of syngas composition, CGE, and HHV with Variable ER is depicted in fig 4.4.

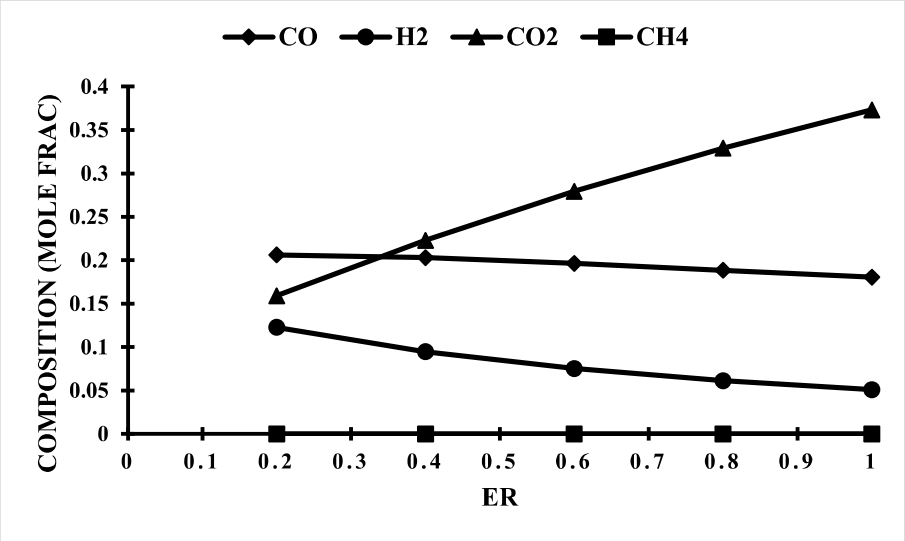

Fig. 4.4. Effect of ER on gas compositions with temperature 800^0C and biomass moisture content of 5 wt%.

It can be inferred from the plot that the magnitude of H_2 content decreases continuously from 12.27% at ER 0.2 to 5.1% at ER 1. The magnitude of CO content also decreases as ER increases. This decline may be attributed to the fact that as ER increases, the quantity of O_2 delivered to the reactor enhances by which the carbon conversion of the fuel upsurges but the additional quantity of oxygen oxidizes the fuel. It results in the decline of CO and H_2 content. It is evident from the plot that the magnitude of CO_2 increases suddenly with the increasing ER. It is due to the initiation of complete combustion. The alteration in the magnitude of CH_4 with escalating ER is found to be insignificant. Results acquired for ER from our model were

in agreement with the other studies in the literature [42, 109]. Han et al. reported the influence of ER on the syngas composition from wood chips in the downdraft gasifier [92]. They reported that the magnitude of H_2 decreases continuously from 23.4% at 0.2 to 9.83% at 0.45 with the increased ER. They also reported that the content of CO decreases continuously from 26.73% at 0.2 to 9.09% at 0.45. The magnitude of CO_2 continuously increases from 9.4% at 0.2 to 17.4% at 0.45. Dang et al.[94] also reported a similar variation of syngas compositions with ER. A comparable trend was stated by Niu et al. wherein the magnitude of CO and H_2 declines whereas CO_2 increases as ER rises [109].

The influence of ER on Cold gas efficiency and HHV is plotted in fig 4.5. Cold gas efficiency depicts the direct relation with the ER. The maximum CGE was 58.47%. This direct relationship may be due to an increase in gas yield as ER increases. HHV shows an inverse relation with increasing ER. The maximum HHV attained was 4.17 MJ/kg at ER 0.2. It is due to the presence of high concentrations of combustibles gases especially CO and H_2 at lower ER. A similar trend for HHV was obtained by Lahijani et al. [107]. They reported a decrease in HHV by increasing the ER by using the sawdust and EFB as feedstock.

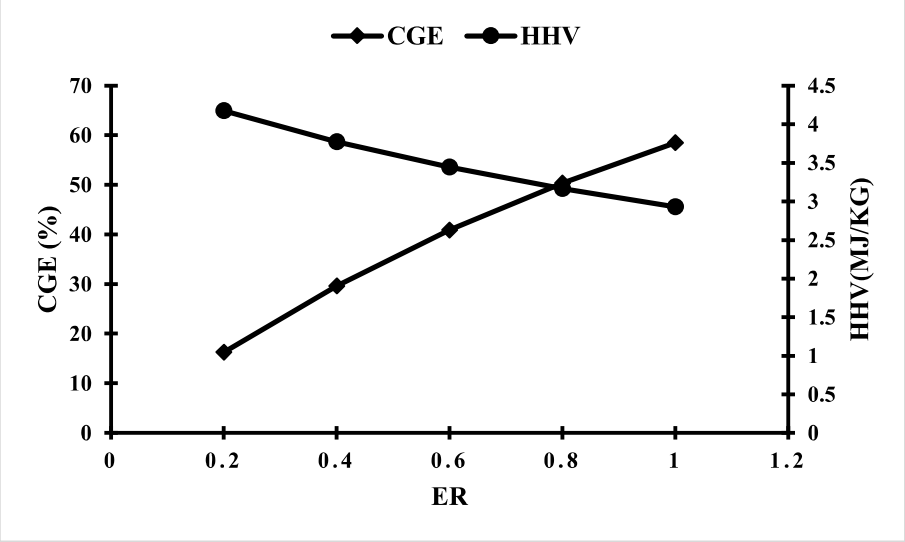

Fig. 4.5. Effect of equivalence ratio on CGE and HHV

4.1.5 Regression analysis

Two independent parameters viz temperature (X_1) and equivalence ratio (X_2) have been taken as the decision variable for the analysis. Three output responses are hydrogen concentration, CGE, and HHV. Table 4.5 illustrates the input and response variables from Aspen plus.

The regression equation for hydrogen concentration in the uncoded unit obtained from ANOVA result is depicted in eq 14

$$H_2 = -0.035 + 0.000379X_1 - 0.005X_2 - 0.000004X_1^2 + 0.028X_2^2 - 0.000158X_1X_2 \quad (14)$$

The regression equation for cold gas efficiency in the uncoded unit obtained from ANOVA result is depicted in eq 15

$$CGE = -25.9 + 0.0652X_1 - 61.7X_2 - 0.000004X_1^2 - 31.8X_2^2 + 0.0291X_1X_2 \quad (15)$$

The regression equation for higher heating value in the uncoded unit derived from ANOVA analysis is given below

$$HHV = -1.31 + 0.01193X_1 + 0.06X_2 - 0.000006X_1^2 - 0.16X_2^2 + 0.0208X_1X_2 \quad (16)$$

4.1.6 Normal probability plots

The normal probability plot is one of the graphical techniques for determining whether the data set is normally distributed or not. In this type of plot, data are charted against a theoreticals normal distributions such that the point should form an approximately straight line, and deviations from this line indicate the departure from the normality. Fig. 4.6 depicts the normal probability plot for all three responses i.e H_2, CGE, and HHV against the residuals. This plot is acquired using Minitab software. It can be inferred from a fig. 4.6 that the predicted value

from the ANOVA tool is having very high accuracy compared with the ASPEN result. Points are scattered very close to the normal distributed straight line.

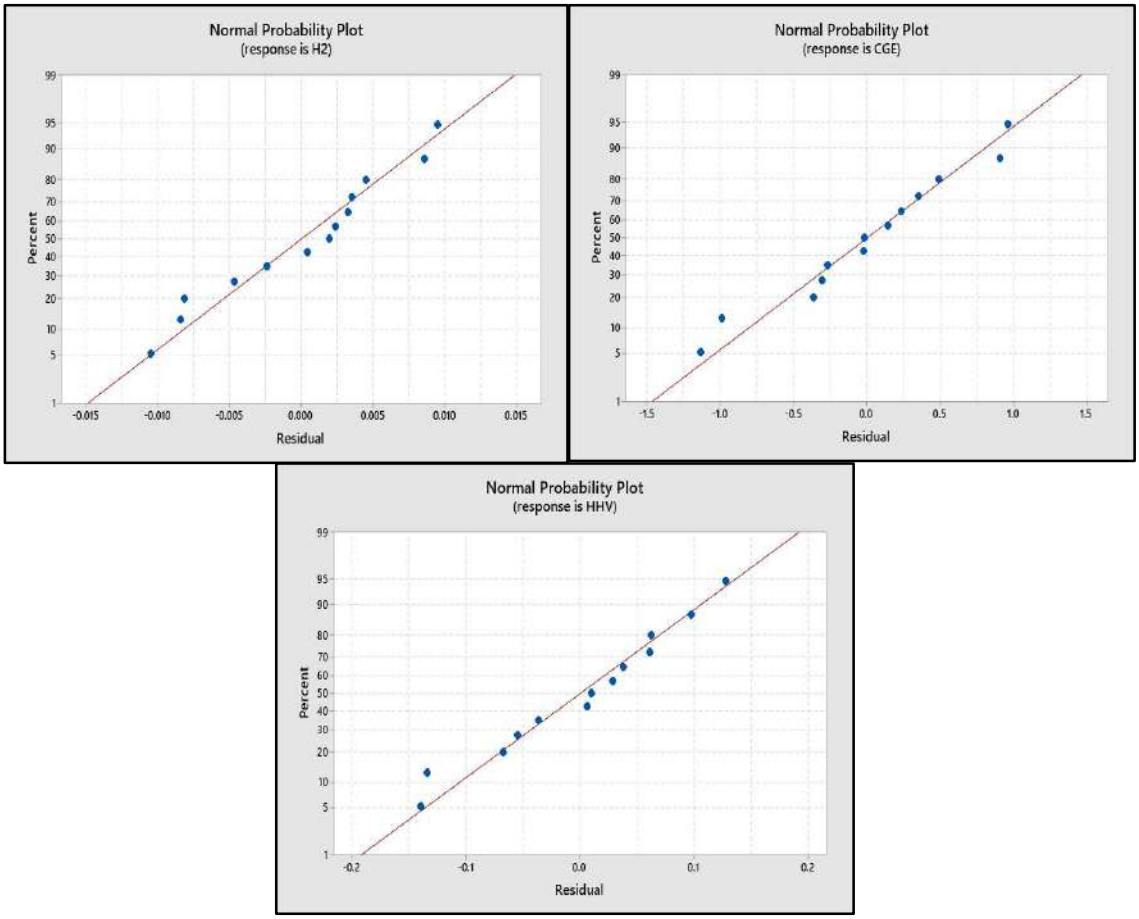

Fig. 4.6. Normal probability plot for output responses against residuals

4.1.7 ANOVA results

ANOVA regression analysis of the RSM models for cold gas efficiency and RSM models conclusion for the CGE is depicted in Tables 4.6 and 4.7 respectively. The P-value is considered to be the most important parameter in the model; P-value is generally considered to be insignificant if the magnitude of this parameter is higher than 0.05 [110]. Results acquired from ANOVA depicted in table 4.6 illustrate that each expression of the regression equations (linear, square, and 2- way interactions) for the response cold gas efficiency are significant

except temperature in the square term. The complete model summary of the ANOVA result is depicted in table 4.6. It can be inferred from table 4.7 that R^2_{adj} value is 99.28% for the CGE. Thus, it can be inferred that the model can predict the response output with high accuracy.

Table 4.6. ANOVA result for the Cold gas efficiency

Source	DF	Adj SS	Adj MS	F-Value	P-Value
Model	5	1132.34	226.47	332.71	0
Linear	2	1121.01	560.51	823.47	0
Temp	1	39.73	39.73	58.37	0
ER	1	1081.28	1081.28	1588.57	0
Square	2	7.95	3.97	5.84	0.032
Temp*Temp	1	2.16	2.16	3.17	0.118
ER*ER	1	4.89	4.89	7.19	0.031
2-Way Interaction	1	3.38	3.38	4.97	0.061
Temp*ER	1	3.38	3.38	4.97	0.061
Error	7	4.76	0.68		
Total	12	1137.1			

ANOVA regression analysis of the RSM models for hydrogen concentration and RSM models conclusion for the concentration of hydrogen in the syngas composition is depicted in table 4.8 and 4.7 respectively. Results developed from ANOVA illustrated in table 4.8 demonstrate that each expressions of the regression equations (linear, square, and 2- way interactions) for the response H_2 are significant except temperature in the linear and square terms. This is because the magnitude of these terms lies above 0.05. Hence, these terms are neglected during the calculation. The complete model summary of the ANOVA result is showed in table 4.8. It can be inferred from table 4.7 that R^2_{adj} value is 78.51% for the H_2.

Table. 4.7. RSM model assessment

	CGE	H_2 yield	HHV
R^2	99.58%	87.46%	95.08%
R^2_{adj}	99.28%	78.51%	91.57%
R^2_{pred}	98.77%	66.55%	86.11%

Table 4.8. ANOVA result for the Hydrogen concentration

Source	DF	Adj SS	Adj MS	F-Value	P-Value
Model	5	0.003438	0.000688	9.77	0.005
Linear	2	0.003284	0.001642	23.33	0.001
Temp	1	0.000031	0.000031	0.44	0.529
ER	1	0.003253	0.003253	46.21	0
Square	2	0.000055	0.000027	0.39	0.693
Temp*Temp	1	0.000053	0.000053	0.76	0.413
ER*ER	1	0.000004	0.000004	0.05	0.826
2-Way Interaction	1	0.000099	0.000099	1.41	0.274
Temp*ER	1	0.000099	0.000099	1.41	0.274
Error	7	0.000493	0.00007		
Total	12	0.00393			

ANOVA regression analysis of the RSM models for higher heating value (HHV) and RSM models summary for the HHV is depicted in table 4.9 and 4.7 respectively. Results developed from ANOVA illustrated in table 4.7 demonstrate that each expression of the regression equation (linear, square, and 2- way interactions) for the response HHV are significant except 2- way interaction and equivalence ratio in the square term. This is because the magnitude of this term lies above 0.05. Hence, these terms are neglected during the calculation. The complete

model summary of the ANOVA result is showed in table 4.9. It can be inferred from table 4.7 that R^2_{adj} value is 91.57% for the HHV. Thus, the model has a high accuracy level in estimating the response output.

Table 4.9. ANOVA result for the Higher heating value

Source	DF	Adj SS	Adj MS	F-Value	P-Value
Model	5	1.58864	0.317728	27.06	0
Linear	2	1.52236	0.761178	64.83	0
Temp	1	0.67181	0.671813	57.22	0
ER	1	0.85054	0.850542	72.44	0
Square	2	0.04895	0.024474	2.08	0.195
Temp*Temp	1	0.04753	0.047534	4.05	0.084
ER*ER	1	0.00013	0.000126	0.01	0.92
2-Way Interaction	1	0.01734	0.017339	1.48	0.264
Temp*ER	1	0.01734	0.017339	1.48	0.264
Error	7	0.08219	0.011741		
Total	12	1.67083			

RSM model assessment for all responses is depicted in table 4.7. It can be inferred from table 4.7 that R^2 assessment is for the H_2 yield, CGE and HHV are 87.46%, 99.58%, and 95.08% respectively. Thus, it can be determined that the model has a very high accuracy level in predicting the response output

4.1.8 Multi-objective optimization using contour and 3-D surface plot

Two independent parameters viz temperature and equivalence ratio have been opted as decision variables for the analysis. It is because these two parameters are the most influential parameters for increasing the gasification efficiency and enhancing the quality of syngas. optimization of

these two parameters leads to increasing the combustible properties of syngas as well as increasing gasification efficiency. Three output responses are hydrogen concentration, CGE, and HHV.

4.1.9 Interaction effect of the decision variables on the Hydrogen concentration

Fig 4.7 represents the influence of decisions variable (temperature and equivalence ratio) on the hydrogen concentration. It can be observed from the surface plot that increasing the temperature increases the concentration of hydrogen but decreases with increasing the ER. This rise is mainly accredited to the water-gas reaction (R7). This reaction also contributed to the enhancement of the calorific value of PG whereas H_2 concentration decrease because as ER increases, the quantity of O_2 delivered to the reactor enhances by which the carbon conversion of the fuel upsurges but the additional quantity of O_2 oxidizes the fuel and thus hydrogen gets oxidized to H_2O.

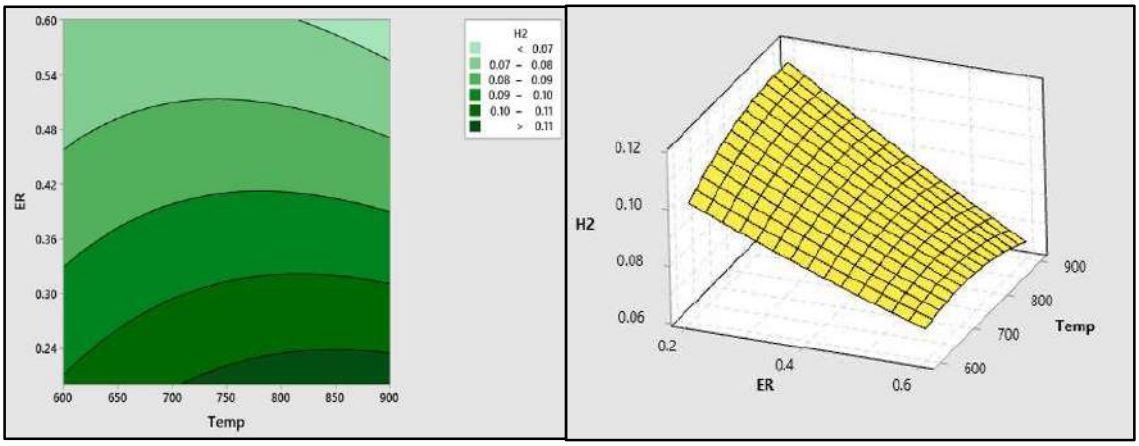

Fig. 4.7. Response surface plots (contour (Left) and 3D (Right)) for H_2 showing the effect of Temp and ER

It can be concluded from the contour plot that the most optimized range for the temperature and ER for maximizing hydrogen concentration is (720-900)^{0}C and (0.24- 0.36) respectively. The optimum value of hydrogen concentration lies in the range of (0.08-0.11)

4.1.10 Interaction effect of the decision variables on the cold gas efficiency

Fig 4.8 depicts the influence of decisions variable on the CGE. It can be observed from the surface plot that increasing the temperature and ER upsurges the CGE. Due to a rise in temperature CGE upsurges because of the continuous increment in the magnitude of CO and H_2 in the syngas composition. CGE depicts a direct relationship with the ER. This may be due to an increase in gas yield as ER increases. It can be concluded from the contour plot that the most optimized range for the temperature and ER for maximizing cold gas efficiency is (770-900)^{0}C and (0.42- 0.48) respectively. The optimum value of CGE lies in the range of (24.1-26.4)%.

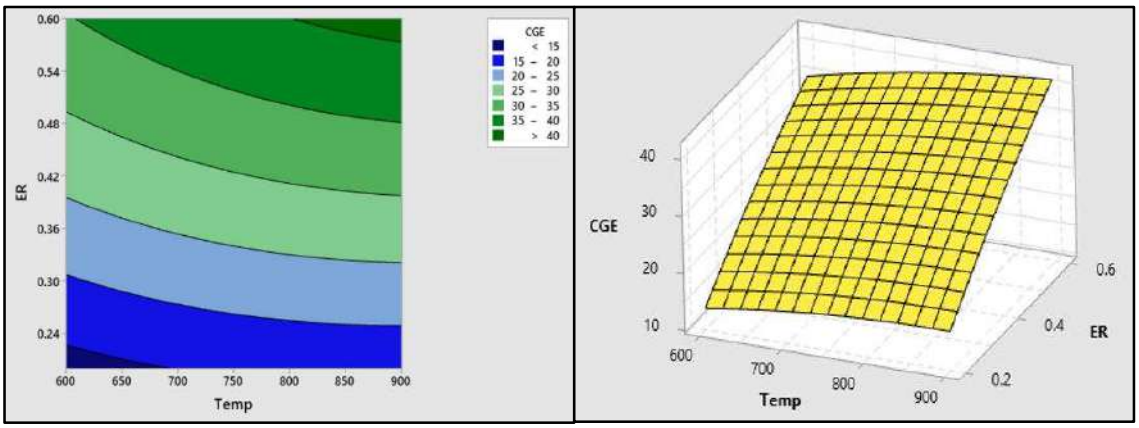

Fig. 4.8. Response surface plots (contour and 3D) for H_2 showing the effect of Temp and ER

4.1.11 Interaction effect of the decision variables on the higher heating value

Fig 4.9 represents the influence of decisions variable on the HHV. It can be observed from the surface plot that increasing the temperature upsurges the magnitude of HHV but decreases with increasing the ER. This may be due to the increment of H_2 and CO magnitude in the syngas composition as the temperature rises. It is already discussed earlier. Similar results for HHV were reported by Lahijani et al. [107]. The magnitude of HHV decreases as ER increases. It is mainly attributed to the fact that the combustible component of producer gas started to decline

as ER increases. It can be concluded from the contour plot that the most optimized range for the temperature and ER for maximizing higher heating value is (770-900)^{0}C and (0.24- 0.36) respectively. The optimum value of CGE lies in the range of (3.8-4.1) MJ/kg.

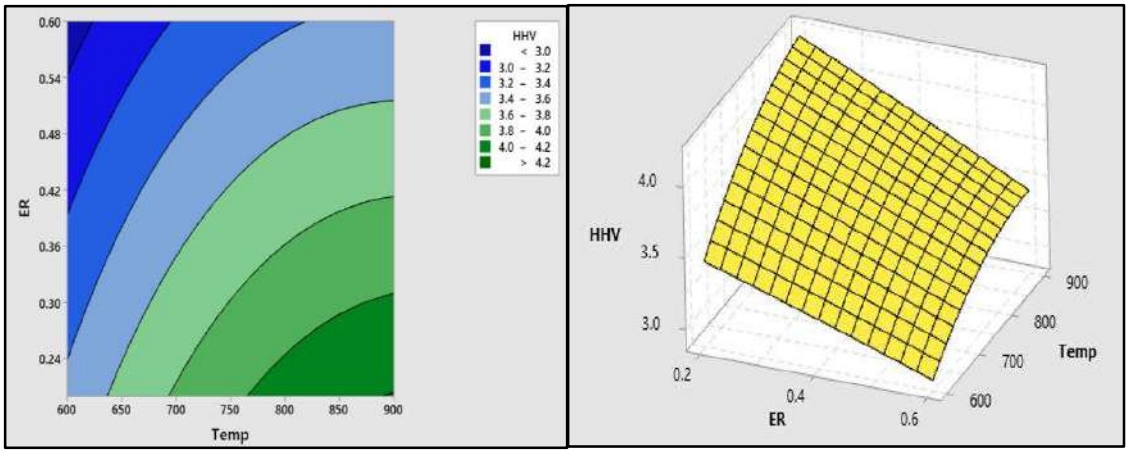

Fig. 4.9. Response surface plots (contour and 3D) for HHV showing the effect of Temp. and ER

4.1.12 Optimal state of decision variables

The optimal performance parameters have been achieved after executing the multi-objective optimizations of the decision variables. It has been acquired from the RSM optimizer section of the Minitab software where each response is characterized by a unitless desirability value (d) and its magnitude reciprocates between 0 and 1. The minimum value 0 depicts ab objectionable response whereas the maximum value 1 represents a required response. The equation of desirability has been categorized as “smaller-the-better” (SB), and “larger-the-better” (LB) type of response [111]. Fig 4.10 depicts the RSM optimizer where results are generated by the RSM optimizer plot. The composites desirability observed was nearby 0.59 which depicts that the setting appears to achieve a favorable outcome for all the responses as a cumulative. The optimal values of H_2, CGE, and HHV are 0.1, 25.23%, and 3.96 MJ/kg respectively. The most optimized point for the temperature and ER is 887.879^{0}C and 0.32.

$$d = \begin{Bmatrix} \left|\frac{y - LL}{UL - LL}\right|^{p'}, LL \le y \le UL \\ 0, y < LL \\ 1, y > UL \end{Bmatrix} \quad (17)$$

$$d = \begin{Bmatrix} \left|\frac{y - LL}{a - LL}\right|^{q'}, a \le y \le UL \\ 0, y > UL \end{Bmatrix} \quad (18)$$

Where exponent p and q are the constants of desirable functions and LL and UL represents lower limit and upper limit whereas a is the minimum magnitude of response output y.

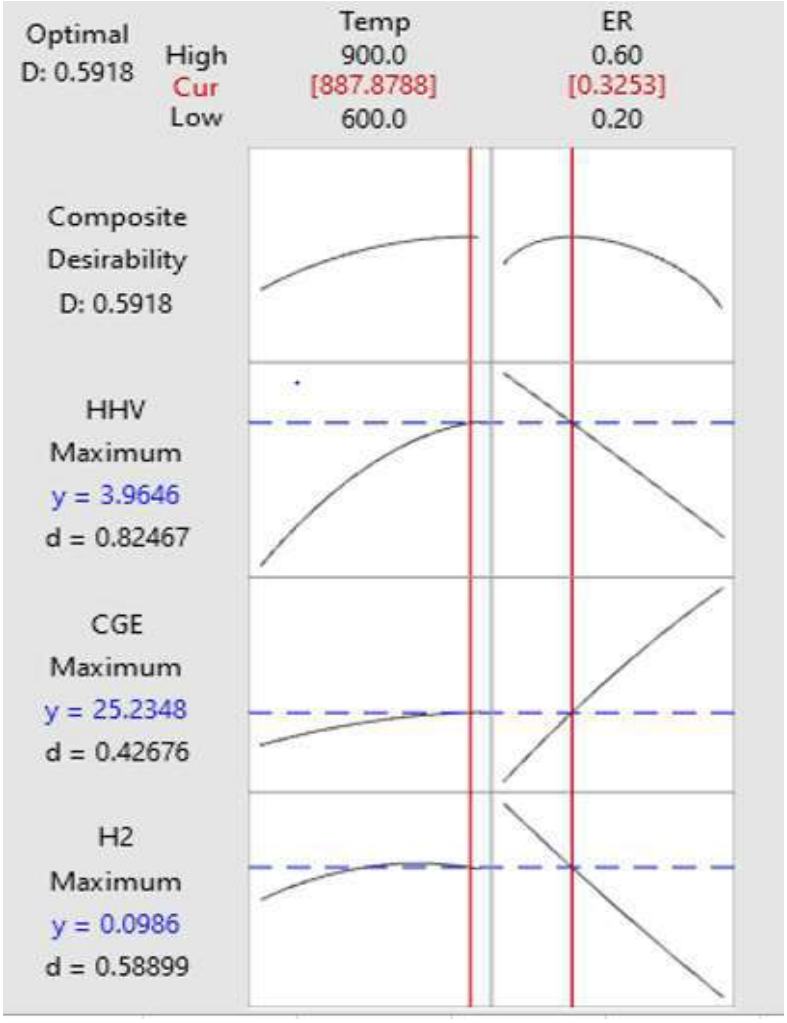

Fig. 4.10. RSM optimizer plot

4.1.13 Summary of the present work

Prediction and multi-objective optimization of the variable air gasification performance parameters by integrating ASPEN Plus with Response surface methodology (RSM) using Syzygium cumini biomass fuel was investigated in this present research work. The model was calibrated and validated using four different feedstock from the literature. Sensitivity and error analysis was performed. Temperature, equivalence ratio of gasifier was selected as the decision variables and the response output was selected as H_2 yield, CGE, and HHV. An optimal working range was obtained to achieve the best possible outputs using RSM. More independent parameters like moisture content, gasifier reactor design can be adopted for the optimization study in the future work. Gasification using torrefied biomass and plastic waste can also be simulated using ASPEN PLUS and optimized using RSM in the further investigation.

The following conclusions can be concluded from the investigation done in this present study

- A comprehensive steady-state stoichiometric kinetic free equilibrium based robust model of biomass gasifier was developed using ASPEN PLUS simulator. It was based on the concept of decreasing Gibbs free energy to the lowest point.
- The model is capable of estimating syngas compositions and gasifier performance under variable operating conditions. Model validation was done and found that results acquired in the present study are in good agreement with the experimental result
- Sensitivity analysis was performed in which the influence of variable gasification temperature, variable equivalence ratio (ER) on the syngas composition, gas yield, cold gas efficiency, and the higher heating value (HHV) was quantified.
- A highly accurate robust regression model has been attained from the ANOVA tool for estimating hydrogen concentration, cold gas efficiency, and higher heating value.

- RSM optimizer estimates that the optimal magnitude of H_2, CGE, and HHV is 0.1, 25.23%, and 3.96 MJ/kg respectively corresponding to temperature at 887.879^{0}C and equivalence ratio 0.32.

- The composite desirability observed was nearby 0.59, which depicts that the setting appears to achieve a desirable outcome for all the responses as a cumulative.

4.2 Numerical Simulation – Gasification of Poultry litter pellet

This present study investigates the processing of waste poultry litter pellet biomass for the generation of enriched hydrogen syngas using biomass gasifier. Modeling of biomass gasifier was performed in Aspen Plus and Model validation was done using four different agricultural waste biomass with the experimental result and, a good agreement was attained. Sensitivity analysis was performed in which the influence of equivalence ratio (ER), gasification temperature, and moisture content on the producer gas (PG) composition, gas yield, H_2/CO ratio, cold gas efficiency (CGE), and the higher heating value (HHV) were investigated. Furthermore, RSM has been employed for the multi-objectives optimization of the variable gasification parameters. with RSM. Fig.4.11 depicts the Aspen plus block diagram.

Table.4.10. Chemical properties of waste Poultry litter pellets

Ultimate analysis (wt. %)	Poultry litter pellets [43]
Carbon	43.98
Hydrogen	5.16
Nitrogen.	4.63
Oxygen	31.98
Sulfur	0.75
Proximate analysis (wt. %)	
Volatile matter	63.6
Fixed carbon	15.3
Moisture	7.6
Ash	13.5

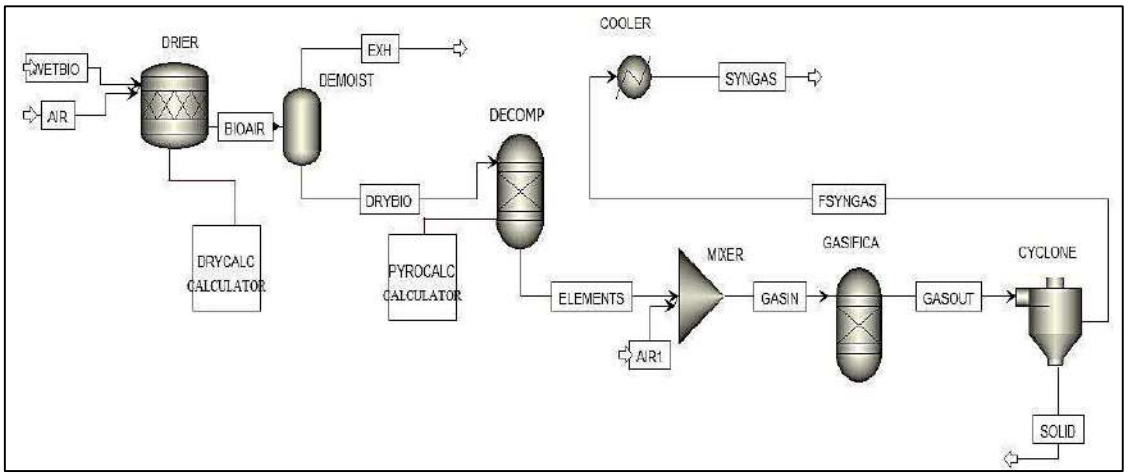

Fig. 4.11. Aspen plus modelling

4.2.1 Model validation

The developed model using Aspen plus was validated against the experimental data which was published by Striguas et al. [43]. Model was validated with four different types of agricultural biomass i.e. Hardwood chip, poultry litter pellets, softwood pellet and rape straw pellet. Model validation in the present investigation depicts that modelling assumptions are generating valid data across the relevant range for multiple types of feedstocks. This builds the confidence in the model for the prediction over the higher range. To achieve the syngas composition, the same operating conditions were used. The values obtained by the established model using Aspen plus simulator are shown in Fig. 4.12 and are compared to experimental values from the literature.

The syngas composition obtained by the current study is in good agreement with those obtained experimentally by Striguas et al. [43], as shown in the Fig. 4.12. The magnitude of CH_4 concentration attains the null value in equilibrium modeling [112]. This under-prediction may be due to the equilibrium model's assumption that tar and heavy hydrocarbons are not included in the syngas composition, despite the fact that they are commonly present in syngas generated by real gasification units.

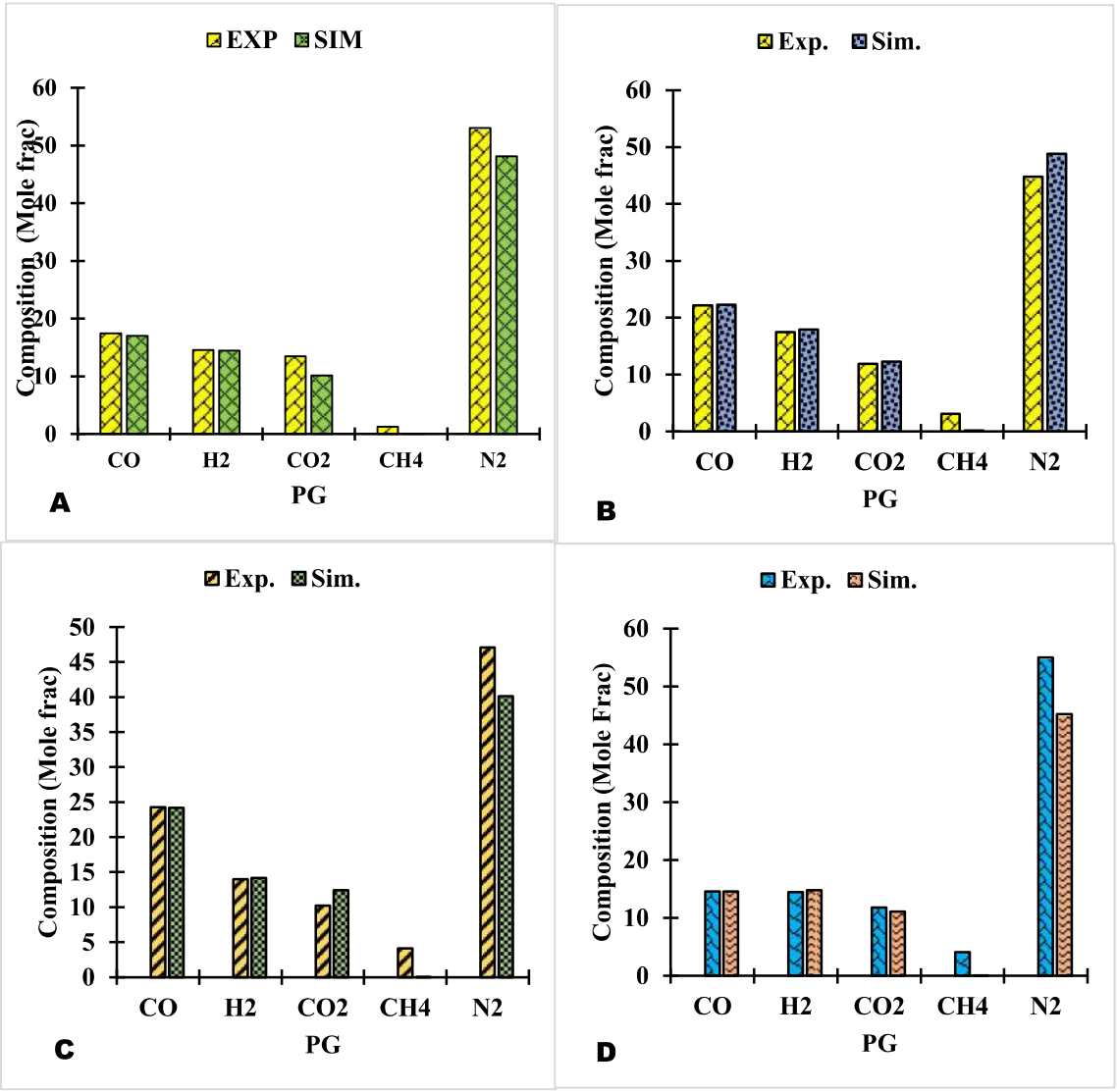

Fig. 4.12. Model validation a. Hardwood chip, b. Poultry litter pellet, c. Softwood pellet d. Rapestraw Pellet

4.2.2 Sensitivity Analysis

Sensitivity analysis was carried out using the existing model. The reaction temperature, equivalence ratio (ER), and biomass moisture content are all important factors in determining syngas compositions and gasification characteristics. For animal waste poultry litter pellets, the effects of variable gasifier temperatures (400-1000°C), variable ER (0.2-1), and variable biomass moisture content (0-30%) on syngas compositions, gas yield (GY), H2/CO ratio, CGE, and HHV were inspected.

4.2.3. Temperature effects on syngas compositions and gasification efficiency

Temperatures for gasification ranged from 400 to 1000 degrees Celsius. Fig.4.13 shows the effect of gasification temperatures on syngas compositions.

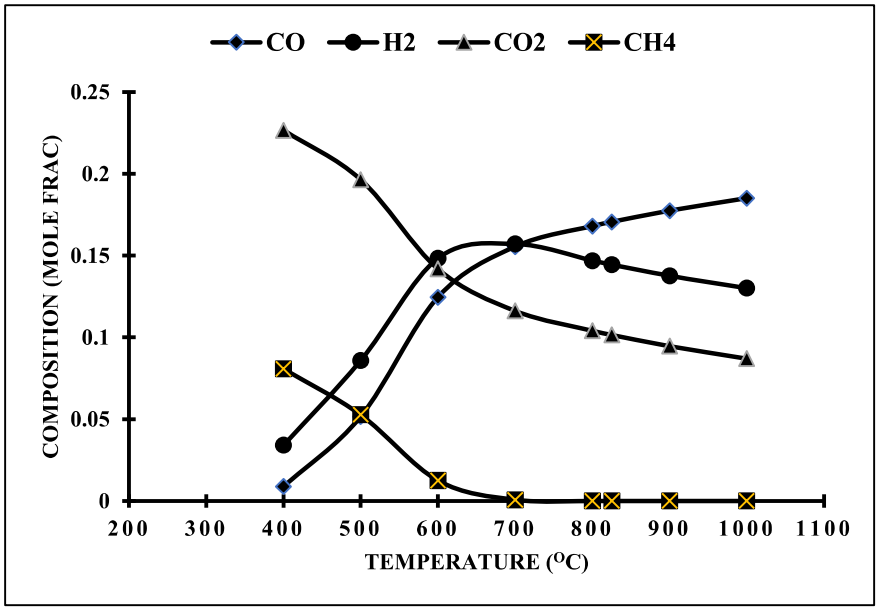

Fig. 4.13 Influence of temperatures on syngas compositions for poultry litter pellets

In the composition of syngas, the temperature of gasification is the most convincing parameter. The temperature at which gasification occurs determines the consistency of syngas. The partial oxidation reaction causes the carbon within the reactor to respond with oxygen and convert it into carbon monoxide as the temperature rises (R4). Another investigation depicts the mechanism of this reaction. [98]. This is a highly endothermic method. CO levels increase as temperature increases, as shown in Fig. 4.13 The water-gas reaction is primarily to blame for this increase (R7). The calorific value of PG was also increased as a result of this reaction. Fig.4.13 shows that the magnitude of CO increases steadily as the variable temperature rises from 400^0C to 1000^0C. This pattern is consistent with the findings of other studies. [98, 103, 104]. Skoulou et al. found a similar pattern when they investigated the effect of gasification

temperature on the magnitude of PG produced from olive kernel and olive tree cuttings. They discovered that as temperatures rise, CO and H2 concentrations increase, while CO_2 and CH_4 concentrations decrease [106].

Fig.4.14 shows the simulated results for gas yield and H2/CO. The plot indicates that the gas yield increases as the temperature rises. This may be because of the following factors: I The initial pyrolysis rate was increased by increasing the temperature, resulting in a higher product gas yield. (ii) At high temperatures, the rate of steam reforming and cracking increases, and (iii) the endothermic reaction of char gasification improves. [113, 114]. A similar trend of gas yield production was obtained by Lahijani et al. [107]. They found that increasing the bed temperature by 50 degrees increases the dry gas yield by sawdust and EFB (empty fruit bunch). As the temperature rises, the H2/CO ratio decreases. It's because CO increases at a faster rate than H2 as the temperature rises. Results obtained for H2/CO from our model were following the result acquired by Han et al. [92]. The variation of cold gas efficiency (CGE) and higher heating value (HHV) with temperature is depicted in Fig 4.15. The CGE is proportional to the temperature of gasification. This may be attributed to the syngas composition's continuous increase in the magnitude of CO and H2. The CGE percentages conveyed in the literature were very similar to the results obtained from our model for CGE values. [115]. Using municipal solid waste (MSW) as a feedstock, Niu et al. investigated the variation of CGE with temperature. They discovered that the magnitude of MSW varies between 39.90 and 78.70 percent at elevated temperatures of $(650\text{-}1000)^0$C and 32.60 to 87.6 percent at lower temperatures of (550-650)0C.[109]. From fig. 4.15, it is clear that HHV is directly propotional to temperature. This may be because the magnitude of H2 and CO in the syngas composition increases as the temperature rises. It has already been debated. Lahijani et al. published similar findings for HHV.[107].

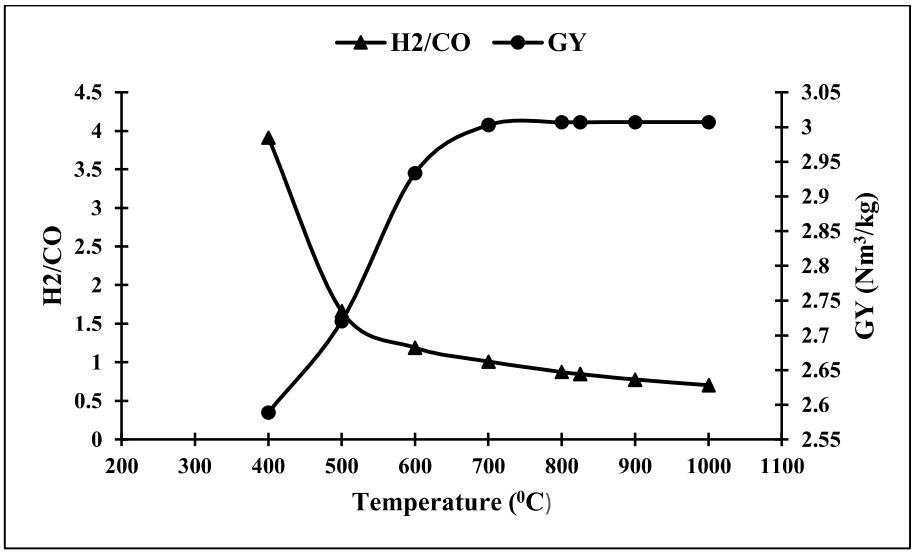

Fig. 4.14 Variation of H2/CO and GY with temperature.

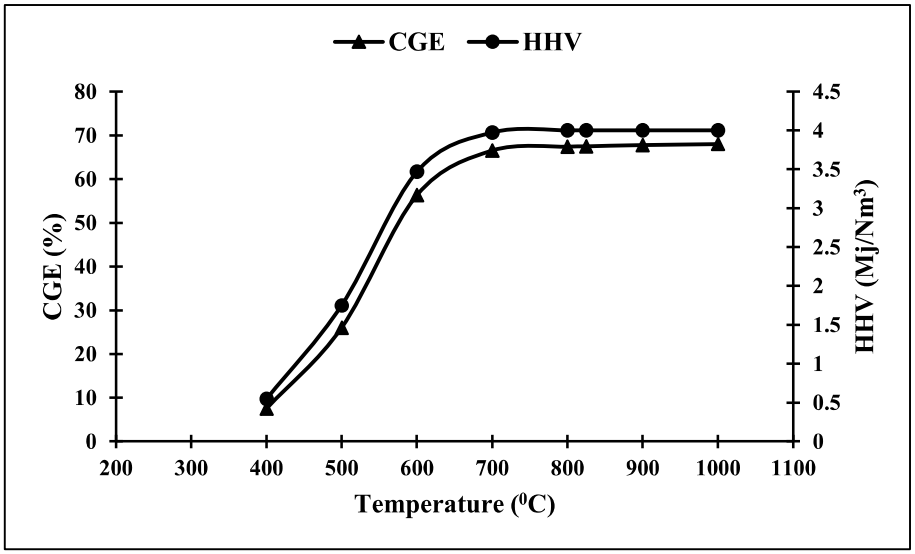

Fig. 4.15 Variation of CGE and HHV with temperature.

4.2.4. Equivalence ratio (ER) effect on syngas composition and its gasification efficiency

The equivalence ratio is known as the difference between the actual and stoichiometric air-fuel ratios. [108]. It's one of the most important factors influencing composition

ns. ER was varied in this investigation from (0.2-1) by varying the airflow amount while holding the temperature steady at 800^0C. Fig.4.16 depicts the changes in syngas composition as ER varies.

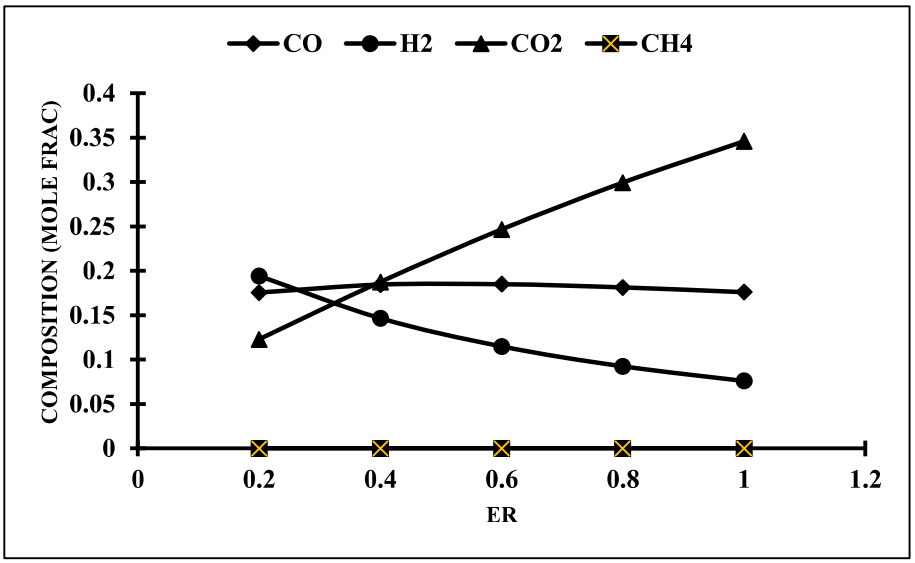

Fig. 4.16. Influence of ER on syngas compositions for poultry litter pellets

The magnitude of H_2 content decreases constantly from 19.41 percent at ER 0.2 to 7.59 percent at ER 1. This can be deduced from the map. As ER rises, the magnitude of CO content decreases as well. This decrease can be explained by the fact that as ER rises, the amount of O2 supplied to the reactor rises, increasing carbon conversion, however the additional oxygen oxidises the fuel completely. CO and H_2 material decreases as a result. It's because full combustion has started. The magnitude of the shift in CH_4 is found to be marginal as ER increases.. Our model's ER results were consistent with those of other studies in the literature. [42, 109].. They also discovered that CO levels drop steadily from 26.73 percent at 0.2 to 9.09 percent at 0.45. CO2 concentrations rise steadily from 9.4 percent at 0.2 to 17.4 percent at 0.45.

Fig.4.17 shows the simulated results for gas yield and H_2/CO. The magnitude of gas yield increased from 0.10 at ER 0.2 to 0.78 at ER 1. This can be seen in Fig.4.17. Lahijani et al.

discovered a similar pattern [107]. Using sawdust and EBF, they registered a steady increase in dry gas yield and carbon conversions, as well as an increase in ER. With increasing ER, H_2/CO has an inverse relationship. Fig.4.18 depicts the effect of ER on CGE and HHV. The direct relationship between cold gas efficiency and the ER is depicted by cold gas efficiency. CGE reached a high of 14.48 percent. This direct relationship may be explained by the fact that as ER rises, gas yield rises as well, while HHV rises in the opposite direction. At ER 0.2, the maximum HHV was 4.69 MJ/Nm^3. The existence of high combustible gas concentrations,especially CO and H_2, is to blame. For gas HHV, increasing ER beyond 0.35 was detrimental. It may be due to the syngas being diluted with N_2, resulting in the gas having a low energy content. Lahijani et al. discovered a similar pattern for HHV.[107]. By growing the ER and using sawdust and EFB as feedstock, they were able to reduce HHV.

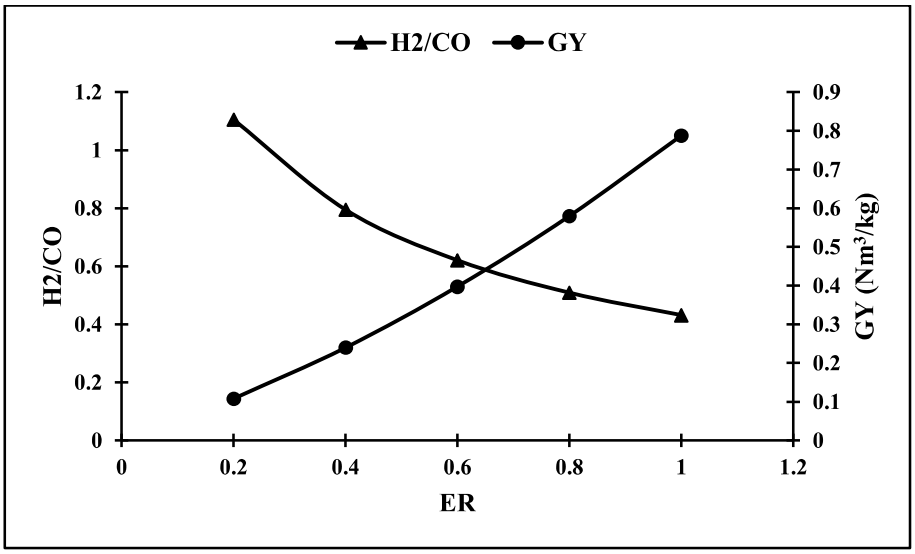

Fig. 4.17. Variation of H2/CO and GY with equivalence ratio.

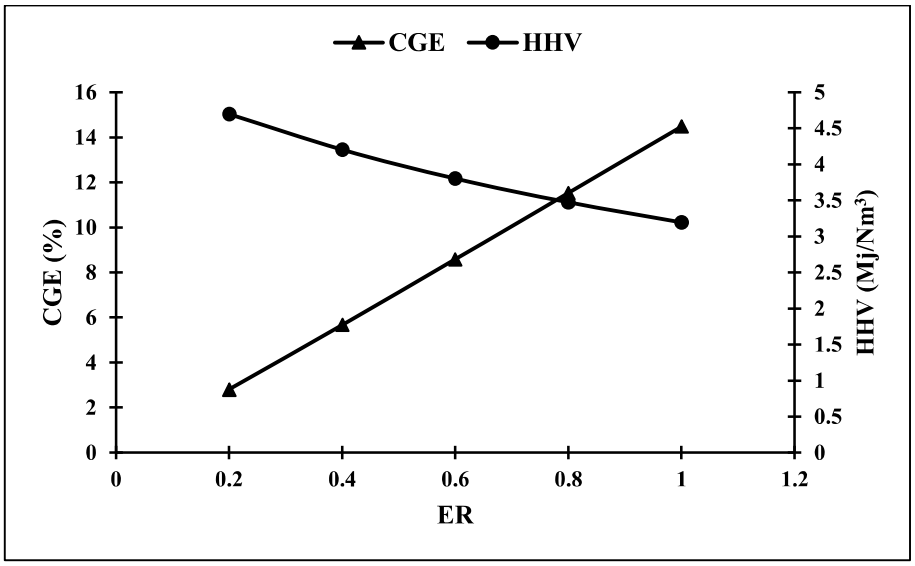

Fig. 4.18. Variation of CGE and HHV with equivalence ratio.

4.2.5. Moisture content (MC) effect on syngas composition and gasification efficiency.

The moisture content of poultry litter pellet has been varied from (0 to 30%). Sensitivity analysis has been implemented to determine the composition of syngas and gasification performance under this range. The influence of moisture contents on the syngas composition was plotted and depicted in fig 4.19.

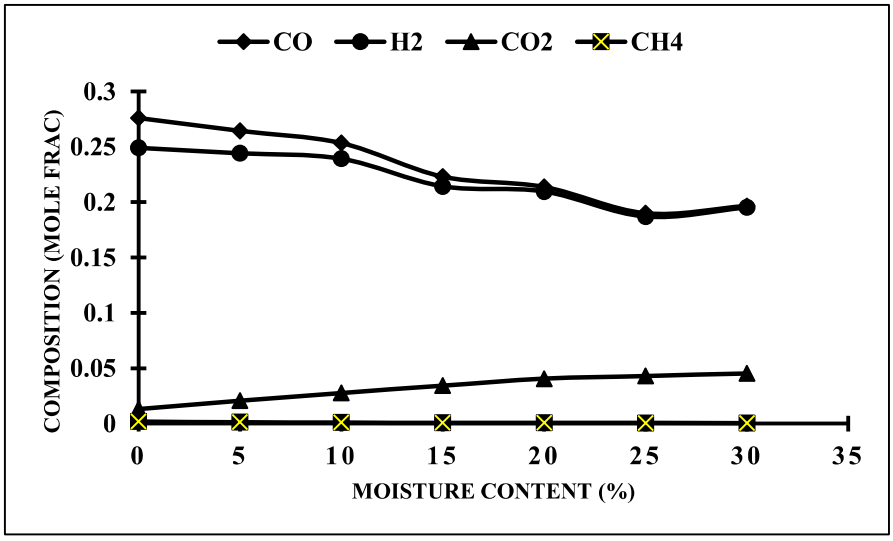

Fig. 4.19. Effect of Moisture Content (%) on syngas composition

The moisture present in the biomass may take part in the chemical reactions, like steam methane reforming reaction (R9), water gas shift reactions (R5), and water-gas reactions (R7). These reactions can control the chemical reaction equilibrium. Eventually, the composition of syngas distribution can be altered [116]. As it is evident from fig 4.19 that while the magnitude of moisture contents increased, H_2 concentration decreases from 24.9% at 0 MC to 19.53% at 30% MC. The magnitude of CO content also follows the same trend of declining as the MC increases. This may be due to the higher heat requirement to vaporize H_2O in the higher MC content feedstock. Reaction temperature drops when MC was enhanced. Lower temperature leads to a decrease in the carbon reduction reaction, along with the decline in the magnitude of CO content. The high content of MC enhances the vapor in the reactor. Eventually, it increases the rate of water gas shift reaction. All of these factors reduce the amount of CO and H2 in the syngas mixture. whereas CO_2 content increases for Poultry litter pellets used in the present study. It is because CO would convert into CO_2. A similar trend was stated by Han et al. [92]. They reported a decrease in the concentrations of CO and H2 while CO_2 content increases as MC increases from 0 to 30% for wood chips as feedstock.

The influence of moisture contents on gas yield and H2/CO has been depicted in fig 4.20 and The influence of moisture contents on cold gas efficiency and HHV is depicted in fig 4.21. Fig.4.21 shows that CGE and HHV levels are decreasing. as MC increases from (0 to 30)%. The magnitude of CGE varies in the range of (53-66)%. . This decline may be due to the decrease in the heating values of syngas as the MC increases. The magnitude of HHV decreases because the content of CO and H2 decreases as the MC increases. Maximum HHV can be obtained in the range of (0-10)% of moisture content. A similar trend of decline was acquired by Han et al. [92]. They reported that LHV constantly decreases from 5.42 MJ/Nm^3 at 0% MC to 3.26 MJ/Nm^3 at 30% MC.). H2/CO ratio tends to increase with increasing MC. It may be

because the magnitude of CO decreases rapidly as compared to hydrogen as moisture content increases. The maximum value of gas yield obtained was 1.91 at 30% MC.

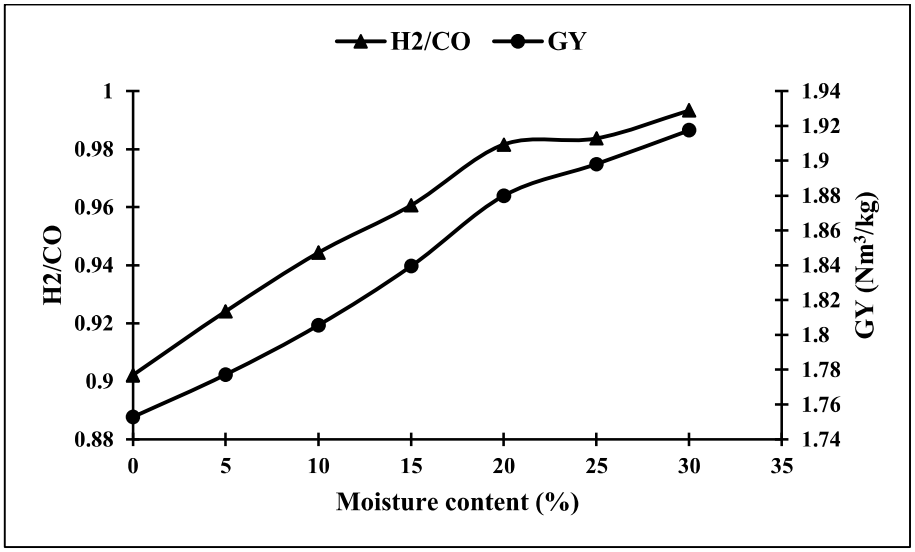

Fig. 4.20. Variation of H2/CO and GY with moisture content.

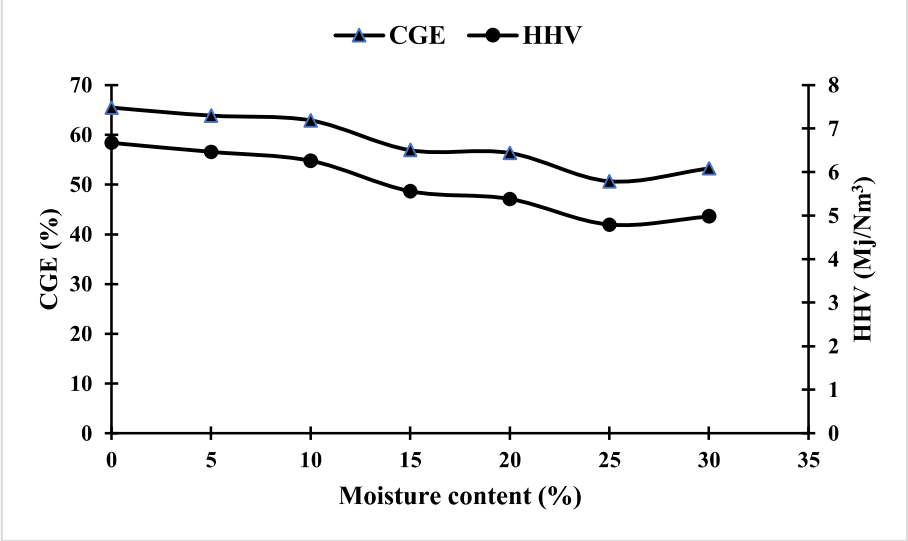

Fig. 4.21. Variation of CGE and HHV with moisture content.

4.2.6 *Regression analysis*

Three independent parameters were chosen: temperature (X1), equivalence ratio (X2), and moisture content (X3). Hydrogen, CGE, and HHV are three performance responses (HHV). Table 4.11 shows the expected design plan as well as the computed response values. Since the two-way interaction concept was trivial, it was left out of the calculations.

The ANOVA analysis yielded for hydrogen concentration

$$H_2 = -0.3999 + 0.001363X_1 - 0.112X_2 + 0.01201X_3 - 0.000001X_1^2 + 0.002X_2^2 - 0.000323X_3^2 \quad (19)$$

The ANOVA analysis yielded for CGE

$$CGE = -69.9 + 0.483X_1 - 374.1X_2 - 1.55X_3 - 0.000277X_1^2 + 262.7X_2^2 + 0.0264X_3^2 \quad (20)$$

The ANOVA analysis yielded for HHV.

$$HHV = -10.83 + 0.03343X_1 - 0.63X_2 + 0.2951X_3 - 0.000020X_1^2 - 0.67X_2^2 - 0.00814X_3^2 \quad (21)$$

Table. 4.11 Parameter settings plan along with the responses

	Parameter				**Responses**	
Trial no	**Temp.**	**ER**	**MC**	**H_2**	**CGE (%)**	**HHV (MJ/Nm^3)**
1	400	0.2	5	0.034130035	7.499004592	0.546367205
2	500	0.2	5	0.085869488	25.97250359	1.748995481
3	600	0.2	5	0.148286535	56.30542016	3.468628042
4	700	0.2	5	0.157165004	66.49327626	3.974526232
5	800	0.2	5	0.146955893	67.41120804	4.000539536
6	825	0.2	5	0.144469873	67.50989772	4.000999897

7	900	0.2	5	0.137662718	67.7494785	4.000818326
8	1000	0.2	5	0.13002299	68.00340787	3.999908523
9	800	0.4	5	0.14661942	5.669877718	4.203581636
10	800	0.6	5	0.114772938	8.583305764	3.80302923
11	800	0.8	5	0.092347979	11.52383681	3.472241226
12	800	1	5	0.075943918	14.48278131	3.194445924
13	800	0.2	10	0.239278257	62.85830773	6.259268667
14	800	0.2	15	0.214370684	56.91030586	5.559075922
15	800	0.2	20	0.209761295	56.3386238	5.380669922
16	800	0.2	25	0.187013436	50.66373946	4.791954306
17	800	0.2	30	0.195322468	53.21380532	4.98045704

4.2.7 Normal probability plots

The normal probability plot for all three output responses is obtained using the RSM technique. These plots are very important for determining the efficiency of the model. in this type of plot, the X-axis is taken as the residuals whereas Y-axis is taken as the percent value. Residual is the difference between the exact value and the predicted value. Exact values are those values that are predicted by using Aspen plus sensitivity analysis. Predicted values are those values that are obtained by using regression equations using ANOVA analysis. These plots have scattered output response points. These scattered points deviate from one straight line that is known as a theoretical normal distribution. The closeness of scattered points from this straight line depicts higher efficiency of the developed model and vice versa. Fig.4.22 depicts the normal probability plots

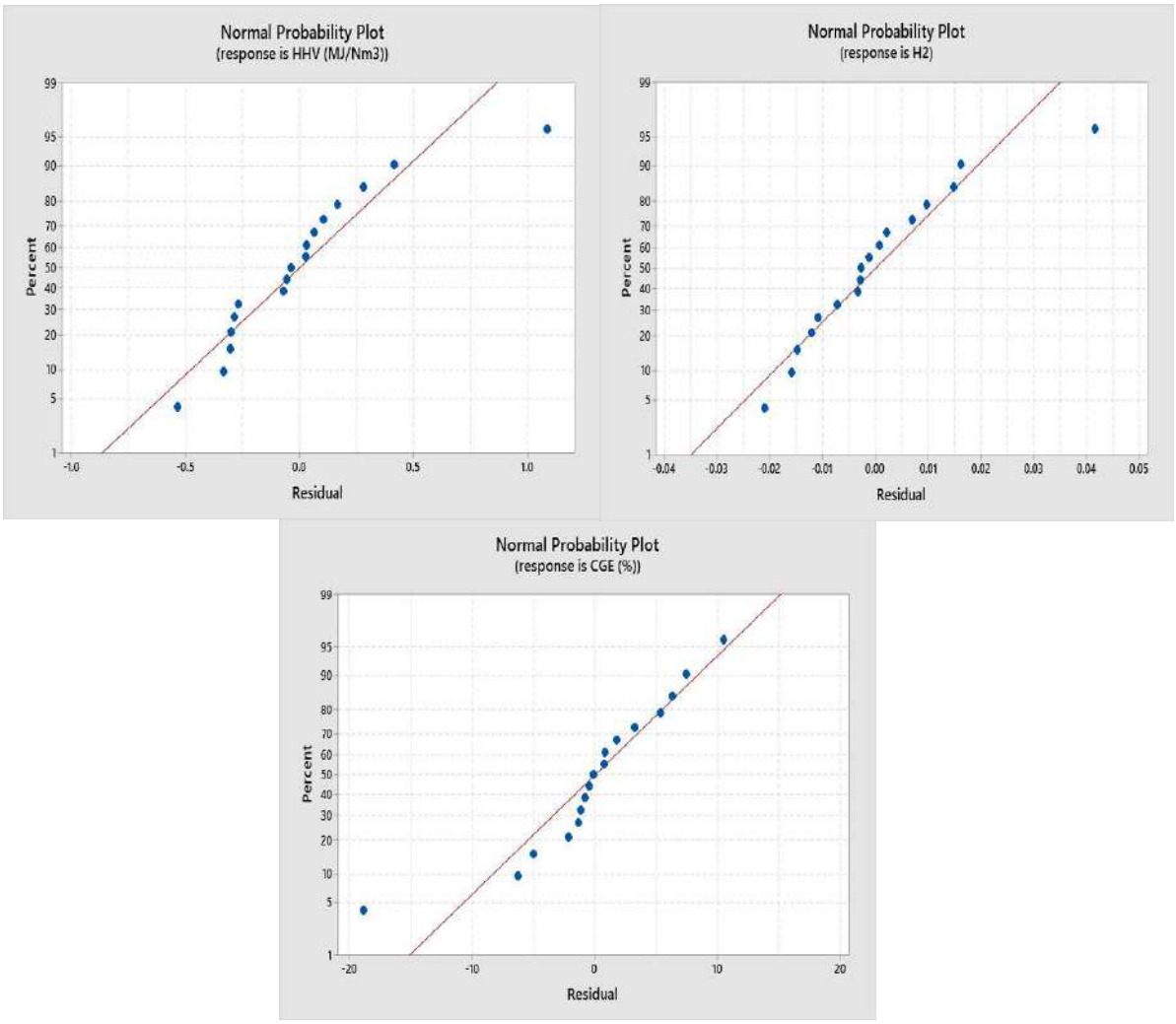

Fig. 4.22. Normal probability plot for output responses

4.2.8 ANOVA results

Tables 4.12, 4.13, and 4.14 show the RSM model's ANOVA results for all three dependent parameter.The F-value in the table depicts the statistical significance of the model as well as factors and their interactions. The higher magnitude of the F factor depicts the higher significance of the effects of the factors on the response variables. The P-value is insignificant if its magnitude is higher than 0.005 [110]. Table 4.12 shows that all expressions of the regression model for the hydrogen are important, with the exception of the equivalence ratio

and moisture content in the square term. It depicts that square term of moisture content and equivalence ratio is insignificant while predicting the response variable using regression analysis. It can be inferrred from table 4.12 that ER is the most predominant paramter for the generation of hydrogen followed by temperature and at last moisture content of biomass. Table 4.13 depicts the ANOVA analysis of CGE. It can be concluded from the table 4.13 that CGE is predominantly affected by temperature follower by equivalence ratio and moisture content. This may be due to the increase concentration of hydrogen and CO at elevated temperature. All terms for predicting CGE in table 4.13 is significant except square term of temeperature as P-value of this square term is greater than 0.005. Same trend like CGE is followed by HHV in table 4.14. Temperature is most predomainent for HHV followed by ER and moisture content of biomass. It can be inferred from the table 4.14 that linear term of temperature and ER are insignificant in predicting HHV of biomass.

Table 4.12. ANOVA analysis for the H_2

Sources	DF	SS	MS	F-Value	P-Value
Models	6	0.043248	0.007208	19.86	0
Linear	3	0.013432	0.004477	12.33	0.001
Temperature	1	0.005899	0.005899	16.25	0.002
ER	1	0.007377	0.007377	20.32	0.001
Moisture content	1	0.000312	0.000312	0.86	0.006
Square	3	0.012843	0.004281	11.79	0.001
Temperature*Temperature	1	0.006947	0.006947	19.14	0.001
ER*ER	1	0	0	0	0.009
Moisture content*Moisture content	1	0.003339	0.003339	9.2	0.013
Error	10	0.00363	0.000363		
Total	16	0.046878			

Table 4.13. ANOVA analysis for the CGE

Sources	DF	SS	MS	F-Value	P-Value
Models	6	9328.7	1554.79	22.85	0
Linear	3	4309.2	1436.41	21.11	0
Temperature	1	2673.7	2673.74	39.3	0
ER	1	2114.2	2114.15	31.08	0
Moisture content	1	248.8	248.82	3.66	0.005
Square	3	2411.1	803.69	11.81	0.001
Temperature*Temperature	1	699.8	699.83	10.29	0.009
ER*ER	1	2051.3	2051.29	30.15	0
Moisture content*Moisture content	1	22.3	22.32	0.33	0.009
Error	10	680.3	68.03		
Total	16	10009			

Table 4.14. ANOVA analysis for the HHV

Sources	DF	SS	MS	F-Value	P-Value
Models	6	27.0707	4.51179	20.3	0
Linear	3	10.3342	3.44475	15.5	0
Temperature	1	9.1833	9.18329	41.33	0
ER	1	1.2498	1.24977	5.62	0.009
Moisture content	1	0.0687	0.06875	0.31	0.009
Square	3	7.2377	2.41256	10.86	0.002
Temperature*Temperature	1	3.6088	3.60882	16.24	0.002
ER*ER	1	0.0132	0.01321	0.06	0.002
Moisture content*Moisture content	1	2.1149	2.11493	9.52	0.012
Error	10	2.2221	0.22221		
Total	16	29.2928			

Table 4.15 shows the RSM model evaluation for all responses. The R^2 magnitude for the H_2, CGE, and HHV is 92.26 percent, 93.20 percent, and 92.41 percent, respectively. As a result, the model can be determined to have a very high degree of accuracy in predicting the response performance.

Table. 4.15. RSM model assessment

	H_2	CGE	HHV
R-sq	92.26%	93.20%	92.41%
R-sq(adj)	87.61%	89.13%	87.86%
R-sq(pred)	68.44%	56.94%	69.43%

4.2.9 Parametric impact using contour and 3-D surface plot

For the study, three independent parameters were chosen as decision parameters: temperature, equivalence ratio, and moisture content. This is because these three parameters have the greatest impact on rising gasification efficiency and improving syngas consistency. Hydrogen composition, CGE, and HHV are three performance responses

4.2.10 Simultaneous influence on the Hydrogen concentration

The surface plot shows that as the temperature rises, the magnitude of hydrogen rises, but as the ER and moisture content rise, the concentration of hydrogen decreases. The water-gas reaction is primarily responsible for this increase (R7). Since as ER rises, the amount of O2 added to the reactor increases, the carbon conversion increases, but the additional quantity of

oxygen oxidises the fuel entirely, this reaction also led to a rise in the calorific value of PG while H_2 concentration decreased. As a result, hydrogen is oxidised to H2O. Fig.4.23 shows a

contour plot and a surface plot of hydrogen yield for (Temperature, ER), (ER, Moisture content), and (Temperature, Moisture content).

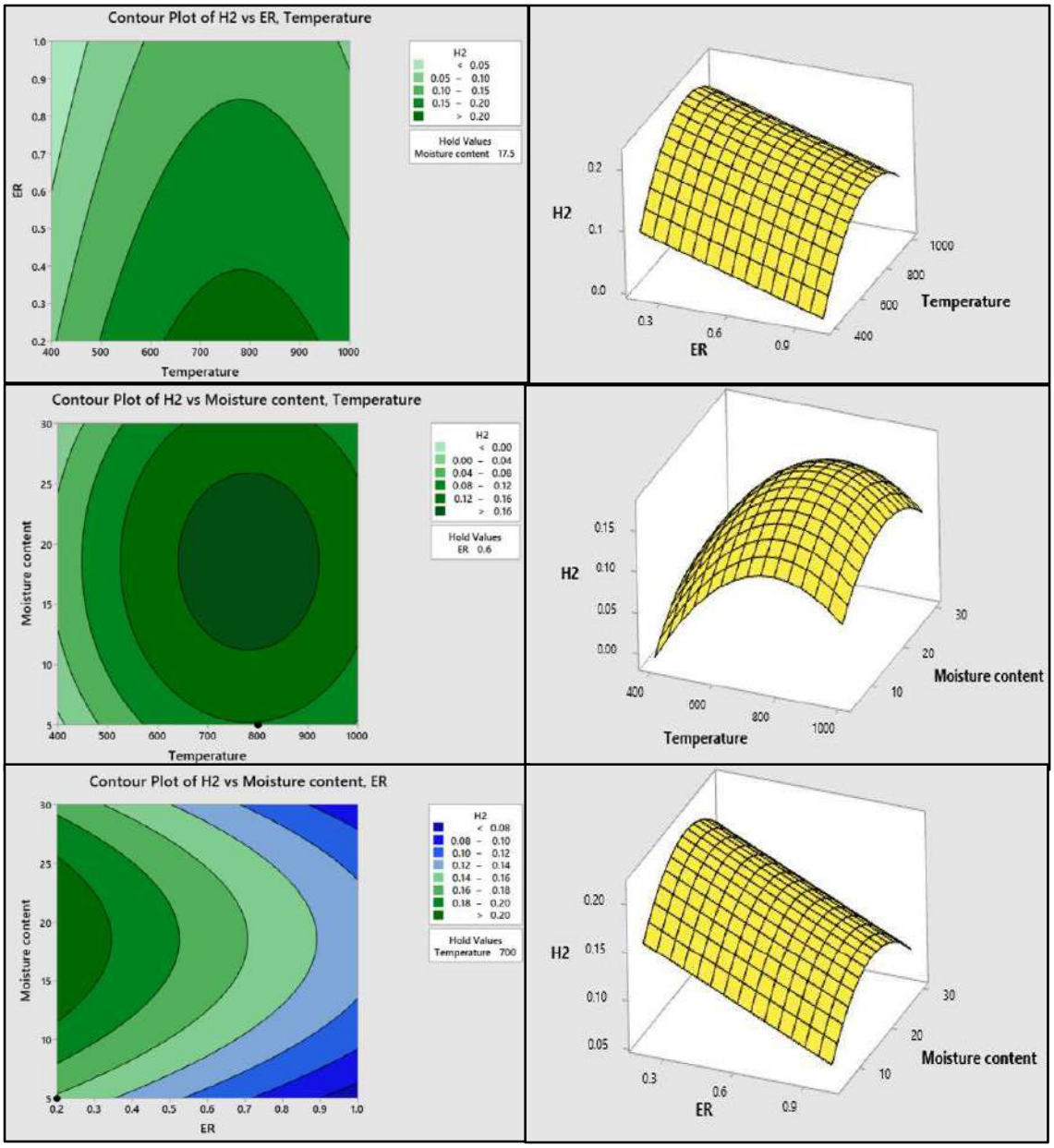

Fig. 4.23. Contour and surface plot of Hydrogen concentration under variable parameters

4.2.11 Simultaneous influence on the cold gas efficiency

The effect of decision variables on cold gas efficiency is depicted in Fig.4.24. The cold gas efficiency increases as the temperature and ER increase, as seen on the surface map. CGE portrays a clear link between the ER. This may be because as ER rises, gas yield rises as well. As MC increases from 0 to 30%, cold gas efficiency (CGE) decreases. This fall may be attributed to a decrease in syngas heating prices as the MC rises. Fig.4.24 shows a contour plot and a surface plot of CGE for (Temperature, ER), (ER, Moisture content), and (Temperature, Moisture content).

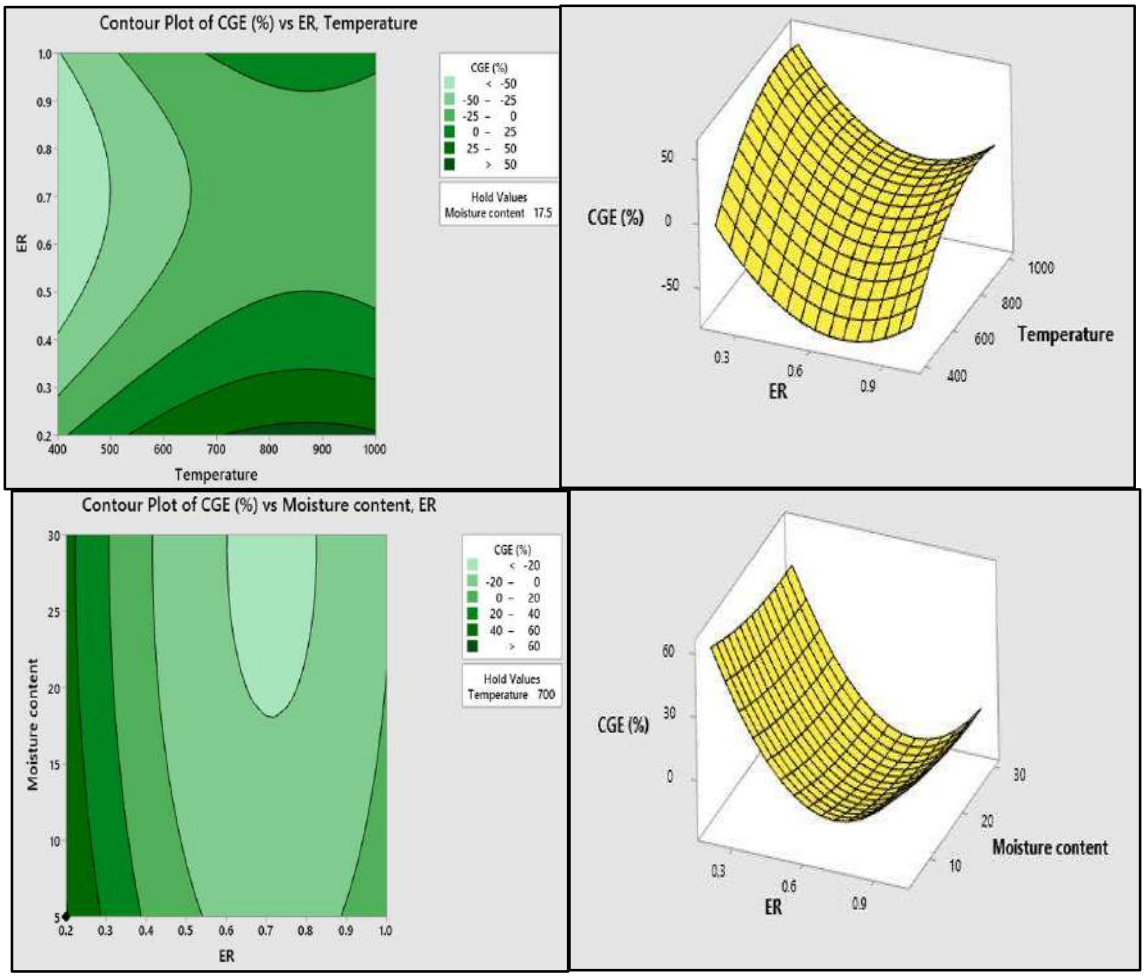

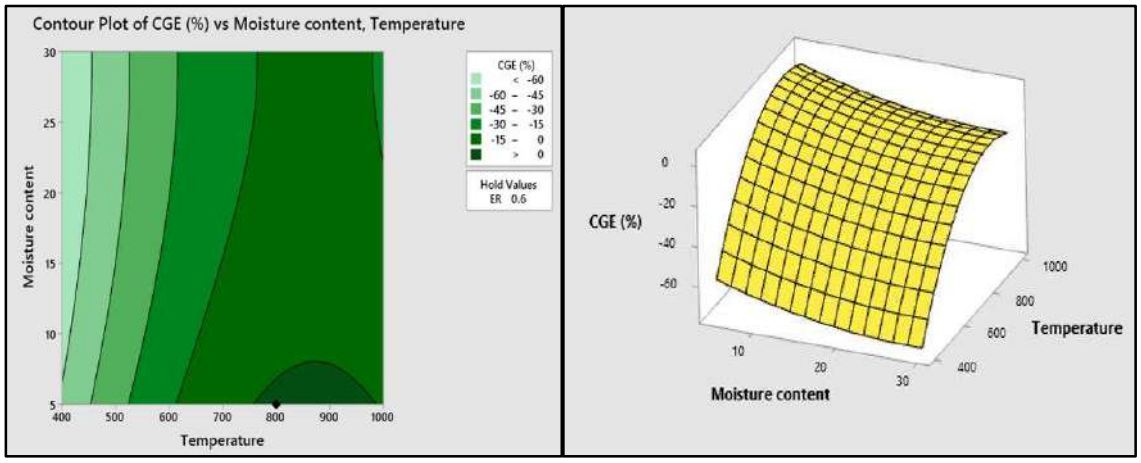

Fig. 4.24. Contour and surface plot of CGE under variable parameters

4.2.12 Simultaneous influence on the higher heating value

The effect of decision variables (temperature, equivalence ratio, and moisture content) on the HHV is depicted in Fig.4.25. The surface plot shows that upsurging the temperature raises the HHV values while upsurging the ER and moisture content decreases it. This may be because the magnitude of hydrogen and CO in the PG composition increases as the temperature rises. It has already been debated. Lahijani et al. published similar findings for HHV [107]. As ER

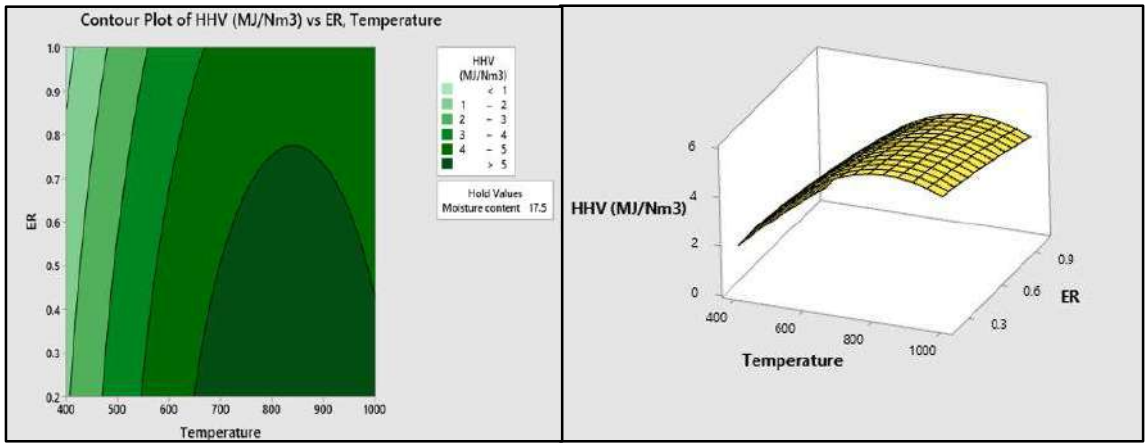

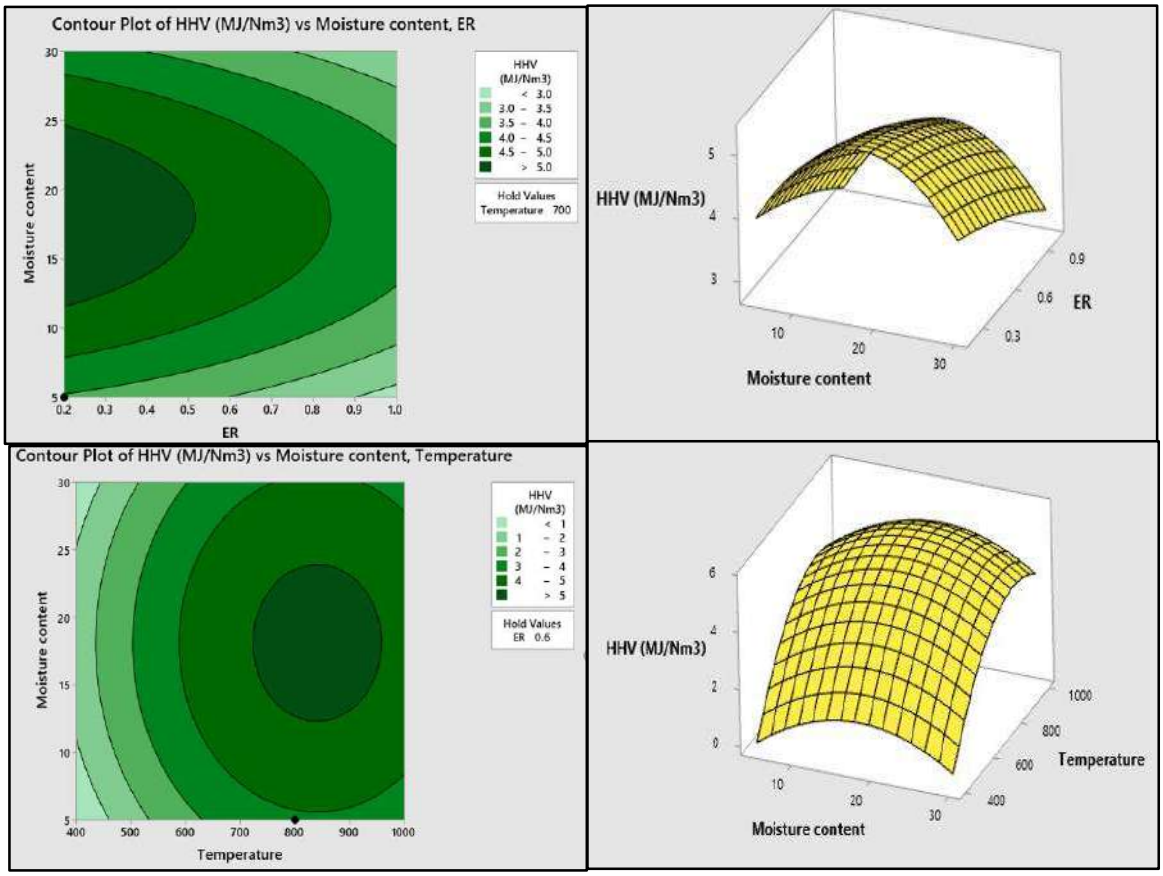

Fig. 4.25. Contour and surface plot of HHV under variable parameters.

rises, HHV declines. It is mostly due to the combustible portion of producer gas began to decline as ER increased, while it decreased due to increased moisture content, as CO and H_2 content decreased as MC increased. Maximum HHV can be obtained in the moisture content range of (0-10) percent. Han et al. discovered a similar downward trend.[92]

4.2.13 Optimal state of decision variables

After running the simultaneous optimization, the optimal output parameters were found. It was obtained from the Minitab software's RSM optimizer module. The lowest value of 0 represents an intolerable response, while the highest value of 1 represents a desirable response. The RSM optimizer is depicted in Fig.4.26, where the optimizer programme generates results. The cumulative composite desirability was found to be about 0.8778, indicating that the cumulative multiple parameters tend to produce a favourable result for all of the responses taken together. H2, CGE, and HHV have ideal values of 0.21, 57.68 percent, and 5.71 MJ/Nm^3 respectively. The temperature, ER, and moisture content are most optimal at 830.30^{0}C, 0.2, and 16.36%. As a result of the current research, it is suggested that animal waste poultry litter pellets can be a viable feedstock for generating power for the rural sector using the gasification technique. The optimization setup is shown in Table 4.16.

Table. 4.16. Optimization setup

Response	Goal	Lower	Target	Importance
HHV (MJ/Nm3)	Maximum	0.54637	6.2593	1
CGE (%)	Maximum	5.66988	68.0034	1
H2	Maximum	0.03413	0.2393	1

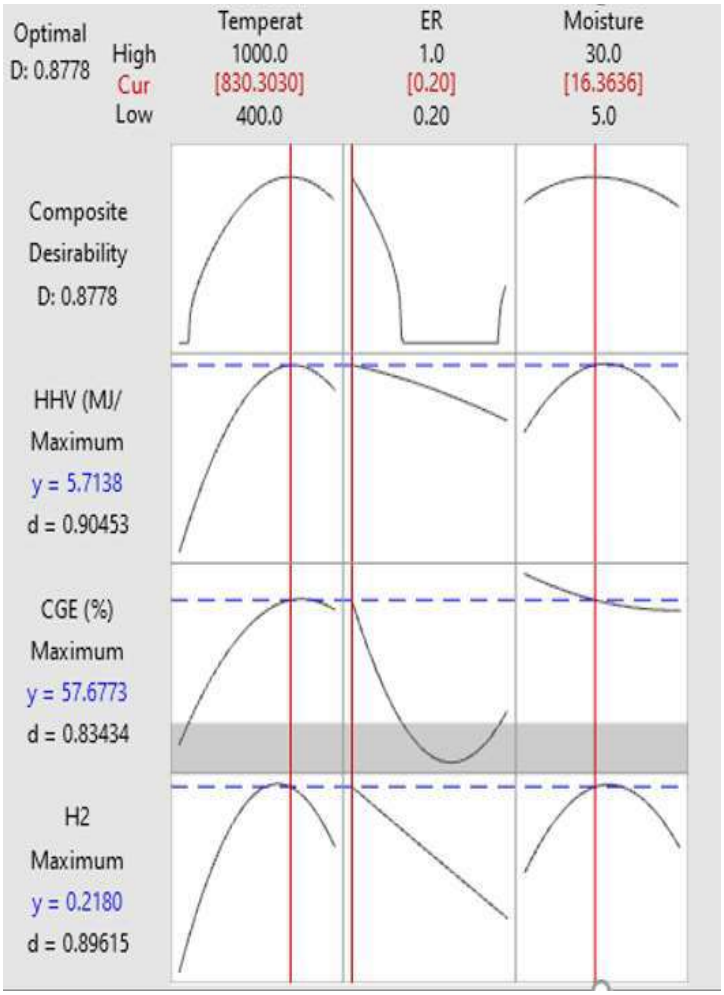

Fig. 4.26. RSM optimizer plot

4.2.14. Summary of the present work

Sensitivity analysis and optimization of waste poultry litter pellet-biomass gasification with Aspen plus and RSM were examined in this work. The model was validated using experimental findings from the literature, and there was a high level of consistency. Temperature, equivalence ratio, and moisture content were employed as independent factors for multi-objective optimization whereas hydrogen yield, CGE, and HHV were used as response variables. The gasifier's optimum operating range was discovered, in which the gasifier produces the best results. The following findings can be drawn from the research conducted in this study:

- The developed model in the present study is capable of predicting producer gas compositions under multiple independent parameteric conditions.
- R^2 value obtained from ANOVA for H_2, CGE, and HHV are 92.26%, 93.2%, and 92.4% respectively
- The optimized independent operating conditions are temperature 830.30^0C, equivalence ratio 0.2, and moisture content 16.36%.
- RSM calculates that the optimized values of responses Hydrogen, CGE, and HHV are 0.21, 57.67%, and 5.71 MJ/Nm^3 respectively.
- Gasification temperature is the most influential parameter in enhancing the H_2, CGE and HHV of syngas followed by equivalence ratio and moisture content.

4.3 Numerical simulation- Gasification of low-density polyethylene waste

This study presents numerical modeling, prediction, and Response Surface Methodology (RSM) based optimization of plastic waste steam gasification. The modeling of the steam-gasification of waste plastic is simulated by Aspen plus simulation tool. Low-density polyethylene waste has been utilised as a feedstock for steam gasification. The model results were validated, and they were found to be in good agreement with the experimental data. The influence of key gasification operating parameters- gasification temperature, equivalence ratio (ER), and Steam/Plastic (S/P) ratio on the syngas composition, cold gas efficiency (CGE), and higher heating value (HHV) have been analyzed. Tar and char concentrations were modelled and their fluctuations with varying temperatures were also quantified.

In the gasification area, it is common that the quality of syngas such as calorific value, tar content, gas composition, and H_2/CO ratio vary with gasification type, gasification operating

conditions, and the properties of the feedstock. Furthermore, for a particular gasification type, optimization of operating conditions plays a significant role in in determining the quality of syngas. However, the combination of Aspen-based gasification results and optimization tools such as response surface methodology (RSM) have not been adequately considered in previous literature works to predict and optimize the input and output parameters. Furthermore, there has been only limited research into plastic waste gasification. Recently, the RSM concept has been successfully applied to determine critical operating conditions and optimize gasification to multiple objective input-output parameters [23],[117], [118], [119, 120]. Hence, this research is aimed to bridge the aforementioned research gaps in a novel way. . The present study includes validation of simulation result with experimental findings, sensitivity analysis and gasification performance prediction and optimization against different performing parameters such as equivalence ratio (ER), temperature (T), and steam to plastic feedstock (S/P) ratio. In addition, the ultimate conclusive results have been made based on the following objectives :-

- To extend the thermochemical equilibrium-based modeling using Aspen plus software to simulate steam gasification using plastic as a feedstock, and validation with reported experimental results.
- To predict, analyze and optimize the impact of equivalence ratios, gasification temperature, and steam to plastic ratio on the composition of the syngas, higher heating value, and cold gas efficiency (%).
- To quantify the magnitude of tar and char concentration with varying reactor temperature.
- To arrange the input-output data according to the response surface methodology and optimize the operating parameters of gasification to the best response of gasification.

- To perform a sensitivity analysis based on Analysis of variance (ANOVA) regression modeling and a Pareto analysis.

4.3.1 Model description

The IDEAL property package was selected for the modeling. The MCINCPSD stream category was chosen due to the presence of another stream category in the procedure. The entire gasification process was modeled using 7 Aspen inbuilt operation blocks in the Aspen plus worksheet. The ASPEN Plus flowsheet is shown in Fig.4.27. Initially, the stream 'WETBIO' was used to discharge raw biomass to the 'DRIER' for pre-drying. The chemical characteristics of 'WETBIO,' a plastic waste, is presented in Table 4.17. Following that, the 'DEMOIST' block is utilized to separate moist and dry air.

The Ryield reactor is used to replicate the gasifier's pyrolysis zone, dubbed "DECOMP." In the model, the pyrolysis yield coefficient is calculated using the FORTRAN algorithm 'PYROCALC.' Air named 'AIR1' and steam designated 'STEAM' are released at the same time. It acts as a gasifing agent in the gasifier 'GASIFICA.' The RGibbs reactor replicates the gasifier's gasification and reduction zones. Finally, the gasification filtration process is mimicked using a splint block of Aspen plus called 'CYCLONE.

Table. 4.17. Proximate and ultimate analysis results of LDPE [121]

Proximate analysis	
Components	**Composition (wt. %)**
Volatile matter	98.85
Fixed carbon	0.57
Moisture	0.01
Ash content	0.57

Ultimate analysis	
Components	**Composition (wt. %)**
Carbon	82.95
Hydrogen	13.54
Nitrogen.	0.07
Oxygen	3.42
Sulfur	0.02

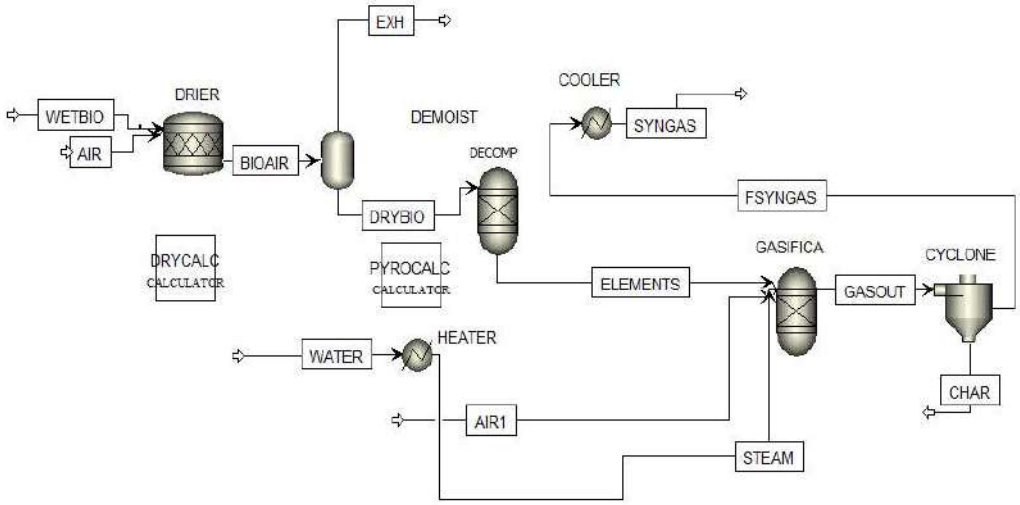

Fig.4.27. Aspen plus flowsheet for steam gasification of plastic waste

4.3.2 Model validation

An Aspen plus model has been developed for the present investigation and was validated by experimental results of Pala et al.[122]. To get the syngas composition, the same operating conditions were used. Fig.4.28 compares the experimental findings with the results obtained by the developed model using the Aspen plus simulator, as well as the data provided by the literature review [122]. The syngas configuration attained by the current study is in good agreement with those obtained by experimental results of Pala et al. [122] as shown in the Fig.4.28.

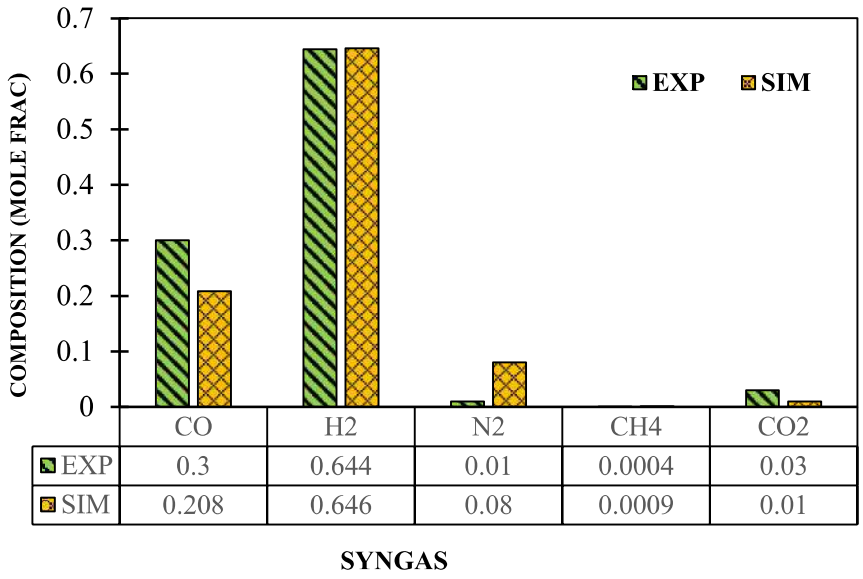

Fig. 4.28. Model validation using food waste

4.3.3 Sensitivity Analysis

A Sensitivity analysis has been applied by the model generated in this work. The investigation's numerous independent operational parameters include the equivalence ratio (ER), gasification temperature, and steam/plastic ratio. The overall heating value of the produced syngas was determined by these factors. For hazardous plastic waste, the effect of gasifier temperature (650-1100)^{0}C, varied equivalency ratios (0.1-1), and variable S/P ratio (0.7-1.2) on syngas compositions, gas yield (GY), CGE, and HHV was investigated.

Equation 9 depicts the calculation for gas yield (GY) [102]

$$GY = \frac{(Qa \times 79\%)}{(Wc \times N_2\ \%)} \tag{9}$$

Cold gas efficiency (%) was calculated by using the following formula (10) [40]

$$CGE(\%) = \frac{LHV(PG)}{LHV(BIOMASS)} \times Y \times 100 \tag{10}$$

$$LHV(PG) = (0.126 \times CO + 0.108 \times H_2 + 0.358 \times CH_4) \tag{11}$$

Equation 12 depicts the expression for predicting the HHV of PG. [102]

$$HHV(PG) = \left((CO\% \times 3018 + H_2\% \times 3052 + CH_4\% \times 9500) \times 0.01 \times 4.1858\right) \quad (12)$$

4.3.4. Influence of temperature on Producer gas composition

Temperatures in the reactor ranged from 650 to 1100^{0}C. The effect of reactor temperature on the composition of the producing gas is seen in Fig.4.29

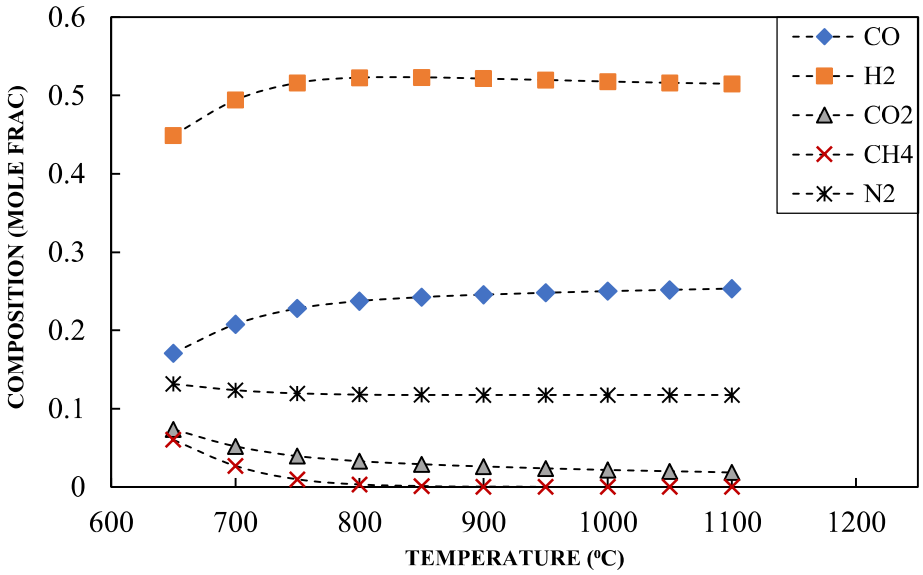

Fig.4.29 Influence of temperatures on syngas compositions for Plastic waste

The temperature at which syngas is gasified has the greatest impact on its heating value. Because some gasification processes need particular temperatures. The temperature was changed between 650^{0}C to 1100^{0}C in this investigation, while the ER and steam/plastic ratios were kept constant at 0.1 and 1, respectively. Fig.4.29 depicts the composition of the PG with varying temperature. It can be inferred from the Fig.that increasing the gasification temperature increases the magnitude of CO and H_2 content in the syngas. It might be due to the exothermic nature of the water gas shift process. As a result, increasing the temperature encourages water gas shift reaction, resulting in an increased concentration of H_2 in the syngas composition. These findings are consistent with prior research. [123]. The increase in the water gas shift

reaction owing to steam injection causes an increase in the magnitude of hydrogen content in the PG. It can be concluded from the Fig.that higher temperature raises the heating value of syngas as it enhances the hydrogen as well as CO concentration in the syngas composition. Other components like nitrogen, CO_2 show an inverse relationship with increasing gasification temperature. The simulation in ASPEN PLUS software was selected according to the inbuilt IDEAL property technique, where the concentration of CH_4 was underestimated,. Because there is a discrepancy between an actual gasification system and an ideal reactor at chemical equilibrium, calculations must make assumptions.[92, 99]. The assumption of the ideal property package used to simulate the real gasifier, as well as uncertainty in the pyrolysis yield coefficients, might be blamed for the underpredictions [124]. Furthermore, by running the gasifier at a temperature lower than 800^0C, these underpredictions may be avoided, and the uncertainty in the pyrolysis yield coefficients can be decreased by utilizing a more powerful supercomputer.

4.3.5. Influence of equivalence ratio (ER) on syngas composition

The equivalence ratio (ER) is defined as the ratio of the actual air-fuel ratio to the stoichiometric air-fuel ratio [108]. It is one of the study's most persuasive parameters. ER was modulated from (0.1-1) by varying the biomass feed rate while maintaining a constant temperature of 900^0C.

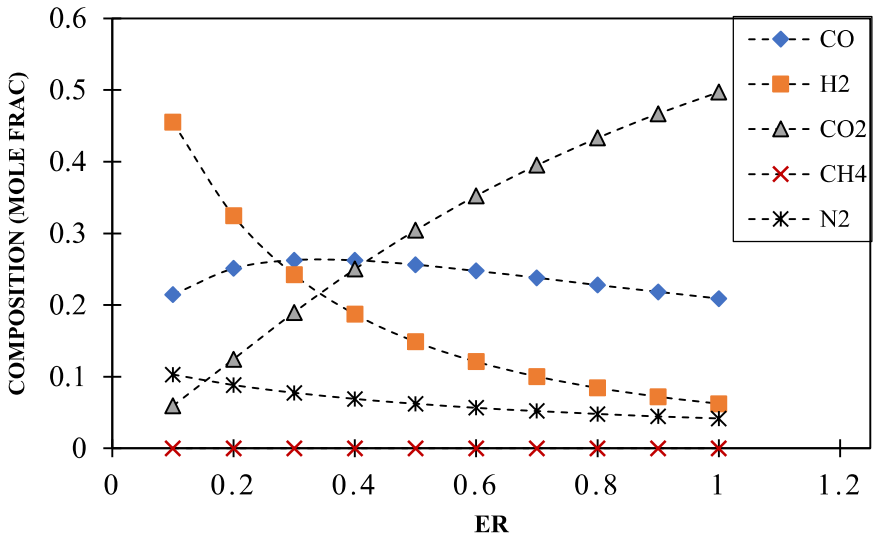

Fig.4.30 Influence of ER on syngas compositions for Plastic waste.

Fig.4.30 shows that the hydrogen concentration drops from 45.5% at ER 0.1 to 6.24 % at ER 1. As the ER rises, the magnitude of CO content reduces as well. The magnitude of the CO content decreases as ER grows. This reduction may be explained by the fact that as the ER increases, so does the quantity of O_2 supplied to the reactor, boosting the carbon alteration of the fuel but oxidizing it more. As a result, the amount of CO and H_2 in the atmosphere drops. CO_2 concentrations rise, as indicated in the graph. It is because a more complete combustion has begun. The amount of shift in CH_4 is judged to be modest as ER increases. The ER results obtained from this model follow the same pattern as those obtained from previous research works [109]. Han et al. stated that the concentration of H_2 decreases from 23.40% at 0.2 to 9.830% at 0.45 with the increased ER [92]. It can be inferred from Fig.4.30 that CO_2 content increases in the syngas as the ER increases. It is due to the increased amount of air coming into the gasifier. It can be inferred from the Fig.that lower ER favours the heating value of syngas.

4.3.6. Influence of steam/plastic on syngas composition

By employing steam as the gasifying agent, the amount of H_2 in the syngas can be increased. [125]. The SPR (steam to plastic ratio) shifted from 0.7 to 1.2, while the temperature of the

gasification and ER were maintained at 800^{0}C and 0.1, respectively. Fig.4.31 depicts the syngas variation as a function of variable SPR. The main cause of enriched H_2 concentration in the syngas is a rise in water vapor partial pressure inside the reactor, which causes the water-gas-shift and steam reforming reactions to increase. [126]. Apart from that, the presence of steam in a gas-phase process causes hydrocarbon breakdown and an increase in the magnitude of H_2 and CO_2 [86]. In the literature, a similar trend of the result was found [127].

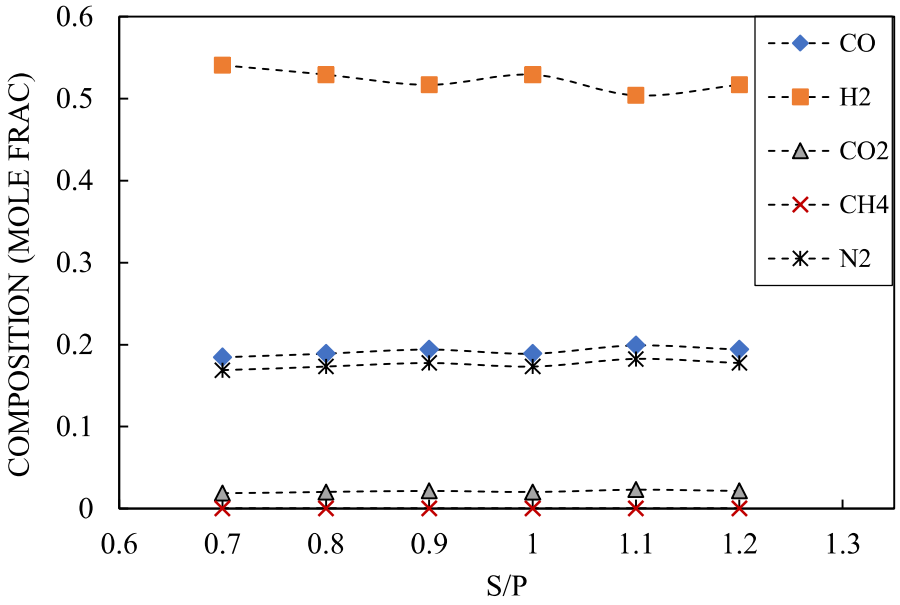

Fig.4.31. Influence of S/B on syngas compositions for plastic waste

4.3.7 Influence of reactor temperature on Tar and Char production

The overall response of the gasification scheme is written as equation 13 [128]

$$\mathrm{CH_aO_b} + w\mathrm{H_2O} + n_{\mathrm{O_2}}(\mathrm{O_2} + 3.76\mathrm{N_2}) \rightarrow n_s \cdot (x_1\mathrm{H_2} + x_2\mathrm{CO} + x_3\mathrm{CO_2} + x_4\mathrm{H_2O} + x_5\mathrm{CH_4} + x_6\mathrm{N_2}) + n_{\mathrm{tar}}\mathrm{C_6H_6} + n_{\mathrm{char}}\,\mathrm{C} \quad (13)$$

where w is the molar moisture content in mol/mol and n is the equivalent substance's molar production in mol/mol. Syngas is denoted by the subscript ‘s’. Dalton's law limits the molar fraction of comparable gaseous components of syngas and is denoted by equation 14.

$$\sum_{i=1}^{6} x_i = 1 \quad (14)$$

By using mass balance from equation 13, following balance can be obtained equation (15-18) The concentrations of tar and char produced can be quantified using equation (19-20)

$$n_{\text{char}} = 0.099 - 0.439 \cdot (1 - e^{-ER+0.0003 \cdot T_r}) \quad (19)$$

$$n_{\text{tar}} = 0.3598 \cdot e^{-0.00298 \cdot T_r} \cdot \left(12 + a + 16b + 18w + 32n_{O_2} + 3.76 \cdot 28 \cdot n_{O_2}\right)/78 \quad (20)$$

In addition, the energy balance can also be obtained from the global reaction scheme [128] :

$$H^0_{f,\text{bio}} + w\left(H^0_{f,H_2O(1)} + H_{\text{vap}}\right) + n_{O_2}\left(H^0_{f,O_2} + 3.76H^0_{f,N_2}\right) + \Delta Q = n_s \sum x_i H^0_{f,i} + n_{\text{tar}} H^0_{f,C_6H_6} + n_{\text{char}} H^0_{f,C} + \int_{T_{\text{amb}}}^{T_r} \left(n_s \sum x_i c_{p,i} + n_{\text{tar}} c_{p,C_6H_6} + n_{\text{char}} c_{p,C}\right) \quad (21)$$

Hf^0 denotes the heat of formation in kJ/mol. Biomass feedstock is denoted by the subscript 'bio'. The vaporization heat of water is represented as $H_{va}r$. The heat input to the gasifier is denoted by Q. The temperatures of the reduction zone of the gasifier and the ambient are T_r and T_{amb}, respectively. The influence of T_{amb} is usually ignored. In this study, T_{amb} is considered to be 298 K.The characteristics of biomass feedstock, *i.e.,* a, b, and w, in the preceding equations, are dictated by the kind of biomass feedstock, which may be considered as known parameters. Variation of the concentration of tar and char with varying temperatures is shown in **Fig.4.32**. The ER is taken as 0.2 for the variation of temperature in the present study. It can be inferred from the Fig.that the magnitude of tar content decreases as the temperature increases form 600^0C to 1100^0C. This might be due to the initiation of enhanced thermal cracking as the temperature rises inside the reactor. Due to the thermal cracking phenomena, heavy hydrocarbon is cracked down to smaller hydrocarbon and thus, the concentration of tar content gets reduced. Fig.4.32 shows the magnitude of char concentration increases as temperature

rises. It is because of the improved combustibility at higher temperatures resulting in more complete burning of plastic waste.

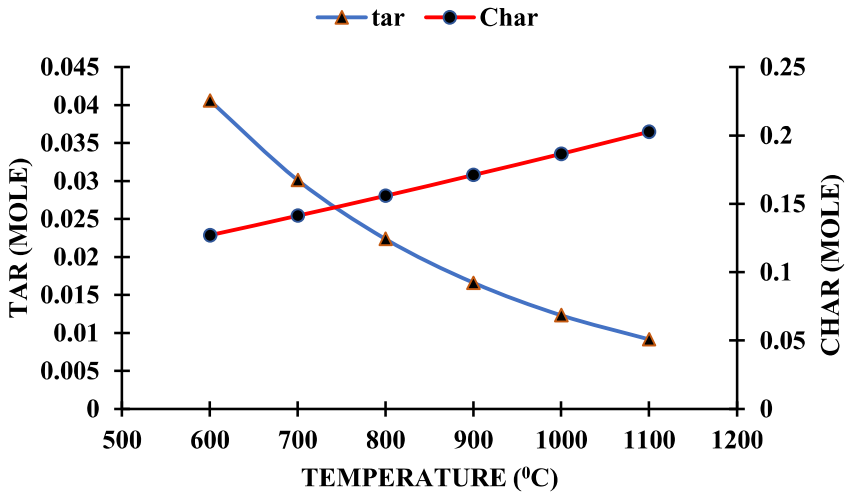

Fig.4.32. Variation of tar and char with varying temperature

4.3.8 Regression analysis

For the investigation, three variable operational parameters were chosen: reactor temperature, ER, and S/P. H_2 and CO concentration, CGE, and HHV are the four output responses. **Table 4.18** shows the expected design plan as well as the computed response values. Because the two-way interaction term was insignificant, it was left out of the calculations. The developed regression equation for predicting H_2 concentration using ANOVA is given in the following correlations :

H_2 = 2.28 - 0.00124 Temperature - 1.656 ER - 2.02 S/P + 0.000001 Temperature× Temperature + 0.973 ER ×ER + 1.016 S/P ×S/P (22)

CGE = -270 - 0.126 Temperature - 11.8 ER + 804 S/P + 0.000091 Temperature ×Temperature+ 8.2 ER ×ER - 418 S/P × S/P (23)

HHV = 17.0 – 0.0082 Temperature – 18.45 ER – 4.3 S/P +0.000006 Temperature ×Temperature + 9.70 ER ×ER + 2.0 S/P×S/P (24)

Table. 4.18. Design matrix plan along with the responses

Trial	Temperature	ER	S/P	CO	H_2	CGE %	HHV (MJ/Nm^3)
1	650	0.2	1	0.170918	0.449064	60.50869	7.896357638
2	700	0.2	1	0.207815	0.494208	73.07749	8.939230379
3	750	0.2	1	0.228062	0.516309	80.2253	9.4773804
4	800	0.2	1	0.237536	0.523001	83.11004	9.682567008
5	850	0.2	1	0.242426	0.523285	84.07927	9.747967482
6	900	0.2	1	0.245618	0.521717	84.41259	9.7682688
7	950	0.2	1	0.248068	0.519809	84.54689	9.774834417
8	1000	0.2	1	0.250088	0.517984	84.61441	9.777042006
9	1050	0.2	1	0.251803	0.516346	84.65644	9.777775008
10	1100	0.2	1	0.25328	0.514901	84.68695	9.777979293
11	900	0.1	1	0.214323	0.455054	67.71282	8.521237049
12	900	0.3	1	0.262625	0.24207	69.88591	6.410436857
13	900	0.4	1	0.262313	0.18707	70.56768	5.703844517
14	900	0.5	1	0.256293	0.148701	71.09528	5.137595542
15	900	0.6	1	0.247645	0.120938	71.51442	4.673660911
16	900	0.7	1	0.237946	0.100233	71.85474	4.286605651
17	900	0.8	1	0.228013	0.084396	72.13618	3.958778808
18	900	0.9	1	0.218268	0.07202	72.37257	3.677548629
19	900	1	1	0.208922	0.062169	72.57378	3.433637277
20	900	0.2	0.7	0.184282	0.54077	54.88739	9.236797706
21	900	0.2	0.8	0.188945	0.529106	53.09022	9.146690577
22	900	0.2	0.9	0.193831	0.516802	51.28029	9.051237866
23	900	0.2	1.1	0.198956	0.503807	49.45737	8.949949141
24	900	0.2	1.2	0.193831	0.516802	51.28029	9.051237866

4.3.9 Pareto Chart

The Pareto chart shows the influence of multiple independent parameters in predicting the output response. It can be inferred from **Fig.4.33** that hydrogen concentration in the syngas is mainly influenced by the equivalence ratio and its square term whereas all other operating parameters are insignificant. It may be because the equivalence ratio controls the amount of air inside the reactor. Cold gas efficiency is mainly influenced by the square term of the S/P ratio followed by temperature and is least affected by the ER. It can be inferred from the Pareto chart of higher heating value that HHV is mainly affected by the ER and least affected by the SP

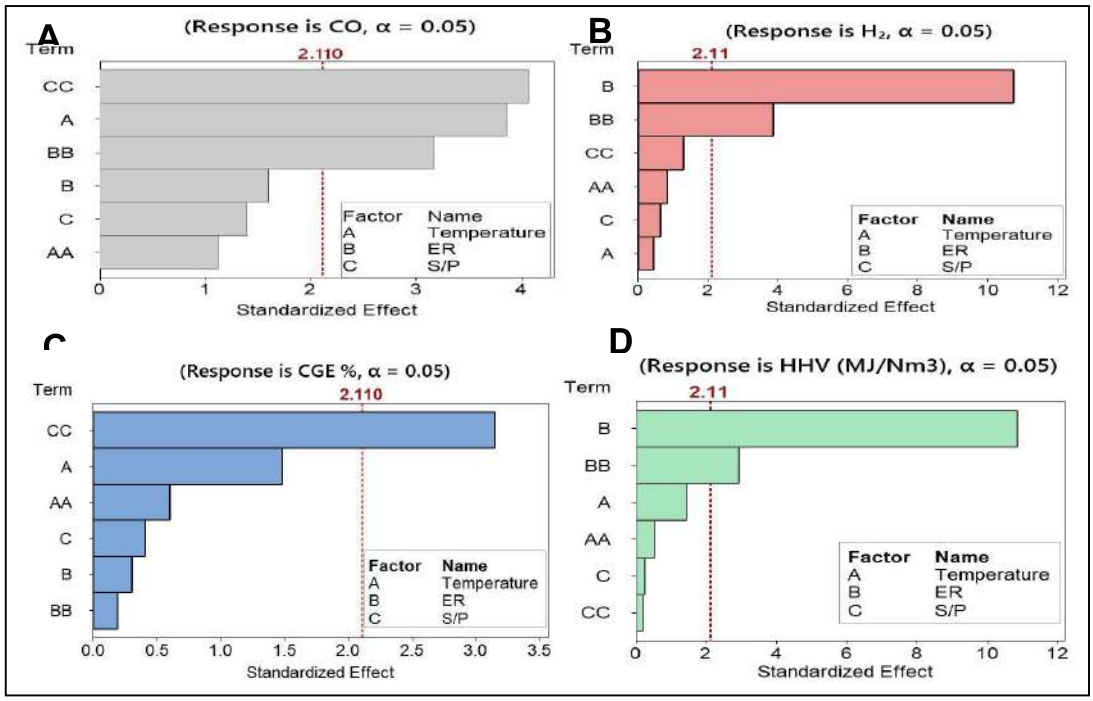

4.3.10 ANOVA results

Tables 4.19 and **4.20** summarise the results of the ANOVA analysis for CO concentration, H_2 yield, CGE, and HHV, respectively. The F-value represents the statistical significance of the model, as well as its components and interactions, in the table. The larger the F-factor, the more important the factors' effect on the response variables is. If the magnitude of the P-value is more than 0.05, it is considered unimportant [110]. It can be inferred from the table 4.19 that

the CO concentration in the syngas is primarily influenced by the reactor temperature followed by the equivalence ratio and the S/P ratio. It might be due to the exothermic nature of the water-gas-shift process. As a result, increasing the temperature encourages the water-gas shift reaction, resulting in an increased concentration of CO in the syngas composition. The H_2 concentration is mainly affected by the ER followed by S/P and least affected by the temperature. This is mainly because ER controls the magnitude of air inside the reactor that eventually affects the water-gas-shift reaction. While predicting the CO concentration in the PG, all operating parameters are significant except ER. It is evident from **Table 4.19** that temperature is insignificant for predicting H_2 concentration in the syngas as the P-value of temperature is greater than 0.005

Table 4.19. ANOVA analysis of CO and H_2 concentration.

		CO		**H_2**	
Source	**DF**	**F-Value**	**P-Value**	**F-Value**	**P-Value**
Model	6	8.06	0	35.26	0
Linear	3	6.16	0.005	39	0
Temp	1	14.86	0.001	0.2	0.658
ER	1	2.53	0.13	115.32	0
S/P	1	1.95	0.181	0.39	0.541
Square	3	9.89	0.001	6.23	0.005
Temp × Temp	1	1.24	0.28	0.7	0.416
ER*ER	1	9.99	0.006	14.92	0.001
S/P × S/P	1	16.5	0.001	1.67	0.214
Error	17				
Total	23				

It can be inferred from **Table 4.20** that CGE is mainly affected by the temperature followed by the S/P ratio and least affected by the ER. This is because CGE is directly proportional to the

CO concentration in the syngas, which ultimately rises due to an increase in reactor temperature. It can be concluded from the table that the S/P ratio is insignificant for predicting the cold gas efficiency of the engine. It is because the P-value of CGE which is larger than the desired magnitude. The higher heating value of the syngas is mainly dependent on the ER and least affected by the S/P plastic. P-value of HHV suggests that temperature is insignificant in predicting HHV of PG.

Table 4.20. ANOVA analysis of CO and H_2 concentration.

		CGE		**HHV**	
Source	**DF**	**F-Value**	**P-Value**	**F-Value**	**P-Value**
Model	6	2.53	0.062	31.14	0
Linear	3	0.8	0.005	39.8	0
Temp	1	2.21	0.001	2.08	0.167
ER	1	0.09	0.007	117.67	0
S/P	1	0.17	0.006	0.06	0.812
Square	3	4.2	0.021	3.16	0.052
Temp × Temp	1	0.36	0.556	0.27	0.61
ER × ER	1	0.04	0.849	8.58	0.009
S/P × S/P	1	9.92	0.006	0.04	0.847
Error	17				
Total	23				

4.3.11 Parametric impact of multiple independent parameters using 3-D surface plot

The optimization of a gasifier's variable operating parameter has a significant impact in achieving a high gasification efficiency. It is extremely difficult for industries to achieve and maintain the gasifier's single operational design value. The contour plot can help to clarify this flaw. The contour map indicated the gasifier's optimal operating range, within which the industry should operate to achieve the higher heating value of producing gas. The 3-D surface

map shows the parametric impact of various operational parameters at the same time. These graphs aid in fully comprehending the behavior of output response when operational parameters are varied at the same time.

4.3.12 CO concentration

Fig.4.34a shows a surface plot of CO concentration corresponding to (Temperature, ER), (ER, S/P), and (Temperature, S/P). It may be inferred from the surface plot that CO concentration rises at higher temperatures and lower equivalence ratio. This could be because of the exothermic nature of the water-gas-shift process. This reaction is enhanced at a higher temperature which leads to higher CO yield in syngas composition. At higher CO content in the PG increases the heating value of syngas. The values were held constant for the CO concentration in the surface plot temperature 875^{o}C , ER 0.55, and S/P 0.95. The SPR should be around 1 for maximizing the CO concentration.

4.3.13 H_2 concentration

Fig.4.34b shows a surface plot of hydrogen yield corresponding to (Temperature, ER), (ER, S/P), and (Temperature, S/P). When ER and temperature are varied simultaneously, the greatest concentration of H_2 is found at ER 0.1 to 0.2 and in the temperature range from 650 to 800 ^{o}C . When ER and S/P are both changed at the same time, the maximum concentration is determined to be between 0.1 and 0.2 for ER and 0.7 to 1.1 for S/P. The parametric impact of several operational parameters is depicted by a surface plot for the H_2 concentration. Lower ER and lower temperature enhance the quantity of hydrogen concentration in the syngas composition, as seen in Fig.4.34B. The temperature 875^{o}C, ER 0.55, and S/P 0.95 were used as the hold values for the surface plot of hydrogen concentration.

4.3.14 Cold gas efficiency

The consequence of decision variables on cold gas efficiency is depicted in **Fig.4.34C**. CGE is described as the ratio of syngas's lower heating value to the biomass's lower heating value multiplied by gas production. The surface plot shows that when the temperature rises, the cold gas efficiency rises as well. When ER and temperature are both changed at the same time, the maximum magnitude of CGE is attained at ER of 0.1 to 0.2 and temperatures of (900 to 1100)^{0}C . The ER and CGE have an inverse relationship. This could be related to a reduction in gas yield when the ER rises. As the S/P ratio rises, the cold gas efficiency (CGE) rises as well. When ER and S/B are both changed at the same time, the highest CGE is attained when the ER is between 0.1 and 0.2 and the S/P ratio is between 1 and 1.2. This could be because as the S/P ratio rises, the heating values of syngas rise as well. In **Fig.4.34C**, the surface plot of CGE for (Temperature, ER), (ER, S/P), and (Temperature, S/P) are shown. **Fig.4.34C** shows that a lower ER, an S/P ratio of approximately 1, and a higher temperature enhance the magnitude of CGE in the syngas composition.

4.3.15 Higher heating value

Fig.4.34D shows the HHV surface plot corresponding to (Temperature, ER), (ER, S/P), and (Temperature, S/P). When ER and temperature are both varied simultaneously, the maximum magnitude of HHV is attained at ER 0.1 to 0.2 and a temperatures range from 750^{0}C to 900^{0}C. When ER and S/P are both changed at the same time, the greatest concentration is found when ER is between 0.1 and 0.2 and S/P is between 0.6 and 1.2. The parametric impact of numerous operating parameters is depicted by a surface plot for the HHV concentration. Lower ER and greater temperature enhance the value of the HHV of syngas, as seen in Fig.4.34D.

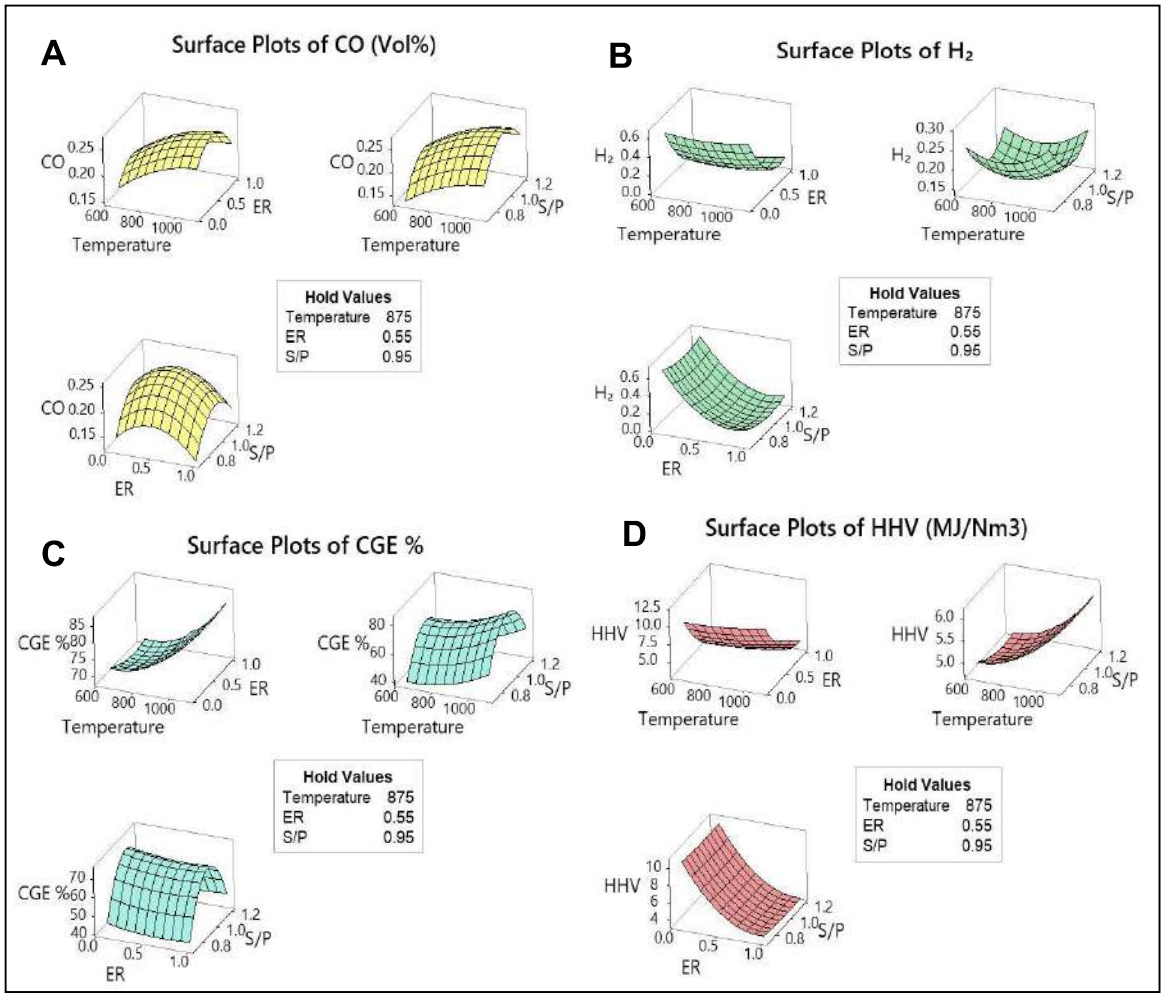

Fig.4.34. Surface plot of A-CO, B-H_2, C-CGE, D-HHV under variable parameters

4.3.16 Multi-objective optimization

The major goal of this research was to find the operating parameters with the best output response. The RSM optimizer is shown in **Fig.4.35**, and the optimizer program setup to generate the results. The observed cumulative composite desirability was 0.9064, indicating that the optimization magnitude was efficient in comparison to the intended value. CO, H_2, CGE, and HHV have optimum magnitudes of 0.24, 0.51, 80.61%, and 9.7 MJ/Nm^3, respectively. 1023.43°C, 0.18, and 0.98 are the best optimal operating independent parameters for temperature, ER, and S/P. As a consequence of this study, it is recommended that hazardous plastic garbage might be a viable feedstock for using steam gasification to generate power for the rural sector.

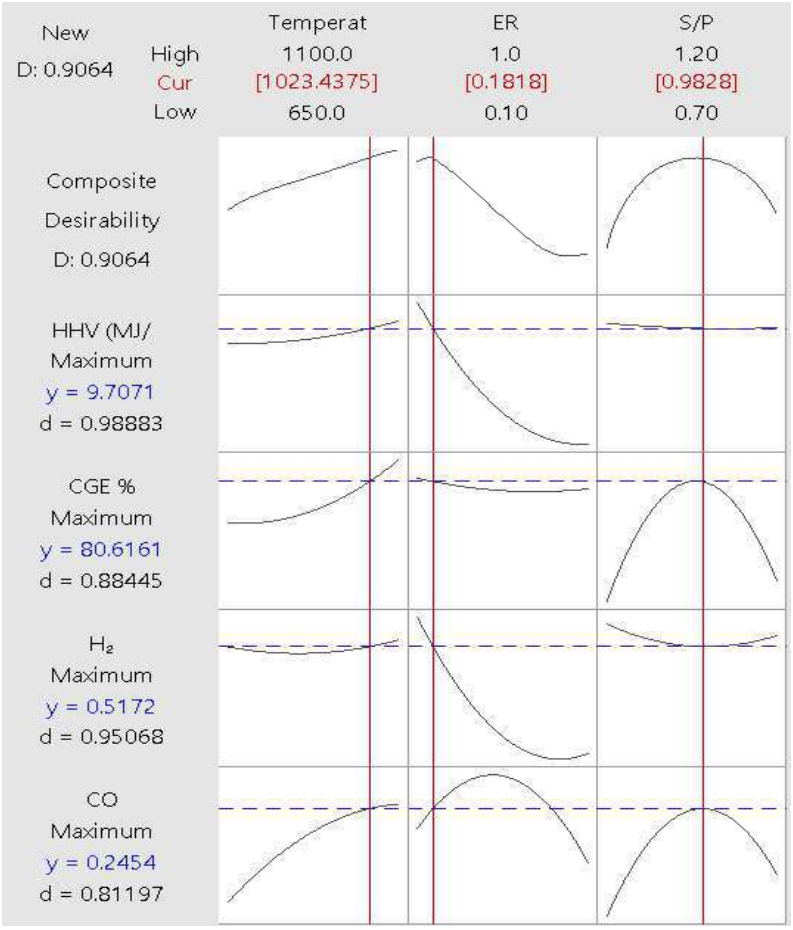

Fig.4.35. RSM optimizer plot

4.3.17. Summary of the present work

This study used hazardous plastic waste to undertake predictive modeling and multi-objective optimization of several gasification performance parameters of steam injected biomass gasifier by combining ASPEN Plus and Response surface methodology (RSM). The model was successfully validated using experimental results from the literature, and there was a high level of agreement. For multi-objective optimization, temperature, equivalence ratio, and S/P were used as independent factors, while CO concentration, hydrogen yield, CGE, and HHV were used as response variables. The gasifier's ideal operating range, in which it produces the best results, was identified. CO- gasification can be the future study of the present work [129]. From the current study, the following findings may be concluded.

- The model established here can forecast syngas compositions and gasifier performance under a variety of different operating conditions.
- Temperature 1023.43^{0}C, equivalence ratio 0.18, and S/P 0.98 are the optimal independent working parameters.
- The ideal values of responses CO, H_2, CGE, and HHV, according to the RSM optimizer, are 0.24, 0.51, 80.61%, and 9.7 MJ/Nm^3, respectively.
- The amount of tar produced shows a direct relationship with temperature whereas char content shows an inverse relationship with increasing temperature.
- The most important factor in increasing syngas CGE is gasification temperature, followed by S/P and ER.

4.4 Modelling of Steam injected Plasma Gasifier

The COVID-19 Pandemic has a detrimental effect on the environment related to the exponential rise in medical waste (MW). Extraction of energy from the toxic MW with the latest gasification technology instead of conventional incineration is of utmost importance to promote sustainable development. This present study investigates the processing of MW for the generation of enriched hydrogen syngas using steam injected plasma gasifier. Modeling of Plasma gasifier was performed in Aspen Plus and Model validation was done with the experimental result and, a good agreement was attained. Sensitivity analysis was implemented on MW in which the influence of gasification temperature, equivalence ratio (ER), and Steam/Biomass (S/B) on the producer gas (PG) composition, gas yield, H_2/CO ratio, cold gas efficiency (CGE), and the higher heating value (HHV) was calculated. Furthermore, Response surface methodology (RSM) has been incorporated for the multi-objective optimization of the variable gasification parameters

4.4.1 Model description

The property package opted for the modeling is the IDEAL property. MCINCPSD stream category was chosen because of the existence of a different category of streams in the process. Fig.4.36 depicts the ASPEN Plus flowsheet. Initially, The stream 'WETBIO' was the raw biomass that was discharged to 'DRIER' for the pre-drying operation. Table 4.21 depicts the chemical properties of 'WETBIO' which is the toxic biomedical waste. Hereafter, the 'DEMOIST' block is used to segregate wet air from the dried air.

Ryield reactor is used to simulate the pyrolysis zone of the gasifier namely 'DECOMP'. Pyrolysis yield coefficient is determined using FORTRAN code namely 'PYROCALC' in the model. At the same instant air named 'AIR1' and steam named 'STEAM' flows are discharged in the heat exchanger called 'PLATORCH'. This heat exchanger is responsible for the

simulation of the plasma arc. The output of 'PLATORCH' is the plasma flow carried by stream 'PLASMA'. It enters into the gasifier 'GASIFICA' as the gasification agent. RGibbs reactor simulates the gasification and reduction zone of the gasifier. Finally, the filtration process of gasification is simulated using sspilt block of Aspen plus namely 'CYCLONE'

Table.4.21. Chemical properties of Medical waste

Ultimate analysis (wt. %)	Medical waste [130]
Carbon	48.99
Hydrogen	7.2
Nitrogen.	0.22
Oxygen	43.52
Sulfur	0.08
Proximate analysis (wt. %)	
Volatile matter	82.37
Fixed carbon	8.7
Moisture	7.04
Ash	1.89

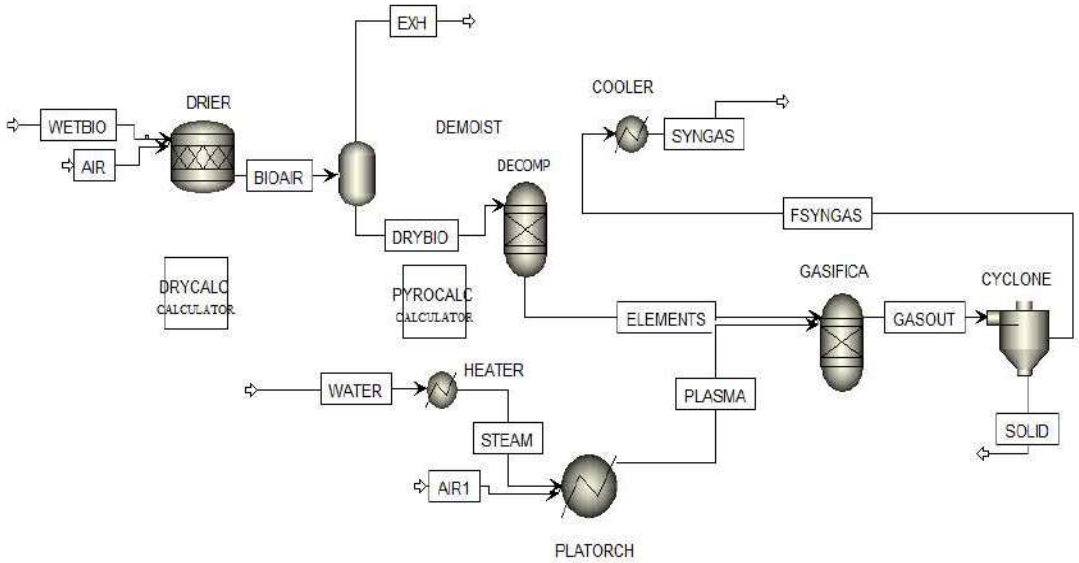

Fig. 4.36. Aspen plus flowsheet

4.4.2 Model validation

Aspen plus model developed in the present study was validated by the experimental investigation performed by Diaz et al. [131]. The same operating condition was employed to attain the syngas composition. Fig.4.37 depicts the values obtained by the developed model using Aspen plus simulator and compared it with the experimental values from the literature [131]. It can be inferred from the Fig.that the syngas composition acquired by the present investigation depicts good agreement with those attained experimentally by Diaz et al. [131]. Model was also validated with the result obtained by Janajreh et al. [132] using Municipal solid waste (MSW). The MW includes 54% paper, 20% textile, 26% organic, 50% plastic, 10% metal-containing, and 15% glass-containing wastes.

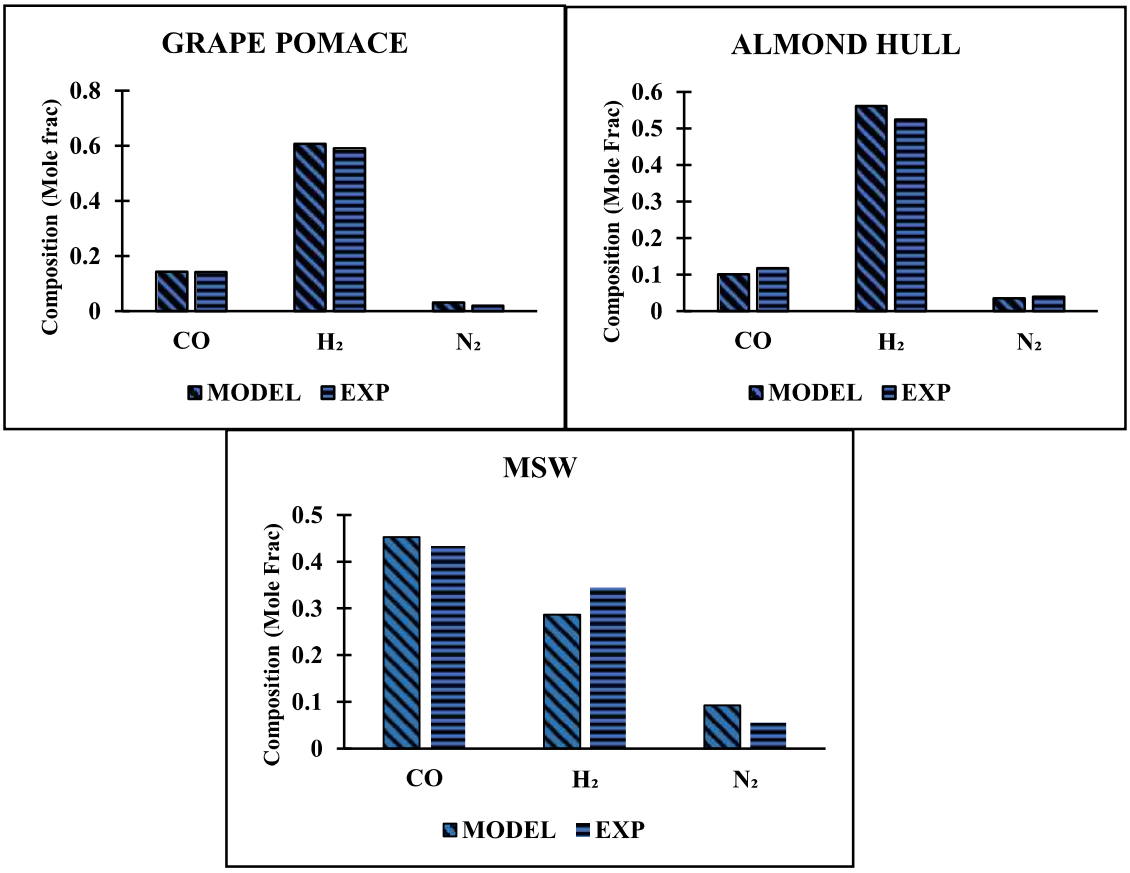

Fig. 4.37 Comparison of experimental and theoretical result on the syngas composition

That's why model was also validated with MSW. It can be inferred from the model validation curve of MSW that present model is well capable of predicting syngas composition of waste medical waste.

4.4.3 Sensitivity Analysis

The developed model performed sensitivity analysis. The gasification temperature, equivalence ratio (ER), and steam/biomass ratio have opted as the multiple independent operating parameters for the investigation. These parameters decided the overall heating value of generated producer gas. Therefore, the influence of gasifier temperature (1500-3000)^{0}C, variable equivalence ratios (0.1-0.5), and variable S/B ratio (0.4-1.4) on the syngas compositions, gas yield (GY), H_2/CO ratio, CGE, and HHV has been scrutinized for toxic medical waste.

4.4.4. Influence of temperature

The reactor temperatures were speckled from 1500^{0}C to 3000^{0}C. The effect of reactor temperature on the composition of the producing gas is seen in the Fig. 4.38

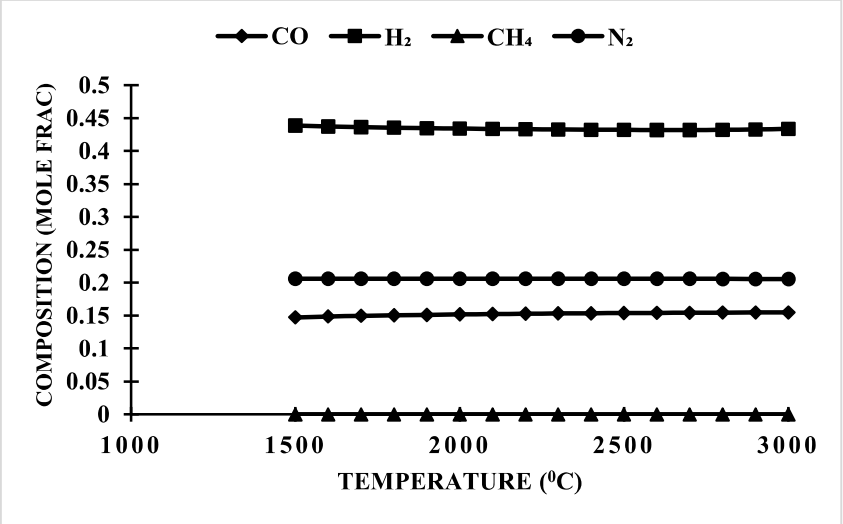

Fig. 4.38. Influence of temperatures on syngas compositions for Medical waste

Gasification temperature is the most influential parameter for enhancing the heating value of syngas. It is because some gasification reactions demand specific temperatures. In the present study, the temperature was varied between 1500^{o}C to 3000^{o}C with a step size of 100^{o}C keeping ER and Steam/biomass ratio constant at 0.1 and 1 respectively. Tavares et al. [133] simulated the plasma gasification using municipal solid waste. They reported that the magnitude of syngas composition (CO and H_2) lies between 0.24 to 0.3 and 0.35 to 0.3 respectively by varying the temperature between 1000^{0}C to 2500^{0}C whereas our present model predicts that the magnitude of syngas composition (CO and H_2) lies between 0.15 to 0.2 and 0.45 to 0.4 respectively by varying the temperature between 1000^{0}C to 3000^{0}C. Fig.4.38 depicts the variations of producer gas composition with variable temperature. It can be inferred from Fig.4.38 that upsurging gasification temperature upsurges CO content in the syngas whereas it depicts opposite relation for H_2 concentration. It may be attributed to the fact that the water shift reaction is exothermic. Therefore, a higher magnitude of temperature does not favor reaction which eventually leads to the lower concentration of H_2 in the syngas composition. These results are following the previous literature [123]. An increase in the magnitude of hydrogen content in the PG is due to the increase in the water gas shift reaction due to steam injection. Inbuilt IDEAL property method was preferred for the simulation in present Aspen Plus Software. It was observed from the simulation result that the concentration of CH_4 was underestimated. It is because of a difference exists between a real gasification system and an ideal reactor at chemical equilibrium [92, 99]. These underpredictions can also be attributed to the assumption of the ideal property package used to model the real gasifier and uncertainty in the pyrolysis yield coefficients. [124]. In addition to this, these under prediction can be overcome by running the gasifier at a temperature lower than 800^{0}C, and uncertainty in the pyrolysis yield coefficients could be reduced by using enhanced super computing device. Besides, prediction of tar, char, and HC can be also be obtained using Aspen plus in future.

Pan et al.[134] have have depicted methodology and predicted the methane concentration in a producer gas composition to a desirable level. They were able to eliminate the constraint of unpredictability of methane by modelling solid oxide electrolyzer cell (SOEC) and methanation unit using Aspen plus. Where, the SOEC unit electrolyzes water to produce H_2, which is necessary for increased CH_4 output in the producer gas composition.

The simulated results for gas yield and H_2/CO against temperature are depicted in Fig.4.39. It can be inferred from the plot that the gas yield rises with a temperature rise. This may be due to the following reason (i) Initial pyrolysis rate was promoted at a higher temperature which increases the product gas yield (ii) Rate of steam reforming and cracking get enhance at elevated temperature and (iii) endothermic reaction of char gasification gets improved at high temperature [113]. A similar trend of gas yield production was attained by Lahijani et al. [107]. They stated that an increase in bed temperatures enhances the dry gas yield by 50% by sawdust and EFB (empty fruit bunch). H_2/CO ratio decreases as the temperature increases. It is due to a higher rate of increase of CO than H_2 with increasing temperature. Results obtained for H_2/CO from our model were following the result acquired by Han et al. [92]. The fluctuation of CGE and HHV with reactor temperature is seen in Fig.4.40. The CGE percentages provided in the literature were extremely close to the results derived from our model for CGE values [115]. Niu et al. reported the variation of CGE with temperature by using Municipal solid waste (MSW) as a feedstock. They found that magnitude of MSW ranges from 39.90 to 78.70% for an elevated temperature between (650-1000)^{0}C whereas 32.60 to 87.6% for the lower temperature range between (550-650)^{0}C [109]. It can be concluded from Fig.4.40 that HHV is directly proportional to temperature.

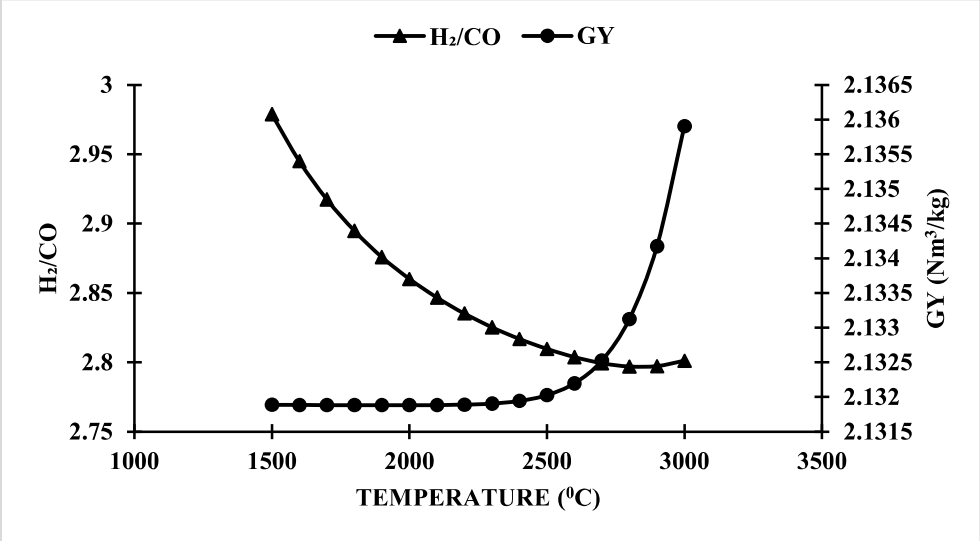

Fig. 4.39. Variation of H_2/CO and GY with temperature.

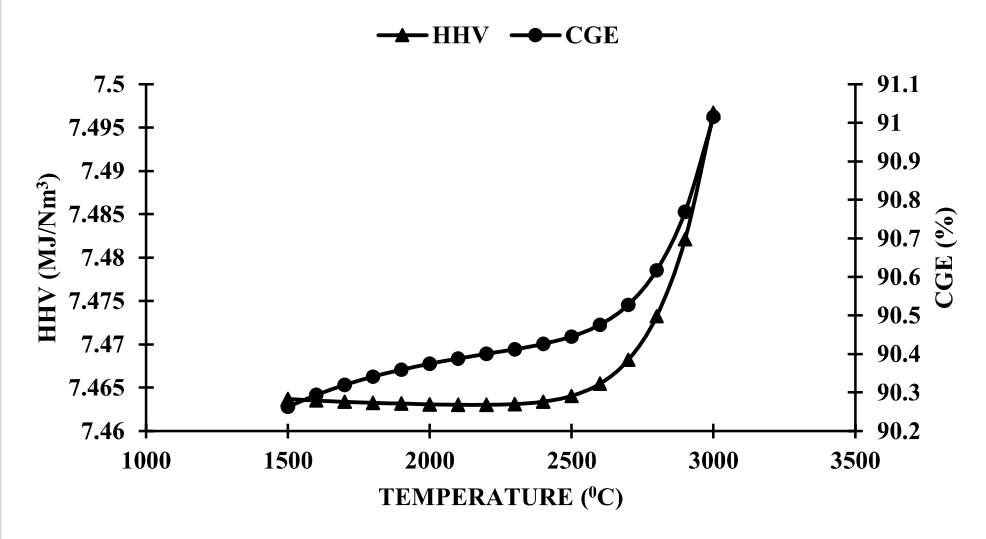

Fig. 4.40. Variation of CGE and HHV with temperature.

4.4.5 Influence of equivalence ratio (ER)

The equivalence ratio is defined as the ratio of the actual by stoichiometric air-fuel ratio [108]. It is one of the most persuasive parameters for the study. ER was varied from (0.1-0.5) by altering the biomass feed rate keeping the temperature persistent at 2500^0C. Fig.4.41 depicts the variation of ER with producer gas composition.

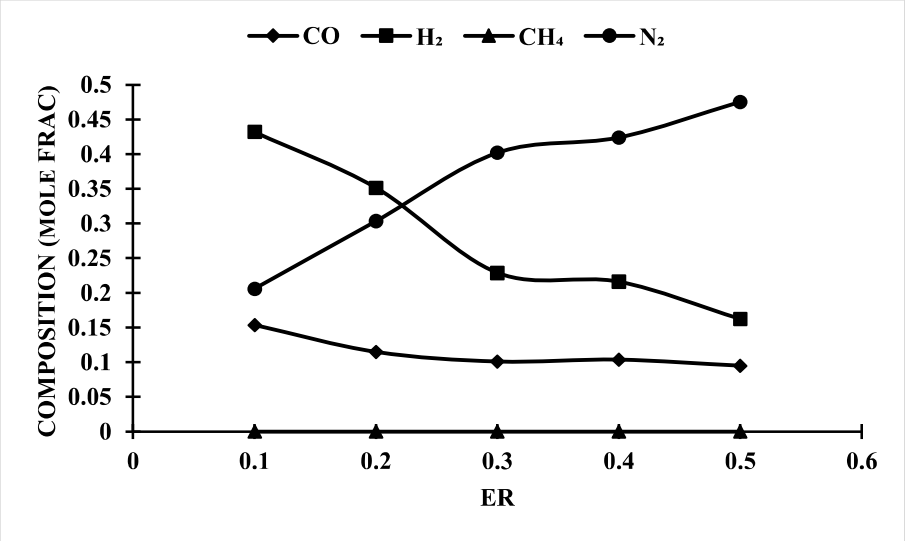

Fig. 4.41. Influence of ER on syngas compositions for Medical waste.

Fig.4.41 concluded that the concentration of hydrogen decreases from 43.21% at ER 0.1 to 16.24% at ER 0.5. As ER upsurges, the magnitude of CO content reduces as well. The ER results obtained from our model follow the same pattern as those obtained from previous research in the literature [109]. Han et al. stated that the concentration of H_2 declines constantly from 23.40% at 0.2 to 9.830% at 0.45 with the increased ER [92]. It can be inferred from Fig.4.41 that N_2 content increases in the syngas as the ER increases. It is due to the increased amount of air coming into the gasifier.

The simulated results for gas yield and H_2/CO against ER are depicted in Fig.4.42. It can be inferred from Fig.4.42 that the magnitude of gas yield was 2.13 at ER 0.1 and 0.92 at ER 0.5. This decrement in GY may be due to an increased amount of N_2 as ER increases. It can be

analyzed from equation 9 that the magnitude of gas yield is inversely proportional to N_2 content in syngas. H_2/CO ratio also shows the same relation as Gas yield. Fig.4.43 depicts the effects of ER on CGE and HHV. The inverse link between CGE and the ER is depicted by CGE. At ER 0.1, the greatest CGE was 90.44 percent. Increased ER has an inverse relationship with HHV. At ER 0.1, the greatest HHV was 7.46 MJ/Nm^3. As ER rises, the size of HHV diminishes. It might be due to the syngas being diluted with N_2, resulting in the gas having a low energy content.

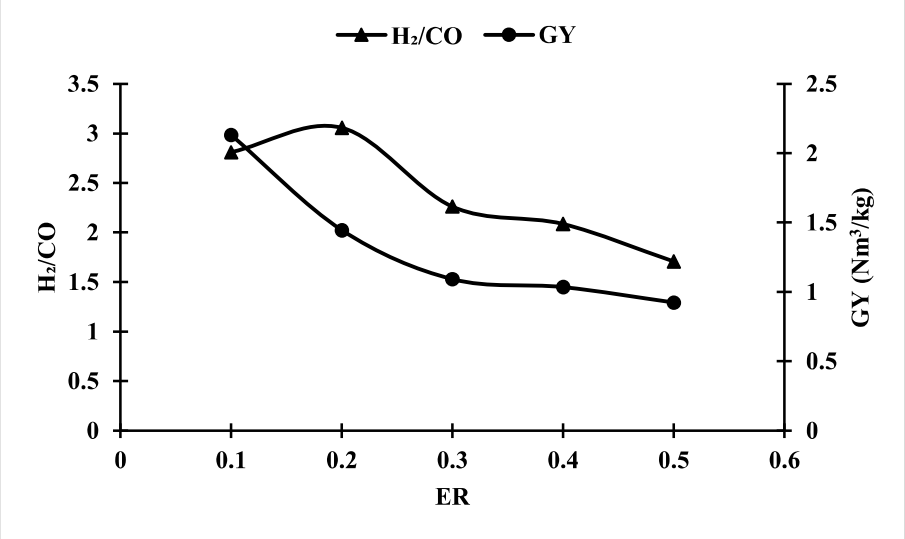

Fig. 4.42. Variation of H_2/CO and GY with equivalence ratio.

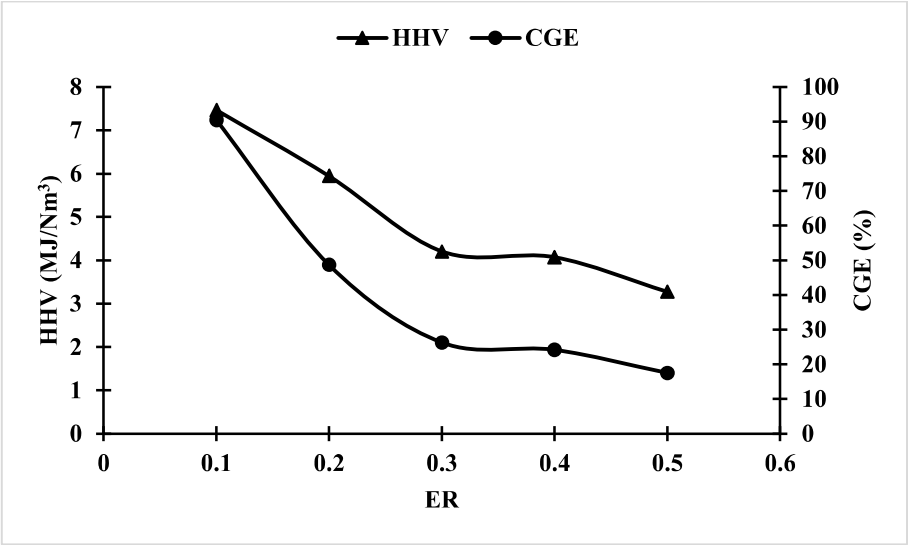

Fig. 4.43. Variation of CGE and HHV with equivalence ratio.

4.4.6. Influence of steam/biomass

The magnitude of H_2 in the syngas can be enhanced by using steam as the gasifying agent [125]. The SBR (steam biomass ratio) was changed from 0.5 to 1.4, while the gasification temperature and ER were maintained at 2500^0C and 0.1, respectively. Fig.4.44 shows the syngas variation as a function of variable SBR. The major cause of enriched H_2 concentration in syngas is a rise in water vapour partial pressure inside the reactor, which causes water gas shift and steam reforming process to rise. [126]. Apart from that, the presence of steam in a gas-phase reaction causes hydrocarbon breakdown and a rise in the magnitude of H_2 and CO_2 [19]. In the literature, a similar tendency of the findings was found. [127]

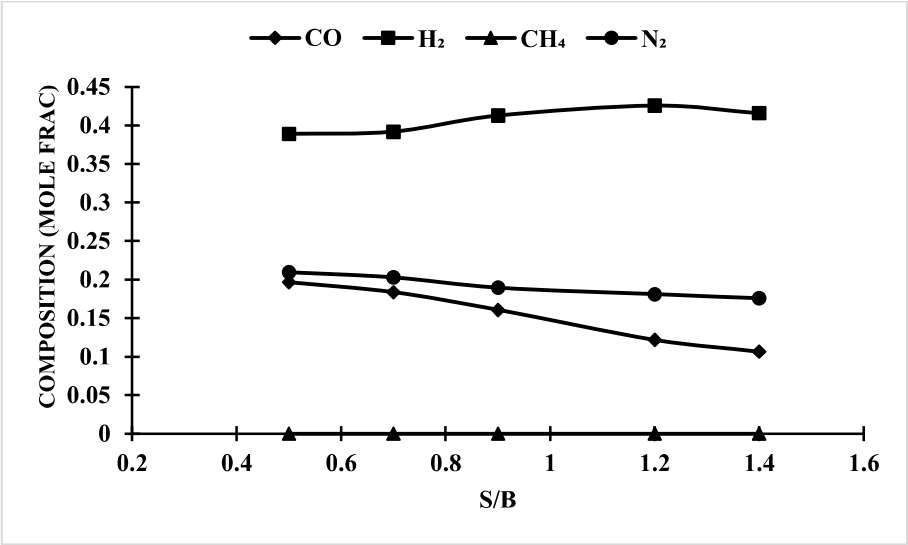

Fig. 4.44. Influence of S/B on syngas compositions for Medical waste.

The simulated results for gas yield and H_2/CO against S/B are depicted in Fig.4.45. It can be inferred from Fig.4.45 that the magnitude of gas yield increases as S/B increases. The magnitude of GY was 2.09 at S/B 0.5 and 2.49 at S/B 1.4. This may be due to a decrease in the concentration of N_2 as SBR increases. A similar trend was shown in was H_2/CO ratio as hydrogen concentration increases while using steam as a gasifying agent. [92]. Fig.4.46 depicts the variation of CGE and HHV with SBR.

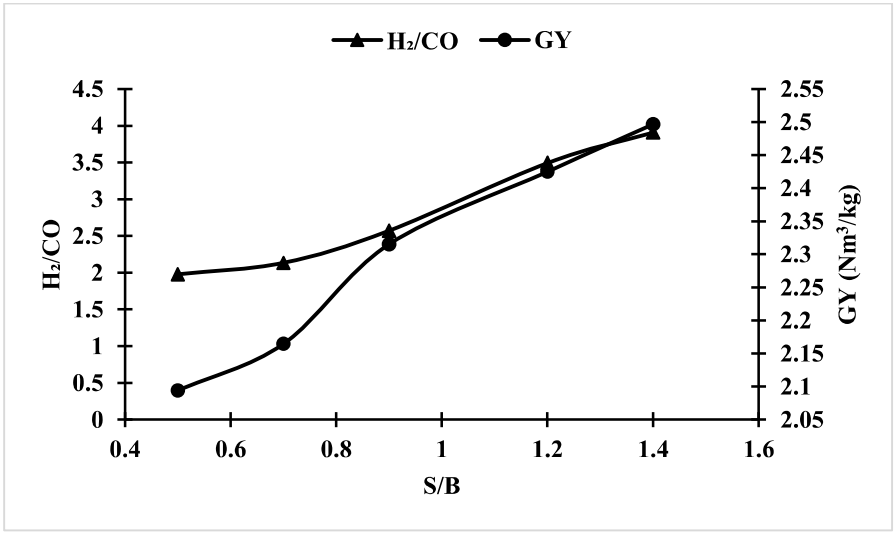

Fig. 4.45. Variation of H_2/CO and GY with S/B.

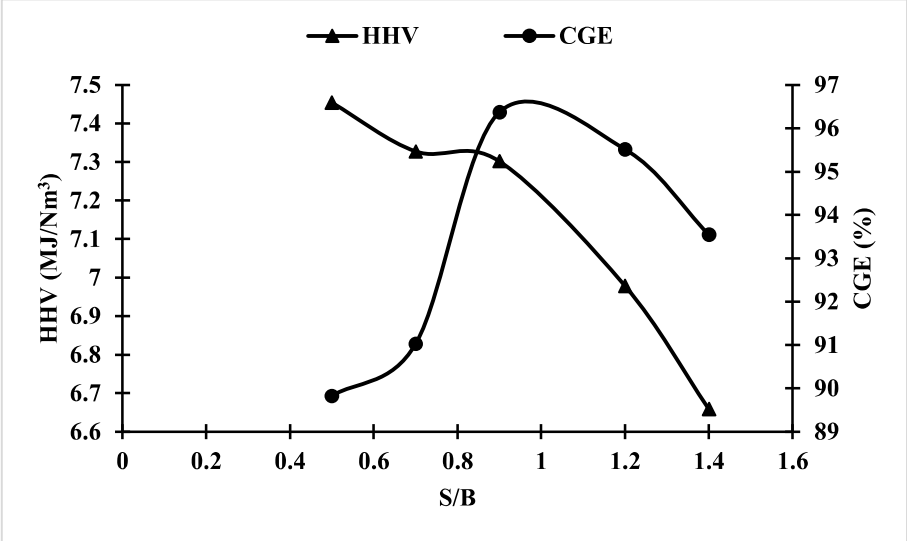

Fig. 4.46. Variation of CGE and HHV with SBR.

4.4.7 Regression analysis

For the investigation, three variable operational parameters were chosen: reactor temperature (X1), ER (X2), and S/B (X3). H2 concentration, CGE, and HHV are the three output responses. Table 4.22 shows the expected design plan as well as the computed response values. Because the two-way interaction term was negligible, it was left out of the calculations.

The developed regression equation for predicting H_2 concentration using ANOVA is given below

$$H_2 = 0.4487 - 0.000056X_1 - 1.292X_2 + 0.3095X_3 + 0.000001X_1^2 + 1.055X_2^2 - 0.1405X_3^2 \quad (13)$$

The developed regression equation for predicting CGE using ANOVA is given below

$$CGE = 137.4 + 0.0059X_1 - 591.2X_2 - 7.9X_3 - 0.000001X_1^2 + 690.9X_2^2 + 6.3X_3^2 \quad (14)$$

The developed regression equation for predicting HHV using ANOVA is given below

$$HHV = 8.94 - 0.000628X_1 - 22.62X_2 + 3.50X_3 + 0.000001X_1^2 + 20.85X_2^2 - 2.255X_3^2 \quad (15)$$

Table. 4.22 Design matrix plan along with the responses

Trial	TEMP	ER	S/B	H_2 (Mole Frac)	CGE (%)	HHV (MJ/Nm^3)
1	1500	0.1	1	0.438614381	90.26248586	7.46368687
2	1600	0.1	1	0.437343987	90.29382631	7.4635155
3	1700	0.1	1	0.436299667	90.31958685	7.463373791
4	1800	0.1	1	0.435431138	90.34101694	7.463255813
5	1900	0.1	1	0.434701263	90.3590559	7.463157973
6	2000	0.1	1	0.43408236	90.37444944	7.463079983
7	2100	0.1	1	0.433553876	90.38787136	7.463028075
8	2200	0.1	1	0.43310115	90.4000878	7.463021894
9	2300	0.1	1	0.432715268	90.41221902	7.463108391
10	2400	0.1	1	0.432394181	90.42618031	7.463386953
11	2500	0.1	1	0.432145446	90.44539381	7.464051414
12	2600	0.1	1	0.431991026	90.47587972	7.465455337
13	2700	0.1	1	0.431974428	90.52779945	7.468204417
14	2800	0.1	1	0.432169841	90.61738334	7.473271886
15	2900	0.1	1	0.432691295	90.76886023	7.482112256
16	3000	0.1	1	0.43369692	91.01540554	7.496712125
17	2500	0.2	1	0.351642487	48.69923388	5.945409356
18	2500	0.3	1	0.228927344	26.26845496	4.203267575
19	2500	0.4	1	0.216106482	24.19371726	4.070423973
20	2500	0.5	1	0.162421273	17.50608414	3.275894873
21	2500	0.1	0.5	0.388940358	89.82220462	7.453573451
22	2500	0.1	0.7	0.391872499	91.02252897	7.327327416
23	2500	0.1	0.9	0.412708932	96.36833652	7.301951085
24	2500	0.1	1.2	0.42567987	95.51293738	6.97790724
25	2500	0.1	1.4	0.415940036	93.54368608	6.658942979

4.4.8 Normal probability plots

The normal probability plot for all three output responses is obtained using the RSM technique. These plots are very important for determining the efficiency of the model. in this type of plot, the X-axis is taken as the residuals whereas Y-axis is taken as the percent value. Residual is the difference between the exact value and the predicted value. Exact values are those values

that are predicted by using Aspen plus sensitivity analysis. Predicted values are those values that are obtained by using regression equations using ANOVA analysis. These plots have scattered output response points. These scattered points deviate from one straight line that is known as a theoretical normal distribution. The closeness of scattered points from this straight line depicts higher efficiency of the developed model and vice versa. Fig.4.47 depicts the normal probability plots

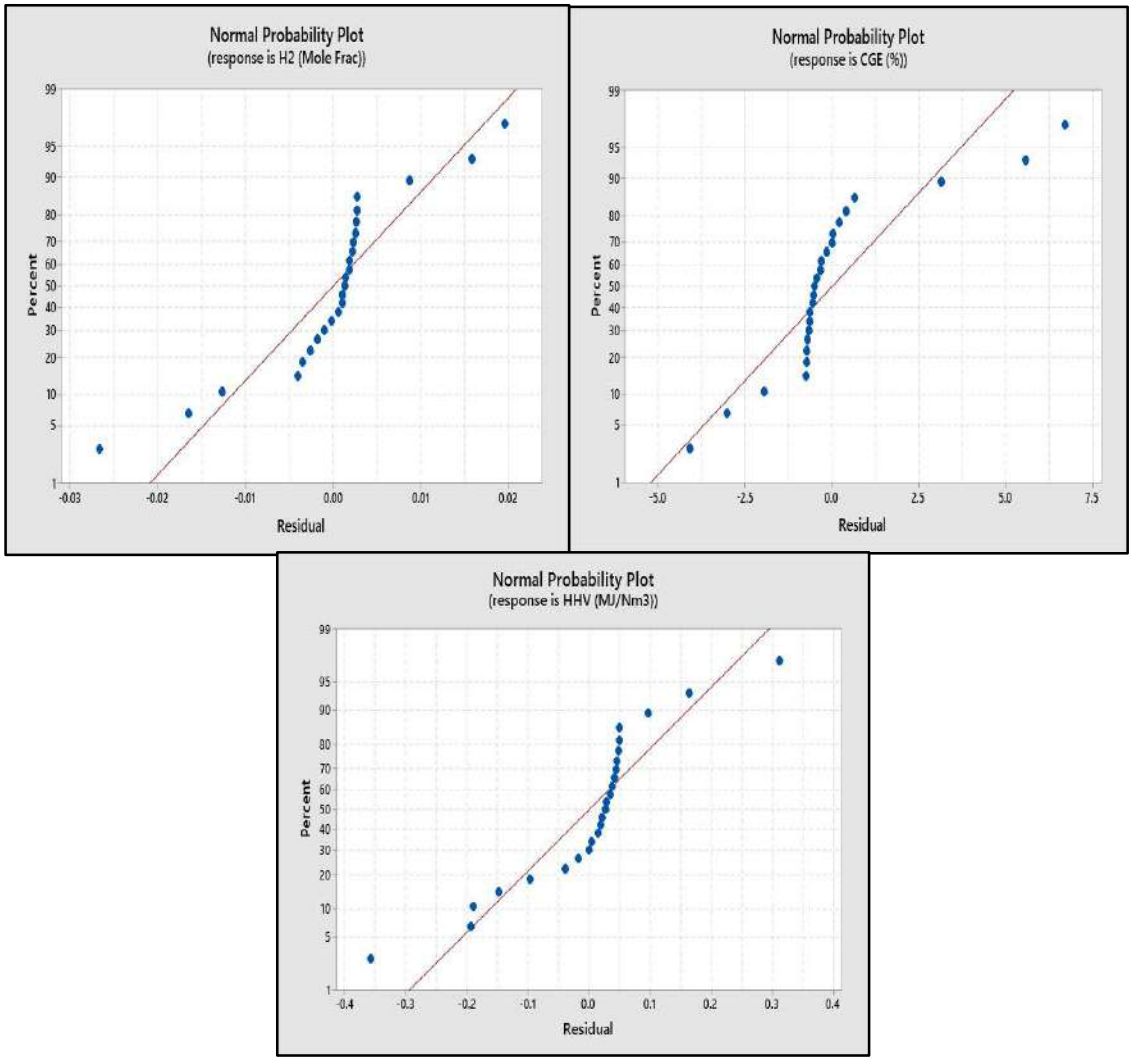

Fig. 4.47. Normal probability plot for output responses

4.4.9 ANOVA results

The results acquired from the ANOVA for H_2 yield, CGE, and HHV were tabulated in table 4.23, 4.24, and 4.25 (attached in Appendix) respectively. The F-value in the table depicts the statistical significance of the model as well as factors and their interactions. The higher magnitude of the F factor depicts the higher significance of the effects of the factors on the response variables. The P-value is insignificant if its magnitude is higher than 0.05 [110]. It can be inferred from the ANOVA result of hydrogen yield is that ER plays an important role in the hydrogen concentration in the syngas composition followed by S/B and temperature. The P-value of temperature is greater than 0.05 in table 4.23 hence it is insignificant. CGE's ANOVA result is shown in table 4.24. it shows that the F-value of ER is higher than S/B and temperature, implying that ER is the most important parameter in increasing syngas CGE. Table 4.25 depicts the ANOVA result of HHV. A similar trend of F-value is observed in the ANOVA of HHV as compared to CGE. RSM model efficiency is shown in table 4.26.

Table. 4.26. RSM model assessment

	H_2	CGE	HHV
R-sq	98.62%	99.10%	98.90%
R-sq(adj)	98.16%	98.80%	98.53%
R-sq(pred)	94.06%	93.62%	94.71%

4.4.10 Parametric impact using contour and 3-D surface plot

Optimization of a variable operating parameter of gasifier is very influential for attaining high gasification efficiency. It is very difficult for industries to attain and retain the single operating value for the gasifier. This drawback can be elucidated by contour plot. The contour plot provided the optimum working range of the gasifier where the industry should operate to attain

the higher heating value of producer gas. The 3-D surface plot depicts the simultaneous parametric impact of multiple operating parameters. These plots help in completely understand the behavior of output response against simultaneous varying of operating parameter

4.4.11 Common impact of the independent parameters on the H_2 concentration

The contour plot and surface plot of hydrogen yield corresponding to (Temperature, ER), (ER, S/B), and (Temperature, S/B) are depicted in Fig.4.48. When ER and temperature vary simultaneously, it is found that the maximum concentration of H_2 is obtained at ER 0.1 to 0.2 whereas temperature ranging between 1500^0C to 2000^0C. when ER and S/B vary simultaneously, it is found that maximum concentration attained at ER ranging between 0.1 and 0.2 whereas S/B ranging between 0.7 to 1.4. surface plot for H_2 concentration depicts the parametric impact of multiple operating parameters. It can be inferred from Fig.4.48 that lower ER and higher temperature increase the magnitude of hydrogen concentration in the syngas composition. Hold values kept for the surface plot of hydrogen concentration was temperature 2250^0C, ER 0.3, S/B 0.95.

4.4.12 Common impact of the independent parameters on the cold gas efficiency

The influence of choice factors on cold gas efficiency is seen in Fig.4.49. CGE is defined as the ratio of producer gas's lower heating value to biomass's lower heating value multiplied by gas production. The surface plot shows that when the temperature rises, the cold gas efficiency rises as well. When ER and temperature are both changed at the same time, the highest magnitude of CGE is attained at ERs of 0.1 to 0.2 and temperatures of 1500^0C to 3000^0C. The ER and CGE have an inverse connection. This might be related to a reduction in gas yield when ER rises. As the S/B ratio rises, the cold gas efficiency (CGE) rises as well. When ER and S/B are both changed at the same time, the highest CGE is attained when ER is between 0.1 and 0.2 and S/B is between 1 and 1.4. This might be owing to the fact that when the S/B ratio rises,

the heating values of syngas rise as well. In fig 4.49, the contour plot and surface plot of CGE for (Temperature, ER), (ER, S/B), and (Temperature, S/B) are shown. Fig.4.49 shows that a lower ER, a S/B ratio of about 1, and a higher temperature enhance the amount of CGE in the syngas composition.

4.4.13 Common impact of the independent parameters on the higher heating value

The contour plot and surface plot of HHV corresponding to (Temperature, ER), (ER, S/B), and (Temperature, S/B) are depicted in Fig.4.50. When ER and temperature vary simultaneously, it is found that the maximum magnitude of HHV is obtained at ER 0.1 to 0.2 whereas temperature ranging between 1500^0C to 2000^0C. when ER and S/B vary simultaneously, it is found that maximum concentration attained at ER ranging between 0.1 and 0.2 whereas S/B ranging between 0.6 to 1.2. surface plot for HHV concentration depicts the parametric impact of multiple operating parameters. It can be inferred from Fig.4.50 that lower ER and higher temperature increase the magnitude of HHV of syngas. Hold values kept for the surface plot of hydrogen concentration was temperature 2250^0C, ER 0.3, S/B 0.95

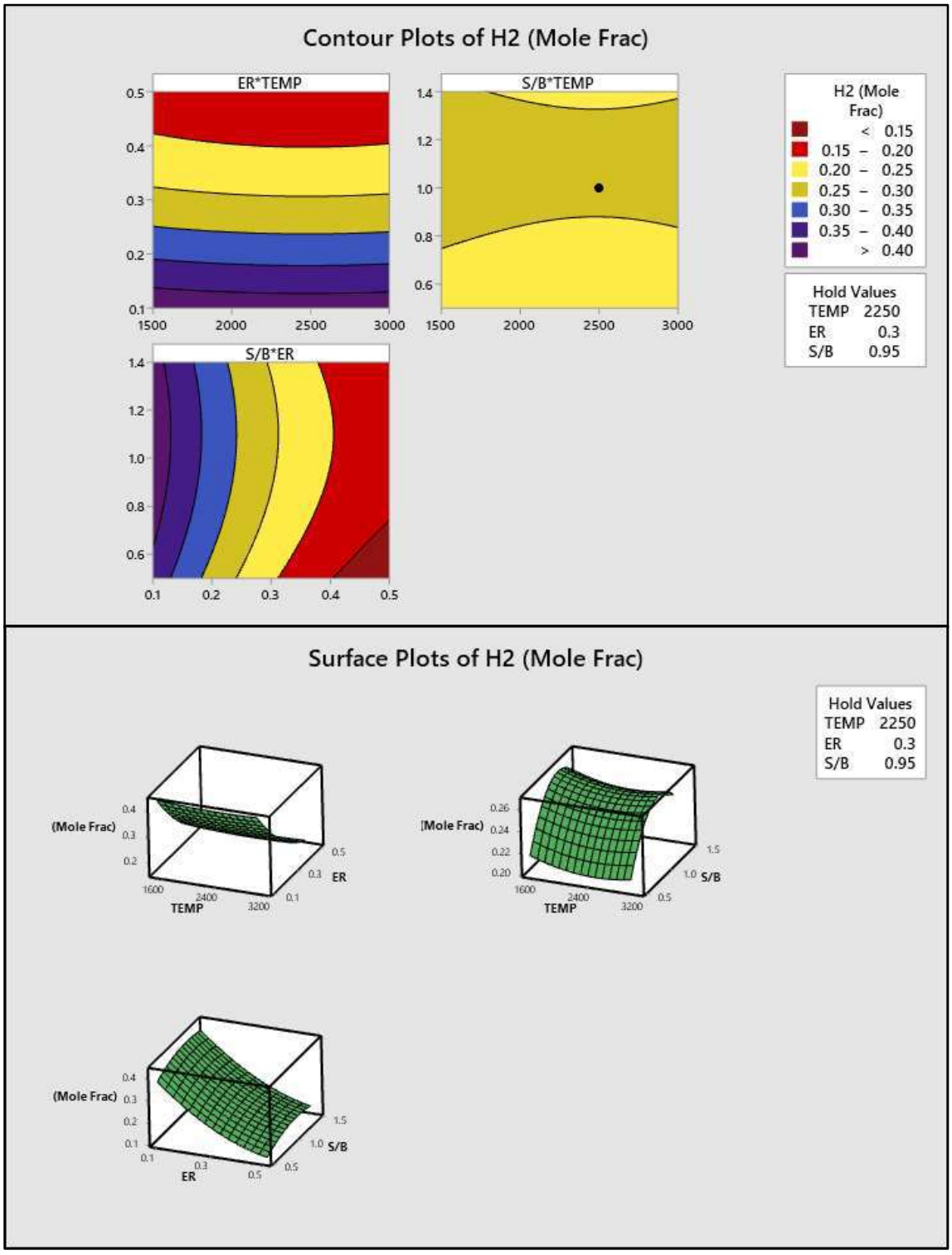

Fig. 4.48. Contour and surface plot of Hydrogen concentration under variable parameters

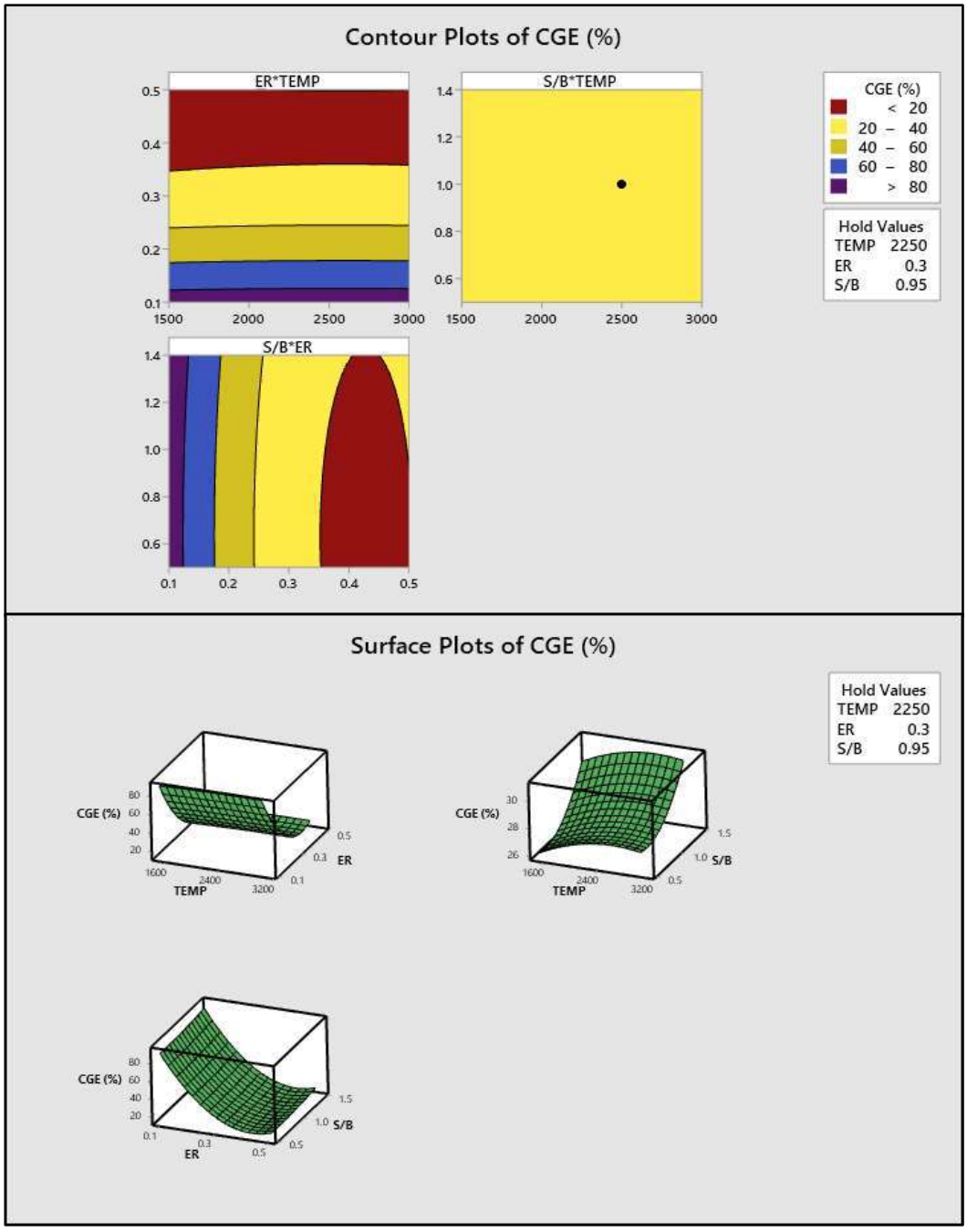

Fig. 4.49. Contour and surface plot of CGE under variable parameters

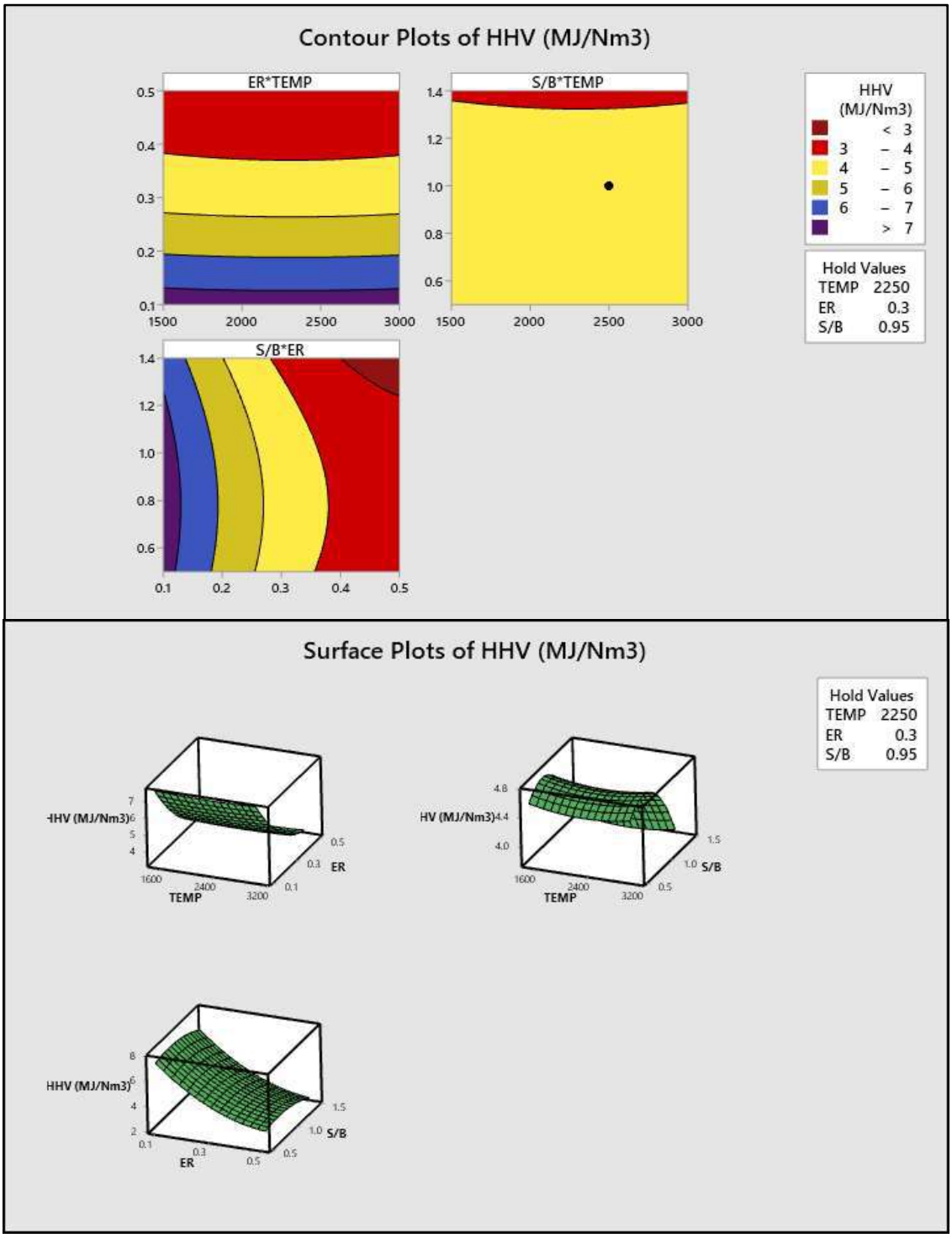

Fig. 4.50. Contour and surface plot of HHV under variable parameters.

4.4.14. Optimal state of decision variables

The primary goal of this research was to find the most optimal operating parameter that corresponded to optimal output responses. The RSM optimizer is seen in Fig.4.51, where the optimizer programme generates results. The cumulative composite desirability found was 0.9721, indicating that the optimization magnitude was efficient in comparison to the intended value. H2, CGE, and HHV have ideal magnitudes of 0.43, 89.95 percent, and 7.49 MJ/Nm3 correspondingly. The most optimized operating independent parameters for the temperature, ER, and S/B are 1560.6^{0}C, 0.1, and 0.99. Therefore, it is recommended from the present study that toxic medical waste can be a viable feedstock to generate power for the rural sector using the technique of plasma gasification. The main goal of the optimization setup is to maximize response output.

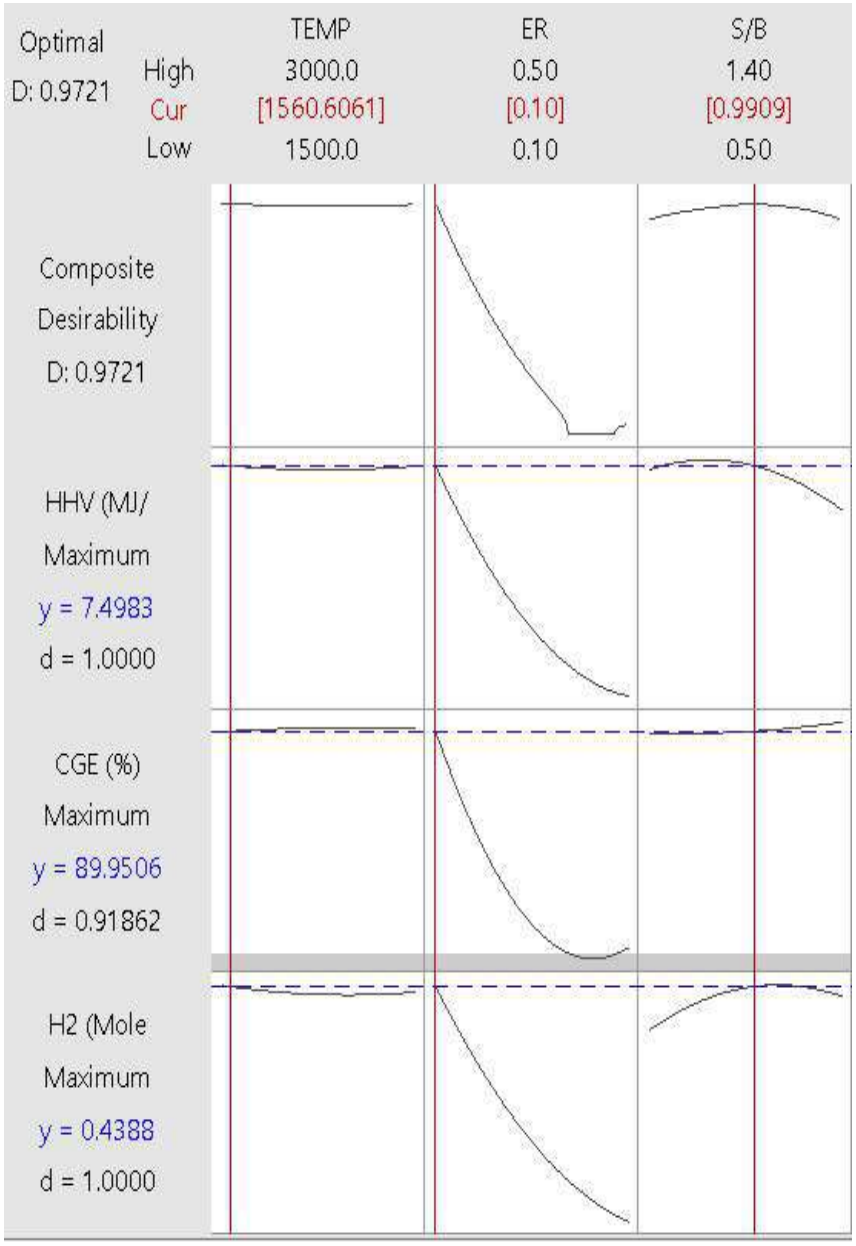

Fig. 4.51. RSM optimizer plot

The simulation was performed again at optimized operating conditions (achieved by RSM) using Aspen plus and the comparative analysis of the hydrogen yield, CGE, and HHV was executed between the predicted value of Aspen plus and RSM under optimized conditions. The result of the comparative analysis was tabulated in table 4.27. The main objective of this analysis was to assess the efficiency of the developed Aspen plus model.

Table. 4.27 Comparative analysis of optimized result between Aspen plus and RSM

Optimized Independent Parameters :Temperature = 1560^0C, ER = 0.1, S/B = 0.99			
Responses	RSM (Fig.4.51)	Aspen Plus	Error
H_2	0.438	0.43	0.008
CGE (%)	89.95	95.55	5.6
HHV (MJ/Nm^3)	7.49	7.61	0.12
Mean error			1.90

4.4.15 Summary of the present work

This study used hazardous medical waste to do predictive modelling and multi-objective optimization of numerous gasification performance parameters of a steam injected plasma gasifier by integrating ASPEN Plus with Response surface methodology (RSM). The model was effectively validated using experimental results from the literature, and there was a good agreement. For multi-objective optimization, temperature, equivalence ratio, and S/B were used as independent factors, while hydrogen yield, CGE, and HHV were used as response variables. The gasifier's optimal operating range was discovered, in which the gasifier produces the best results.

From the current study, the following findings may be drawn.

- Under numerous independent operating situations, the created model in this study is capable of forecasting producer gas compositions and gasifier performance.
- R^2 value obtained from ANOVA for H_2, CGE, and HHV are 98.62%, 99.10%, and 98.9% respectively

- The optimized independent operating conditions are temperature 1560.60^{0}C, equivalence ratio 0.1, and S/B 0.99.
- The ideal values of responses H_2, CGE, and HHV, according to the RSM optimizer, are 0.43, 89.95 percent, and 7.49 MJ/Nm^3, respectively.
- Injecting steam as a gasifying agent enhances the hydrogen concentration in the syngas
- ER is the most influential parameter in enhancing the CGE of syngas followed by S/B and temperature.

4.5 Experimental analysis-Gasification of coconut shell

Producer gas or syngas generation from biomass gasification reveals one of the pronounced perspectives to substitute conventional fossil fuel. In the present experimental studies, performance, emission, and fuel consumption of VCR engines run with diesel and coconut shell-based producer gas (PG) with varying load, CR, and gasification equivalence ratio (GER) have been performed. Apart from this analysis, the response surface method has been applied to optimize engine operating inputs like CR, load, and gasifier ER to improve the performance by maximizing brake power (BP) and brake thermal efficiency (BTE) and minimizing brake specific fuel consumption (BSFC) and exhaust emission (CO, UHC, CO_2, and NOx). In the experiment, Total 48 experimental data set was executed for the RSM based optimization and ANOVA sensitivity test. The formation of regression models using ANOVA showed high accuracy in forecasting output response variables with a confidence interval of 95%. The RSM predicted a good relationship between the range of inputs and output parameters with high accuracy. The coefficient of determination of the RSM value was found to be equal to 0.9520, which shows the high accuracy level in the relationship between statistical-based prediction and experimental values. As per the results obtained by using RSM optimization, the best operating conditions of the engine were obtained to be 0.12 gasification equivalence ratio, 16 compression ratio with 12 kg engine load. The optimum responses predicted under these operating parameters were obtained equals to 3.5 kW, 26.41%, 0.48 kg/kWh, 0.0042% (vol%), 15.15 (ppm), 1.27 (vol%), and 2.94 ppm for BP, BTE, BSFC, CO, UHC, CO_2, and NO respectively. Thus, RSM is a useful approach for assessing and improving the performance and exhaust emission of a CI engine powered with diesel and PG corresponding to optimized input variables

4.5.1 Experimental arrangement

For the conduction of the experiment, the coconut shell, a feedstock for gasifier, was collected from the temple area of Varanasi, Uttar Pradesh, India. Here, mostly, coconut used to arrive from South India. The photograph of coconut feedstock is shown in Fig.4.52, where the hemispherical diameter of a broken part was about 75-85 mm and thickness 4-5 mm. The chemical property details of coconut shell and producer gas from gasifier are mentioned in table 4.28. In the gasifier-ICE experimental setup, downdraft gasifier fitted with reaction chamber with thermocouple integrated, blower, air control valve, scrubber, cyclone separator, test flare, water pump, three-chamber for the fine filtering system. An air-based, batch-type, fixed-bed downdraft with self-heating is made of thick mild steel with a 73 cm diameter and 200 cm height. Water-based cleaning, cyclone separation, and filtering is integrated with the reactor so that producer gas can pass through it. Then, to confirm flammability, PG was passed through a series of checkpoints until the testing flame changed colour and flared. To eliminate residual contaminants, PG was permitted to flow through three-chamber filtering in a sinusoidal trajectory, first through a fine filter, then through a fabric filter utilising Rice husk, wood dust, and cotton cloth. The compression ignition engine (CIE) functions primarily with naturally air aspirated, direct injection, water-cooled, variable compression ratio (VCR) system, eddy current load dynamometer, and auto governing system to maintain 1500 engine rpm, etc. The characteristics of engine combustion, fuel consumption, and performance were logged on a computer through a data acquisition system-Engine Soft. AVL DIGAS 444 was used for measuring engine emission during the experimental analysis. Exhaust gas emission testing is a procedure that involves measuring the gases generated by an engine exhaust pipe using test equipment. It is based on the Differential Optical Absorption Spectroscopy (DOAS) concept. The light source is a xenon lamp, and the detector is a spectrometer in its most basic form, revealing the fine details of a certain wavelength range, or "window." To detect various

gaseous species, or groups of such species, different windows are utilised. The actual gas concentration may be estimated using mathematical processing of the observed spectrum and comparison with pre-recorded spectra of known gases and known concentrations within the specified timeframe. A probe is inserted into the engine exhaust tailpipe, and the exhaust gases are monitored according to a precise protocol. The exhaust gas analyser measures four gases: carbon monoxide (CO), carbon dioxide (CO_2), and hydrocarbons (HC), and NOx. These measures add up to a highly precise method of determining an engine's combustion efficiency.. A Certified Reference Standard developed in line with ISO17025 must be used to calibrate the instrument. Box type orifice meter and manometer were used to measure the air and gas flow rate separately. During the experimental campaign, a total 48 test runs were implemented to execute the whole experimental investigation.

Fig. 4.52. Coconut Shell: A-supply feedstock (before gasification), B-Coconut char (after gasification)

Table. 4.28 Chemical property of fuel- coconut shell [135, 136]

Particular	**Value**
Proximate analysis	
Volatile matter	72.93%
Fixed carbon	19.48%
Ash	0.61%
Moisture content (%)	6.98%
Ultimate analysis	
Carbon	53.73%
Hydrogen	6.15%
Oxygen	38.45%
Nitrogen	0.86%
Sulphur	0.02%
Calorific value (MJ/kg)	20.88
Producer gas composition	
CO	21%
H_2	20%
CO_2	13%
CH_4	< 3%
N_2	50%
Producer gas calorific value (MJ/Nm^3)	5.4

4.5.2 Experimental uncertainty

Due to the obvious experimental metering variability, variance has mostly been incorporated during the experiment. Calibration of findings, instrument selection, standardized testing, working conditions, and data interpretation are the other factors contributing to the inclusion of experimental errors and uncertainty in a system. Table 4.29 shows the instruments used in the experiments, as well as the equipment range, resolutions, system accuracies, and system percentage uncertainty. These uncertainties may be due to systematic and precision errors, as well as instruments used to collect data and rounding off errors during data observation. The total amount of uncertainty in the experiment was calculated.

Total percentage uncertainty

$= [\text{Uncertainty of } \{(\text{Brake power})^2 + (\text{Tachometer})^2 + (\text{Thermocouple})^2 + (\text{Dynamometer})^2$

$+ (\text{Pressure transducer})^2 + (\text{Crank angle sensor})^2 + (\text{Fuel measurement})^2]^{(1/2)}$

$= [(0.39)^2 + (0.33)^2 + (0.16)^2 + (0.2)^2 + (0.04)^2 + (0.2)^2 + (1.0)^2]^{1/2})$

$= \pm 1.16\ \%$

Table. 4.29. Instrument details and the associated uncertainties

SN	Apparatus	Range	Resolution	Accuracy	Uncertainty (%)
1.	Brake power	0-3.4 kW	0.1 kW	±0.1 kW	±0.39
2.	Tachometer	1200-1500 rpm	1 rpm	±5 rpm	±0.33
3.	Thermocouple	0-12000C	10C	±20C	±0.16
4.	Dynamometer	0-50 kg	0.01 kg	±0.1 kg	±0.2
5.	Pressure transducer	0-5000 psi	---	±2 psi	±0.04
6.	Crank angle sensor	0-3600	10	±10	±0.2
7.	Burette fuel	---	---	±0.1 cc	±1.0

4.5.3 *RSM Normal Probability Plots*

The normality hypothesis for the calculated data was specifically validated using normal probability plots. [137]. It's also known as investigation plot, and it's a kind of plot that's used to look at the distribution of residuals. Responses are scattered against a theoretical normal distribution, with the point forming an approximately straight line, and deviations from this line indicating the residual magnitude. The X-axis represents residual, while the Y-axis represents percent worth. Minitab software was used to create this storyline. Normal probability graphs of BP, BTE, BSFC, CO, CO_2, HC, and NO_X are depicted in Figures 4.53 and 4.54 that have a normal distribution, which is one of the requirements for ANOVA's validity. The least-square methodologies, which are multiple regression techniques that apt a model to set the experimental results with fewer issues, were used to acquire these mathematical models.

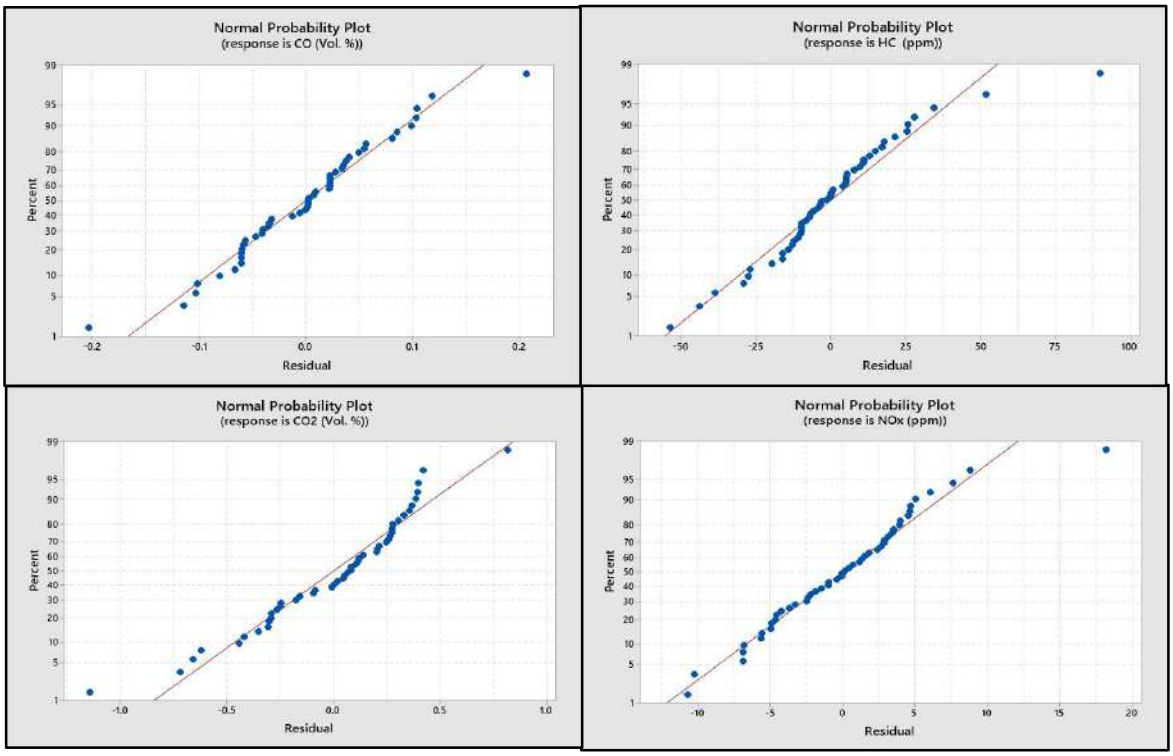

Fig. 4.53. Normal probability plots for emission characteristics

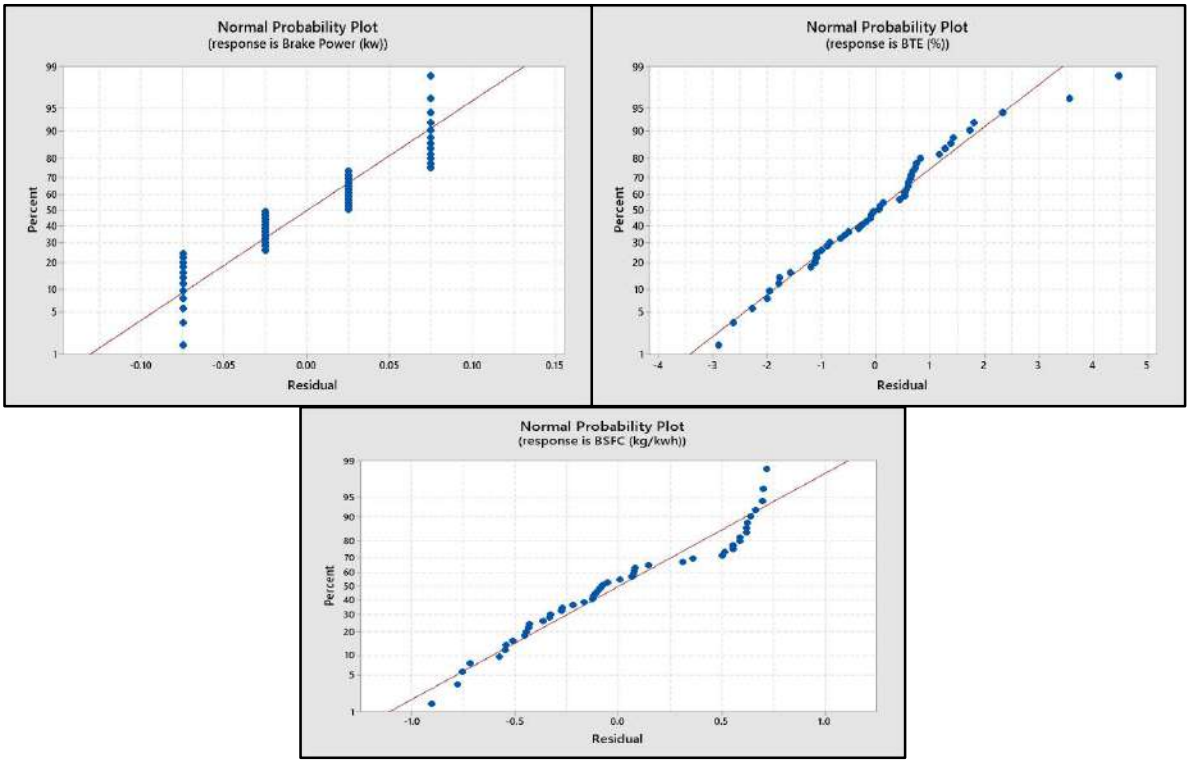

Fig. 4.54. Normal probability plots for performance characteristics

4.5.4 RSM regression analysis

The decision variable for the study was chosen from three independent parameters: Equivalence ratio (ER), Compression ratio (CR), and Engine Load. BP (kW), BTE (percent), BSFC (kg/kWh), HC (ppm), CO (vol. percent), CO_2 (vol. percent), and NO_X (vol. percent) are the seven production responses (ppm). RSM constructed second-order equations to estimate performance-dependent parameters based on independent parameters, which are shown in Eqs. 2-8.

$$\boldsymbol{BP} = 0.07 - 0.001\,\boldsymbol{ER} + 0.0001\boldsymbol{CR} + 0.2687\boldsymbol{EL} + 0.000\mathit{O}4\boldsymbol{BR} * \boldsymbol{BR} - 0.001563\boldsymbol{EL} * \boldsymbol{EL} - 0.000005\boldsymbol{ER} * \boldsymbol{CR} - 0.000015\boldsymbol{ER} * \boldsymbol{EL} \quad (2)$$

$$\boldsymbol{BTE} = -54 + 30.9\boldsymbol{ER} + 5.5\boldsymbol{CR} + 0.74\boldsymbol{EL} + 18.8\boldsymbol{ER} * \boldsymbol{ER} - 0.133\boldsymbol{CR} * \boldsymbol{CR} - 0.1174\boldsymbol{EL} * \boldsymbol{EL} - 2.42\boldsymbol{ER} * \boldsymbol{CR} + 0.436\boldsymbol{ER} * \boldsymbol{EL} + 0.1727\boldsymbol{CR} * \boldsymbol{EL} \quad (3)$$

$$\boldsymbol{BSFC} = 40.6 - 12.3\boldsymbol{ER} - 3.63\boldsymbol{CR} - 1.834\boldsymbol{EL} + 0.85\boldsymbol{ER} * \boldsymbol{ER} + 0.089\boldsymbol{CR} * \boldsymbol{CR} - 0.06688\boldsymbol{EL} * \boldsymbol{EL} + 0.678\boldsymbol{ER} * \boldsymbol{CR} - 0.027\boldsymbol{ER} * \boldsymbol{EL} + 0.0027\boldsymbol{CR} * \boldsymbol{EL} \quad (4)$$

$$\boldsymbol{CO} = -23.16 + 6.66\boldsymbol{ER} + 2.744\boldsymbol{CR} - 0.1713\boldsymbol{EL} - 0.979\boldsymbol{ER} * \boldsymbol{ER} + 0.0789\boldsymbol{CR} * \boldsymbol{CR} + 0.002312\boldsymbol{EL} * \boldsymbol{EL} - 0.331\boldsymbol{ER} * \boldsymbol{CR} - 0.0368\boldsymbol{ER} * \boldsymbol{EL} + 0.00552\boldsymbol{CR} * \boldsymbol{EL} \quad (5)$$

$$\boldsymbol{HC} = -2921 + 302\boldsymbol{ER} + 377\boldsymbol{CR} - 52.3\boldsymbol{EL} + 446\boldsymbol{ER} * \boldsymbol{ER} - 11.37\boldsymbol{CR} * \boldsymbol{CR} + 0.908\boldsymbol{EL} * \boldsymbol{EL} - 6.2\boldsymbol{ER} * \boldsymbol{CR} - 3.67\boldsymbol{ER} * \boldsymbol{EL} + 1.51\boldsymbol{CR} * \boldsymbol{EL} \quad (6)$$

$$\boldsymbol{NO} = -519 - 809\boldsymbol{ER} + 79.1\boldsymbol{CR} - 15.46\boldsymbol{EL} + 239.1\boldsymbol{ER} * \boldsymbol{ER} - 2.72\boldsymbol{CR} * \boldsymbol{CR} - 0.0195\boldsymbol{EL} * \boldsymbol{EL} + 38.57\boldsymbol{ER} * \boldsymbol{CR} - 38.57\boldsymbol{ER} * \boldsymbol{EL} + 6.74\boldsymbol{CR} * \boldsymbol{EL} \quad (7)$$

$$\boldsymbol{CO2} = 18.6 + 0.0782\boldsymbol{BR} - 2.21\boldsymbol{CR} + 0.0197\boldsymbol{EL} + 0.000602\boldsymbol{BR} * \boldsymbol{BR} + 0.0691\boldsymbol{CR} * \boldsymbol{CR} - 0.000205\boldsymbol{EL} * \boldsymbol{EL} - 0.00574\boldsymbol{BR} * \boldsymbol{CR} - 0.000057\boldsymbol{BR} * \boldsymbol{EL} + 0.000079\boldsymbol{CR} * \boldsymbol{EL} \quad (8)$$

4.5.5 ANOVA analysis

The results of the ANOVA for engine efficiency and emission were tabulated in Tables 4.30, 4.31 respectively. The statistical significance of the model, as well as variables and their interactions, is depicted in the table by the F-value. The greater the F factor's magnitude, the greater the importance of the factors' impact on the response variables. The P-value is the most critical parameter in the model; if the magnitude of this parameter is greater than 0.05 [118, 138], the P-value is usually considered negligible.[110].The magnitude of F-value in the case of BP is highest for engine load, indicating that the engine's BP is primarily affected by varying engine load, according to engine output ANOVA review. For BP, higher-order terms like 2-way interaction and square are irrelevant. The reason for this is that the P-Value is greater than 0.05. Variable engine load is the primary control factor for BTE, followed by the Equivalence ratio and compression ratio. Table 4.30 shows that the magnitude of the F-Value of engine load is greatest for BSFC and BTE. This demonstrates that engine load is the most important factor in improving the engine's efficiency.

Table. 4.30. ANOVA for engine performance parameters.

		BP		BTE		BSFC	
Source	**DF**	**F-Value**	**P-Value**	**F-Value**	**P-Value**	**F-Value**	**P-Value**
Model	9	2234.4	0	238.3	0	68.99	0
Linear	3	6674.72	0	686.26	0	140.24	0
ER	1	0	0.001	2.49	0.123	0.05	0.005
CR	1	0	0.001	22.17	0	2.9	0.0001
EL	1	20024.15	0	2034.13	0	417.77	0
Square	3	2.53	0.071	21.34	0	64.95	0
ER*ER	1	0	1	1.02	0.008	0.02	0.009
CR*CR	1	0	1	0.07	0.003	0.3	0.006
EL*EL	1	7.6	0.009	62.92	0	194.51	0
2-Way Interaction	3	0	1	3.03	0.041	1.45	0.245
ER*CR	1	0	1	1.01	0.002	0.75	0.391
ER*EL	1	0	1	0.98	0.008	0.04	0.85
CR*EL	1	0	1	7.09	0.011	3.55	0.067
Error	38						
Total	47						

According to an ANOVA study of emission parameters, the equivalence ratio has a greater impact on emissions than the compression ratio. Table 4.31 shows that square terms for CO emission prediction are negligible since the magnitude of the P-Value is greater than the required level of significance. Increasing the equivalence ratio increases the concentration of HC in the emission, according to the experiment. The table shows that engine load has the greatest impact on unburned hydrocarbon, followed by the equivalence ratio. The CO_2 F-value indicates that CR is the most important parameter for regulating CO_2 composition in emissions.

For the experimental investigation of engines, emissions are the most influential parameter. The emission table shows that the Equivalence ratio has the greatest effect on NOx concentration, followed by engine load, and finally compression ratio. It's because increasing the equivalence ratio raises the concentration of air within the gasifier, which raises the NOx concentration in the emissions when the gasifier is coupled with an engine. It can be inferred that the equivalence ratio has the greatest effect on the emission parameter.

Table. 4.31. ANOVA for engine emission characteristics

		CO		**HC**		**CO_2**		**NO_x**	
Source	**DF**	**F-Value**	**P-Value**	**F-Value**	**P-Value**	**F-Value**	**P-Value**	**F-Value**	**P-Value**
Model	9	62.07	0	34.44	0	28.32	0	9.99	0
Linear	3	175.09	0	96.43	0	79.44	0	8.33	0
ER	1	6.33	0.016	1.19	0.002	13.66	0.001	11.33	0.002
CR	1	0	0.993	0.3	0.008	61.54	0	5.28	0.027
EL	1	519.36	0	287.8	0	163.13	0	8.38	0.006
Square	3	7.25	0.001	6.13	0.002	3.77	0.018	5.2	0.004
ER*ER	1	1.14	0.292	2.18	0.008	3.69	0.062	13.12	0.001
CR*CR	1	10.26	0.003	1.95	0.001	2.51	0.122	2.33	0.005
EL*EL	1	10.02	0.003	14.26	0.001	5.11	0.03	0.14	0.002
2-Way Interaction	3	4.44	0.009	0.78	0.51	3.26	0.032	16.84	0
ER*CR	1	7.92	0.008	0.02	0.006	3.97	0.053	20.37	0
ER*EL	1	2.92	0.096	0.26	0.001	3.3	0.077	18.68	0
CR*EL	1	2.85	0.1	2.06	0.159	2.52	0.121	11.46	0.002
Error	37								
Total	46								

4.5.6.Parametric impact using contour plot and 3-D surface plot

Equivalence ratio, compression ratio, and engine load have been chosen as decision variables for the analysis as three independent parameters. This is since these three parameters have the greatest influence on raising engine efficiency and lowering emission characteristics. BP, BTE, BSFC, CO, HC, CO2, and NO are the seven production responses.

4.5.7 Common impact of the independent parameters on Brake Power

The power of any engine is mainly attributed to the engine brake power. Brake power is defined as the power available at the crankshaft. Fig.4.55 depicts the simultaneous impact of Equivalence ratio, CR, and EL on the Brake power of the engine. It can be concluded from the Fig.that brake power increases linearly with increasing engine load. It may be due to the reduction in heat loss and increase in power with an increase in load [139]. Brake power almost remains constant with increasing compression ratio. The present optimum results depicts 3.5 kW brake power which is comparable with the results equals to 3.14 kW (BMEP load of 458.37 kPa) obtained by somboatwong et al. [140]. The Fig.also illustrates that the brake power of the engine is almost independent of the Equivalence ratio of the gasifier.

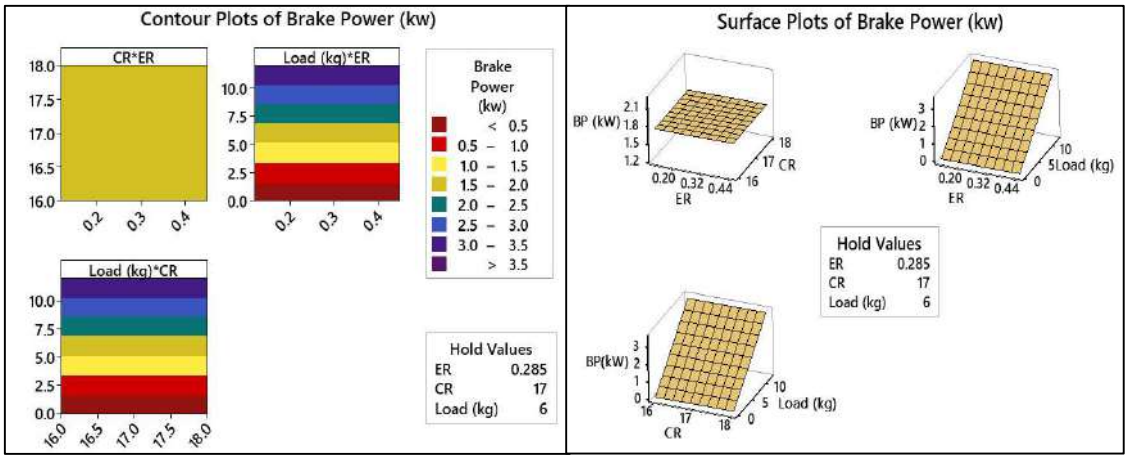

Fig. 4.55. Simultaneous impact of Equivalence ratio, Compression ratio, and Engine load on Brake power

4.5.8 Common impact of the independent parameters on Brake thermal efficiency

Brake thermal efficiency is one of the most important factors to consider when estimating and comparing an engine's output. The BTE authorizes the use of a portion of the fuel energy converted to power the crankshaft. [141]. Fig.4.56 depicts the effect of several independent parameters on the BTE at the same time. The Fig. shows that a higher load and a lower Equivalence ratio of the gasifier improves the engine's brake thermal efficiency. This may be because a low ER increases the engine's combustion efficiency. Result of present study was validated by the experimental result of somboatwong et al. [140], where it shows they have revelead that maximum BTE achieved was 26.65% at pilot diesel whereas it was found from the present investigation that maximum BTE achieved was 31.7% at dual fuel system. On the other hand, it was discovered that engine load and BTE have a clear relationship with the surface plot of BTE. It may be because the engine's thermal performance is higher at higher loads than at lower loads. BTE, on the other hand, was found to increase marginally as the compression ratio was increased. It's possible that the higher compression ratio improves efficiency because of the reduced ignition delay. Because the producing gas is less volatile, the engine's efficiency improves, resulting in improved combustion at high temperatures. Reduced heat loss and increased braking power with applied load also contribute to increased efficiency. The extra oxygen in producer gas promotes better burning, which improves efficiency. Due to lower compression temperature and pressure, a slower combustion process, and more dilution by residual gases, a drop in compression ratio affects efficiency.

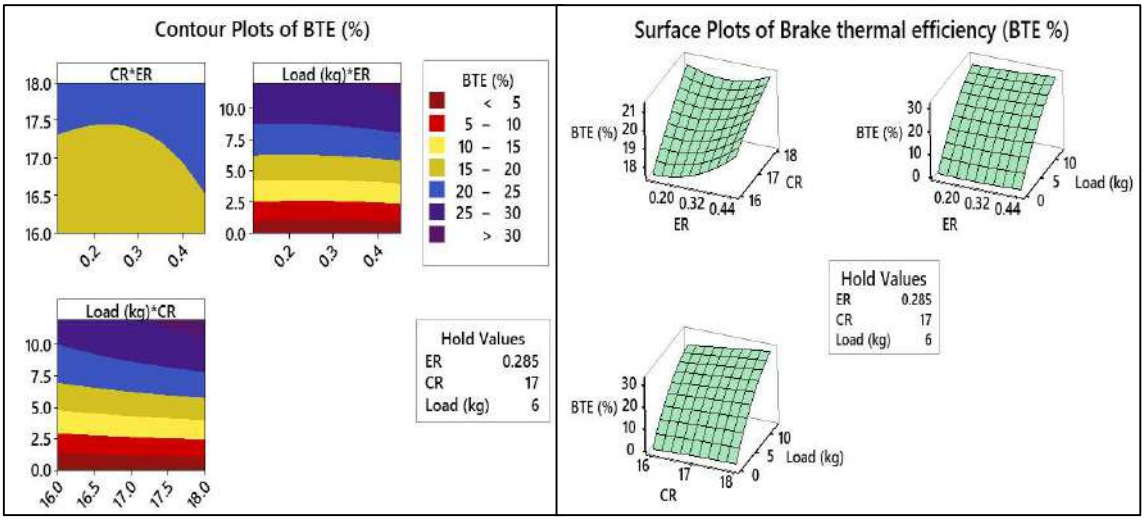

Fig. 4.56. Simultaneous impact of Equivalence ratio, Compression ratio, and Engine load on BTE

4.5.9 Common impact of the independent parameters on Brake specific fuel consumption.

The thermal efficiency of an engine has a gradual impact on the engine's fuel economy. The rate of fuel consumption to generate a unit of BP is known as brake-specific fuel consumption (BSFC). Fig.4.57 depicts the typical effect of multiple decision variables on the BSFC. The Fig.shows that BSFC can be reduced by using a higher Equivalence ratio. However, a deeper examination reveals that the BSFC falls as the compression ratio rises. The explanation for this tendency might be that when CRs rise, the maximum cylinder pressure rises as fuel is fed into a hotter combustion chamber, resulting in more effective power. As a result, fuel consumption per unit of output power will fall [142]. The engine load is directly proportional to BSFC. This is due to a rise in engine power as engine load rises, necessitating the use of more fuel to produce the increased load. BSFC showed a similar pattern of results when the compression ratio on the E6 engine was changed. [143]. It can be concluded that increasing the equivalence ratio reduces BSFC.

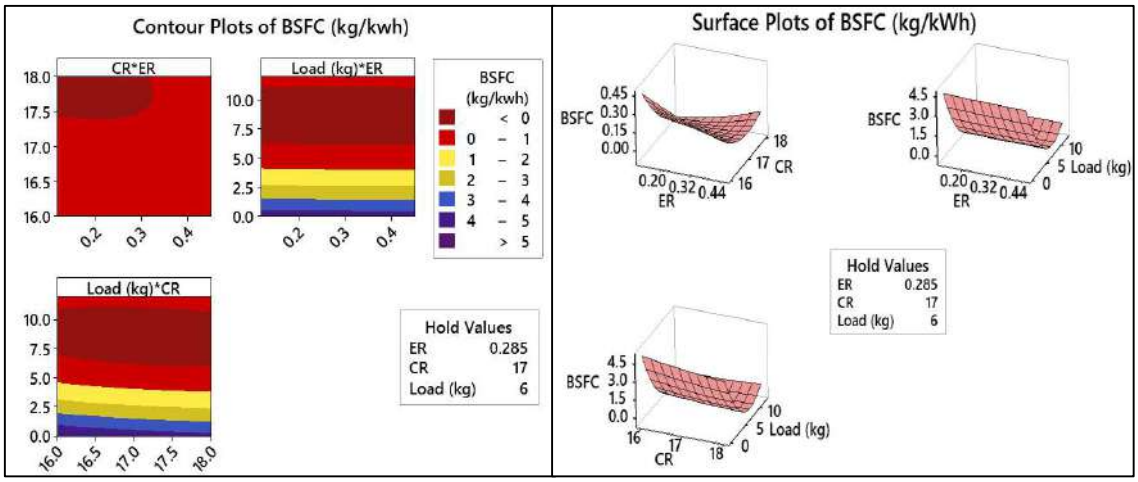

Fig. 4.57. Simultaneous impact of Equivalence ratio, Compression ratio, and Engine load on BSFC

4.5.10 Common impact of the independent parameters on engine exhaust emission

Figures 4.58 and 4.59 show the simultaneous effects of equivalence ratio, engine load, and compression ratio on NOx and CO_2. At room temperature, nitrogen is considered an inert gas. It can only react when the temperature is extremely hot, above 1100^0C.[144]. The amount of NOx produced is determined by the cylinder pressure and temperature. Higher in-cylinder temperature and pressure cause more valance oxygen and nitrogen atoms to develop via air dissociation, resulting in higher NOx emissions at the exhaust. As a result of the greater compression ratios, increased cylinder pressure and temperature result in higher NOx emissions.After reacting with oxygen, it transforms itself into nitrogen oxide [145]. The magnitude of NOx concentration in the emission increases as the equivalence ratio rises above 0.2, as seen in the graph. It may be attributed to the increased amount of oxygen found in rising equivalence ratios, as well as temperature availability. The concentration of NOx also rises as the load rises. This is because as the load on the engine increases, the temperature within the engine rises. Similar results have also been observed by Samet et. al. [144]. The experiment

also shows that increasing the compression ratio raises the magnitude of NOx concentration. It is because of increased combustion inside the cylinder at a higher compression ratio than the temperature inside the engine cylinder gradually rises. The root cause of greenhouse gas and global warming is CO_2 [146]. Fig.4.59 depicts the collective effect of multiple decision variables on CO_2 emission. An upsurge in the concentration of CO_2 emissions is seen till 66.66% of the load. It can been inferred from Fig.4.59 that CO_2 concentration gets increased with increase in the compression ratio. It may be due to higher peak pressure and temperature inside the cylinder.

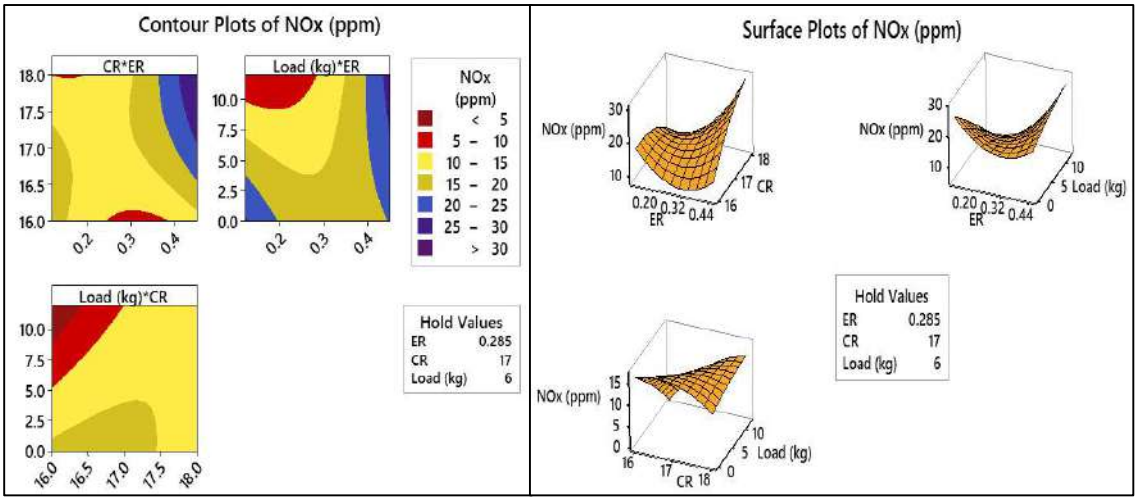

Fig. 4.58. Simultaneous impact of Equivalence ratio, Compression ratio, and Engine load on NO_x emission.

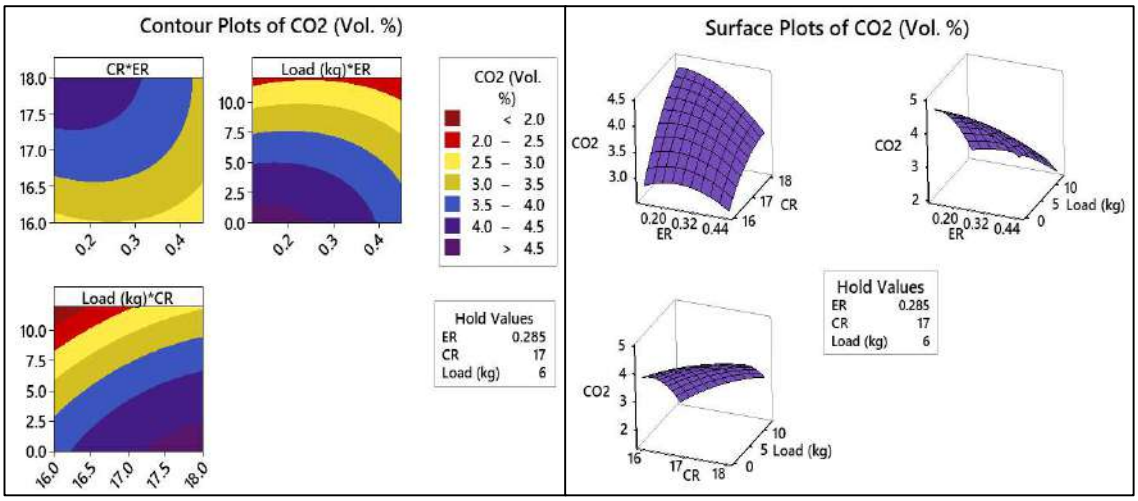

Fig. 4.59. Simultaneous impact of Equivalence ratio, Compression ratio, and Engine load on CO_2 emission

Fig.4.60 depicts the effect of the equivalence ratio and engine load on the unburnt hydrocarbon (UHC). The minimum magnitude of unburned UHC reveals the fuel's combustion efficiency. It has been discovered that growing the ER raises UHC. The increased equivalence ratio is due to the high presence of oxygen. The magnitude of HC decreases as the compression ratio rises. The minimum magnitude of HC can be achieved at a higher compression ratio, i.e. 18, and a lower Equivalence ratio and load percentage, as seen in the plot. Fig.4.61 depicts the impact of the Equivalence Ratio, Engine Load, and Compression Ratio on CO emissions as a whole. Fig.4.56 shows that a higher compression ratio, i.e. 18, and a higher load percentage, i.e. more than 85 percent, minimize CO emission concentration in the exhaust.

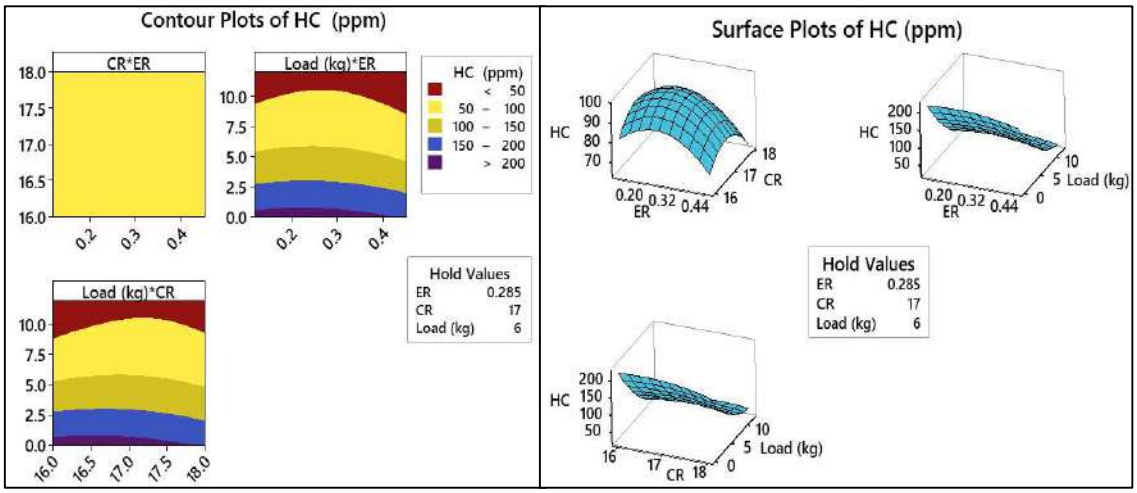

Fig. 4.60. Simultaneous impact of Equivalence ratio, Compression ratio, and Engine load on UHC emission.

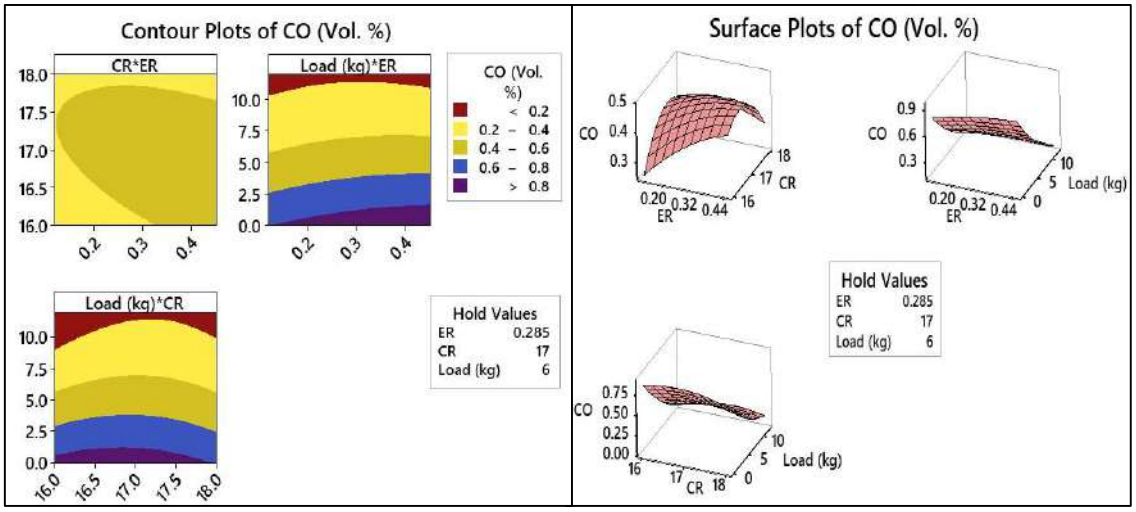

Fig. 4.61. Simultaneous impact of Equivalence ratio, Compression ratio, and Engine load on CO emission.

4.5.11 Response optimizer

After running the simultaneous optimizations of the decision variables, the best output and emission parameters were found. It was obtained from the Minitabs RSM optimizer module, where each answer is described by unitless desirabilities values (d) and magnitude counters ranging from 0 to 1. The minimum value of 0 denotes an unacceptable response, while the maximum value of 1 denotes a desirable response. The answer to the equation of desirability has been classified as either “smaller-the-better” (SB) or “larger-the-better” (LB). The RSM optimizer is depicted in Fig.4.62, where the optimizer program generates results. About 0.9520 was found to be the cumulative composite desirability. 3.52 kW, 26.41 %, 0.48 kg/kWh, 0.0042 percent (percent vol), 15.15 (ppm), 1.27 (vol percent), and 2.94 ppm are the optimum values for BP, BTE, BSFC, CO, UHC, CO2, and NO, respectively. The magnitude for the independent parameters Equivalence ratio 0.12, compression ratio 16, and engine load 12 kg that was optimized. As a result of the current research, it is suggested that coconut shell can be a viable feedstock for generating power for the rural sector using the biomass gasification technique.

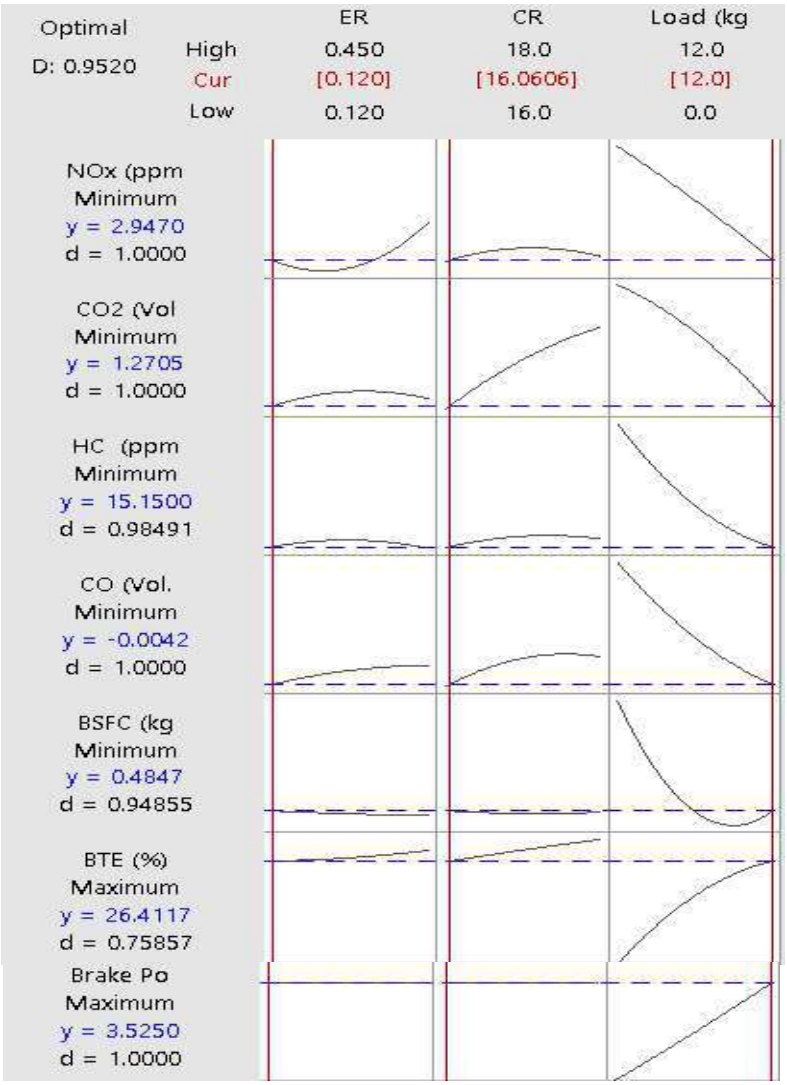

Fig. 4.62. RSM optimizer plot

4.5.12 Summary of the present work

This study aims to optimize three operating parameters: equivalence ratio, compression ratio, and engine load. The RSM optimization technique is used to optimize seven output responses, including efficiency and emission parameters, namely BP, BTE, BSFC, CO, UHC, CO2, and NOx. For the production of producer gas, the Coconut shell was chosen. On the dual-fuel VCR

CI engine, a total of 48 experimental trials were conducted. With a confidence interval of 95%, regression models built from ANOVA results are found to be highly accurate in predicting performance response variables. The most influential parameter for engine performance characteristics, according to the F-Value from ANOVA regression analysis, is engine load. The engine's emission parameters, on the other hand, are largely determined by the gasifier's Equivalence ratio. Using the response optimizer, the optimal values of independent parameters, such as equivalence ratio, compression ratio, and engine load, are 0.12, 16, and 12 kg, respectively. 3.52 kW, 26.41 %, 0.48 kg/kWh, 0.0042 percent (% vol), 15.15 (ppm), 1.27 (vol %), and 2.94 ppm are the optimum values for BP, BTE, BSFC, CO, UHC, CO2, and NO, respectively. The magnitude for the independent parameters Equivalence ratio 0.12, compression ratio 16, and engine load 12 kg that was optimized. The cumulative composite desirability observed was around 0.9520. The RSM model is a useful technique, applied successfully to measure the best engine operating parameters for optimizing engine performance and emissions responses.

4.6 Triple fuelled gasification utilizing Biodiesel, Diesel and Producer gas

At present, there is an escalation of electric power demand because of the exponential growth of population and rapid industrialization. Literature reveals that a gasification-based captive power plant is one of the suitable alternatives. Biomass gasification is one of the promising alternates for gaseous fuel generation due to its renewability and availability. The present work deals with the gasification of waste Madhuca longifolia biomass for producer gas generation and simultaneously induction of PG, Diesel, and Safflower biodiesel in the triple fuel CI engine. The oil output from safflower seed in the lab and the biodiesel yield obtained were 26% and 91%, respectively. Biodiesel was blended with diesel with a blending ratio B20. To

enhance the gasifier-engine performance, the main objective of this analysis is to conduct a parametric experiment and optimization of operating variables for maximizing the engine power and minimizing the exhaust emission. Response surface methodology (RSM) was employed to optimize the input parameters (gasification equivalence ratio, engine compression ratio, and Engine load (EL)) for the best response of output parameters (BP, BTE BSFC, HC, CO, NOx, CO_2). RSM result found indicated the optimum combination of inputs is at 0.2 ER, 17.2 CR, and 73.4% EL, and respective outputs are 2.49 kW BP, 27.57% BTE, 3.31 kg/kWh BSFC, and emission 0.0081 vol% CO, 8.60 ppm-UHC, 1.53 vol.% CO_2, and 182.32 ppm NO_x with the overall desirability of 0.49. Thus, in practice, RSM results could satisfactorily be applied to an integrated co-gasification and triple fuelled mode CI engine with optimum conditions

4.6.1 Experimental setup

The mahua wood, a feedstock for gasifiers, was acquired for the experiment at a local market in Varanasi, Uttar Pradesh, India. The reason for selecting the Mahua tree branch waste was its readily available in the forest site and can be easily transported to the required location. Lohan et al. [147] reported that the Mahua tree is being cultivated in around 62,500-hectare areas in India for a different purpose. The details of Mahua cultivation are shown in **Table 4.32a**. This has a suitable thermal property for gasification like heating value, low ash, and a minor amount of sulfur. The raw safflower seed oil was purchased from a local Varanasi merchant. The oil produced from the seed accounted for 26% of the total. After many weeks of monitoring, the mixes were determined to be stable. **Table 4.32b** depicts the chemical properties of Madhuca longifolia biomass**. Table 4.33** shows the results of a comparative property study of safflower oil and safflower biodiesel using conventional techniques. The output of biodiesel produced from the oil was 91%.

Table 4.32a: Particular Mahua tree (Madhuca longifolia)

***Mahua plant growth* (A-B-C)** 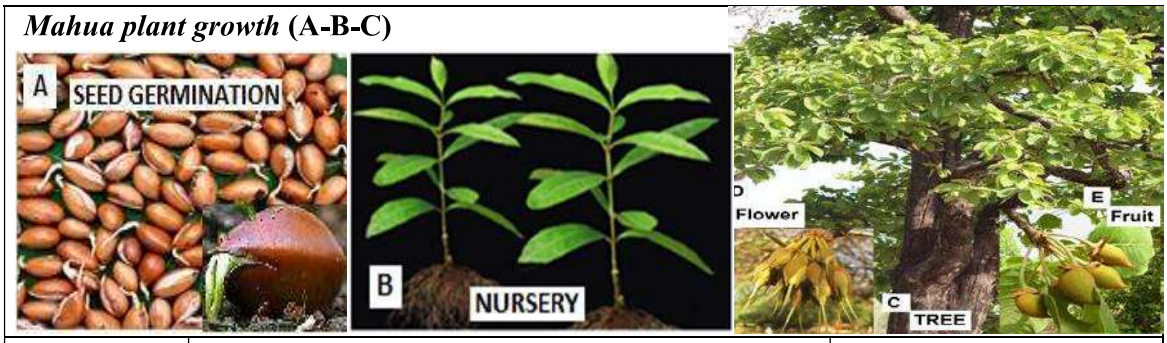		
Particular	**Properties (**for adult tree/ year)	**Reference**
Land	Deep/sandy-loam soil, clayey and calcareous soil	[148] ,[149]
Climate	Mean Temperature: 2-46^{0}C, humidity: 40-90%	[148], [150]
Rain	550-1500mm annual rainfall	[148],[150]
Period	8-15-year gestation and 9-year maturation	[147], [151, 152]
Spacing	7m X 7m plant to plant	[148]
Number	Plants per hectare: 200 no.	[147]
Fruit (kg)	Seed 40-56%, husk 44-60%	[153],[154], [155]
Tree size:	Height 21-23 m, stout trunk, 80 cm diameter	[147],[156]

Table 4.32b: Proximate and ultimate analysis of Madhuca longifolia Biomass

Particular	**Value**
Proximate analysis	***Mahua biomass***
VM	77.05 ± 0.2 %
FC	12.63 ± 0.3 %
Ash	2.08 ± 0.05 %
Moisture content	7.88 ± 0.5 %
Ultimate analysis	***Mahua biomass***
C	47.577 %
H	6.400 %

N	0.722 %
S	0.34 %
CV (MJ/kg)	25.88 ± 0.18
Cellulose	37.92 ± 0.13 %
Hemicellulose	27.33 ± 0.13 %
Lignin content	14.20 ± 0.11 %

The gasifier-ICE experimental design includes a downdraft gasification system with a blower, thermocouple integration, cyclone separator, scrubber, air control valve, test flare, and three-chambered fine filtering system, a compression ignition (CI) engine, and a water pump. Engine regulated 1500 rpm of the engine in a (VCR) CI engine with a water-cooled, naturally aspirated, direct-injection engine. The Engine Soft integration program was used to record engine combustion and performance information on a computer. A manometer and an aperture were utilized to monitor the gas and airflow rates solely. To bring the experimental study to a close, 48 experiments were conducted.

Table. 4.33 Comparative property analysis of safflower oil and its methyl ester [157]

Parameters	**ASTM standard**	**Safflower oil**	**Safflower Biodiesel**
Carbon	--	67	59.5
Kinematic Viscosity (mm^2/s)	D445	28	5.8
Heating value (MJ/kg)	D2015	39	38.122
Density (g/ml)	D1298	0.95	0.88

4.6.2 Experimental procedure

The generation of producer gas from the gasification of mahua wood followed the ICE experimental research. To do so, mahua biomass feedstocks were first led into the gasifier reactor at the same weight fraction in a layer-by-layer fashion through a hopper at the top entrance, and a tiny amount of diesel was sprayed at the ignition point for fast ignition. The air blower was powered. The conflagration was kept close to both the spigot port and the feedstock to avoid catching fire. When the coal was a little red hot and the temperature in the oxidation reaction zone reached around 500^0C and beyond, the valve was opened, enabling water-based scrubbing, cyclone separation, and filtration to proceed. Producer gas is first scrubbed and then cooled in the scrubbing and cooling stage, where the temperature is reduced to near-ambient levels and circulating water attempts to remove water-soluble contaminants such as Hydrogen Sulphide (H_2S) and SO_2 (sulfur dioxide), as well as tar, soot particles, and other contaminants from the PG. A cyclone separator was also used to purify PG further. The flammability of PG has been tested at the checkpoint regularly since then, till the color of the testing flame changes and flares. When the temperature reached 650^0C, the testing flame changed color and flared. Following that, using three-chamber filtering devices, the produced gas was allowed to flow in a sinusoidal pattern (wood dust, rice husk, and heavy cotton fabric). The producer gas from the filtering unit was then endorsed to get in the producer gas storage, the mixing chamber, where the right amount of Producer Gas was combined with the right amount of air, and the control, the valve, and finally the input section of the Engine at a temperature of $35\text{-}55^0$C.

Following the ICE experiment, lab-scale biodiesel conversion from safflower non-edible seed oil was carried out. **Fig.4.63** shows the conversion method for obtaining biodiesel from safflower seed. Initially, safflower oil was taken from its seed then biodiesel was produced from the oil using a transesterification method. Volumetrically, 20 percent methyl alcohol was mixed with 0.4 percent NaOH for the transesterification procedure. The mixture of alcohol and

NaOH was then poured into the glass borosil containing the safflower oil. The combination of all three mixtures was heated to an endurance temperature of 55–65°C and agitated in the transesterification reactor for 2 hours at about 1000 RPM. The mixture was maintained in the separating funnel for 24 hours after 2 hours to allow for the separation of glycerine and methyl ester. Biodiesel was rinsed three times after separation to eliminate any impurities from the methyl ester. Finally, the biodiesel was heated to 110^0C to eliminate any remaining moisture. The obtained fuel, biodiesel, was volumetrically added to diesel fuel at 20%. B20 were the fuel mixtures that resulted from the mixing.

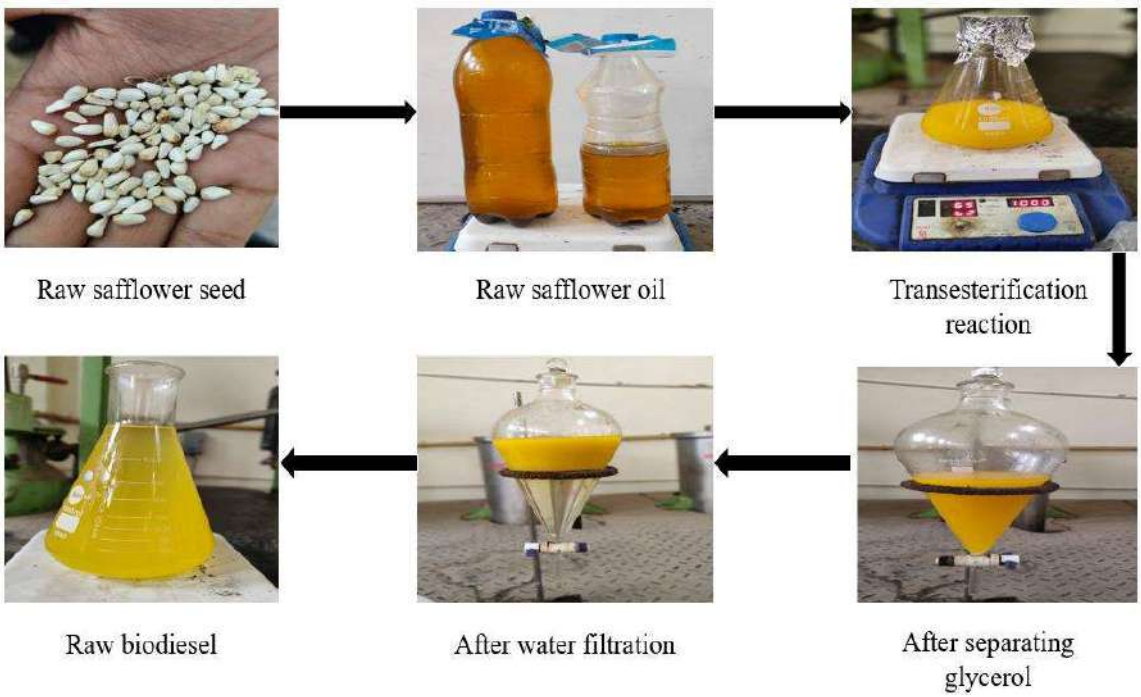

Fig.4.63 Conversion step for extracting lab-scale biodiesel from safflower seed

The test was first carried out in (diesel + biodiesel + producer gas) triple mode only to evaluate the performance of the engine, fuel usage, and emissions with various CR (16,17,18) and engine EL variations (0 to 12 kilogram) at a constant 1500 rpm for a comparative study of the performance of the engine between traditional Diesel and dual-fuelled PG and Diesel engines. The engine's performance and emissions were then evaluated in triple fuel mode at various

compression ratios and ELs. The impact of nozzle opening on the gasifier equivalency ratio on engine performance parameters was also investigated. In cogasification, The mass ratio between the empirical fuel-to-air ratio and the stoichiometric fuel-to-air ratio is called the equivalency ratio (ER). The airbox U tube manometer technique was utilized to calculate the rate of producer gas flow. The "enginesoft" program was used to monitor and record thermal performance metrics such as fuel consumption, braking power, BSFC, BTE, CO, NO, UHC and CO_2.

4.6.3 Experimental uncertainty

Uncertainty is induced as a result of the experimental metering variation. Experimental mistakes and uncertainty in a system are caused by a variety of variables, including result calibration, selecting of instruments, preparation of the test, working conditions, and analysis of data. **Table 4.34** shows the instruments utilized in the experiment, together with the instruments, resolutions, system precisions, and the percent uncertainty of the system. Systematic and precise mistakes, together with the equipment utilized to gather records and round off inaccuracies while observing data, might all contribute to these uncertainties. The entire experimental uncertainty cost was calculated using the equation below.

Total percentage uncertainty

$$= \sqrt{\left\{ \begin{matrix} BP^2 + \text{Tachometer}^2 + \text{Thermocouple}^2 + \text{Dynamometer}^2 + \text{Pressure transducer}^2 \\ +\text{Crank angle sensor}^2 + \text{Fuel measurement}^2 \end{matrix} \right\}}$$

$$= \{(0.39)2 + (0.33)2 + (0.16)2 + (0.2)2 + (0.04)2 + (0.2)2 + (1.0)2\}1/2$$

$$= \pm 1.16$$

Table. 4.34. Apparatus details & Associated uncertainties

SN	Device	Range	Resolution	Precision	Uncertainty (%)
1.	BP	0-3.4 kW	0.1 kW	±0.1 kW	±0.39
2.	Tachometer	1200-1500 rpm	1 rpm	±5 rpm	±0.33
3.	Thermocouple	0-12000C	10C	±20C	±0.16
4.	Dynamometer	0-50 kg	0.01 kg	±0.1 kg	±0.2
5.	PT	0-5000 psi	---	±2 psi	±0.04
6.	Crank angle sensor	0-3600	10	±10	±0.2
7.	Burette	---	---	±0.1 cc	±1.0

4.6.4 Normal Probability Plots

The normality of the data can be verified by plotting the residuals' normal probability plot (NPP). A normal probability plot is a graphical tool for determining if a data set is roughly normally distributed. The residual is the difference between the experimental and the regression's anticipated value (or fitted value). The major distinction between straight lines and scattered data points is residuals. The magnitude of the Residuals in this study ranges from -0.5 to +0.5. The data are regularly distributed if the points on the plot are pretty close to the straight line. The experimental points appeared to be fairly aligned, implying a normal distribution. This demonstrates that the Predicted RSM model is well trained at predicting dependent responses. The main reason behind the difference between straight lines and data points may be attributed to neglecting the higher-order term from the regression equations. The residuals are randomly distributed around zero, implying that the errors have a constant variance. All other points were determined to fall inside the range, and the residuals appear to be randomly spread about zero. The diagonal line (which runs through the theoretical

distribution's bottom and upper quartiles) serves as a visual aid for determining whether the connection between the theoretical and sample percentiles is linear. The theoretical percentiles and the sample percentiles have a nearly linear relationship. As a result, the residuals' normal probability plot indicates that the error terms are normally distributed. For every dependent and independent output and input, the RSM technique is utilized to construct a normal probability plot. The effectiveness of the model is determined by these graphs. The percent value is represented on the Y-axis, while the residuals are plotted on the X-axis. This plot was made with the Minitab program. **Figures 4.64 and 4.65** provide probability graphs for Brake Power, BTE, BSFC, CO, UHC, CO_2, and NO. On these graphs, the output response points are spread. A theoretical normal distribution is a single straight line, but these scattered dots are not. The more deviation of the scattered points from this straight line depicts the lesser efficiency of the RSM model.

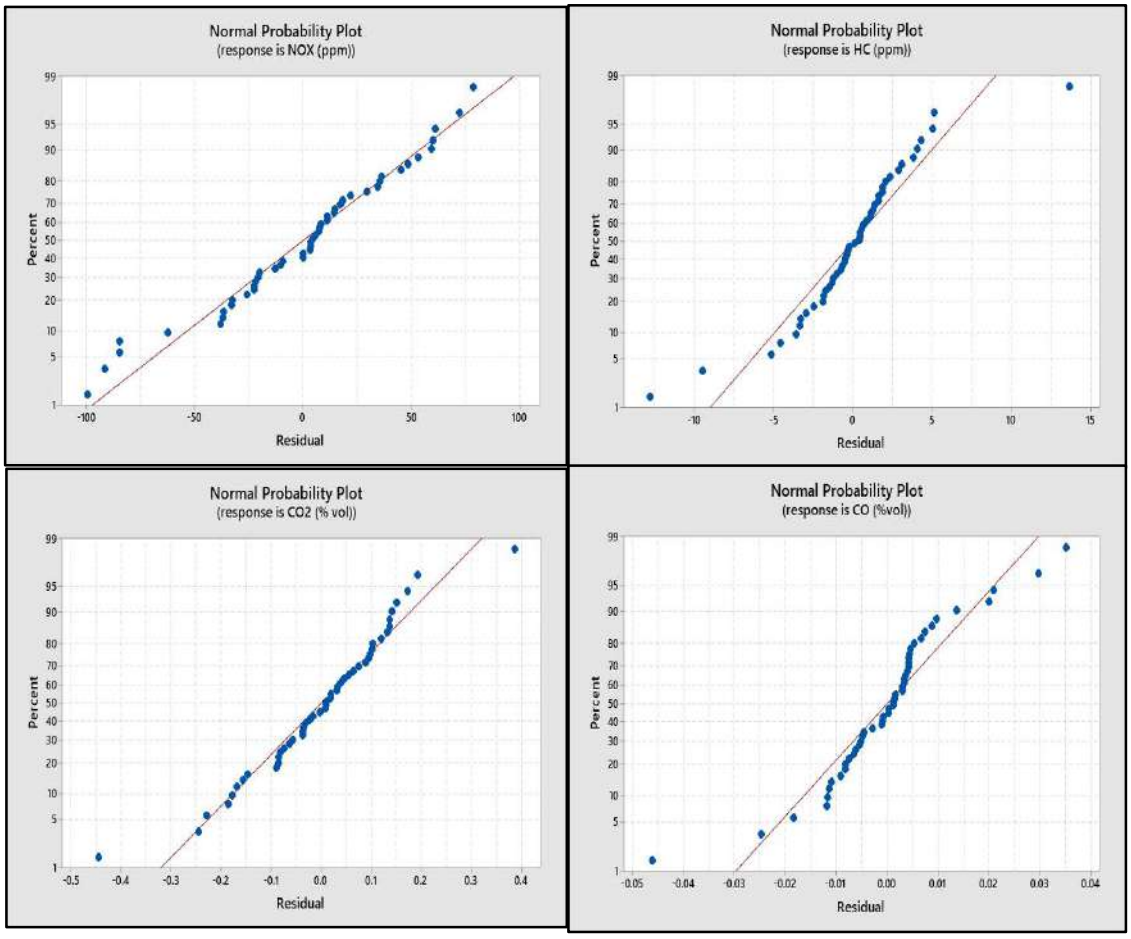

Fig.4.64 Normal probability plots for emission parameter

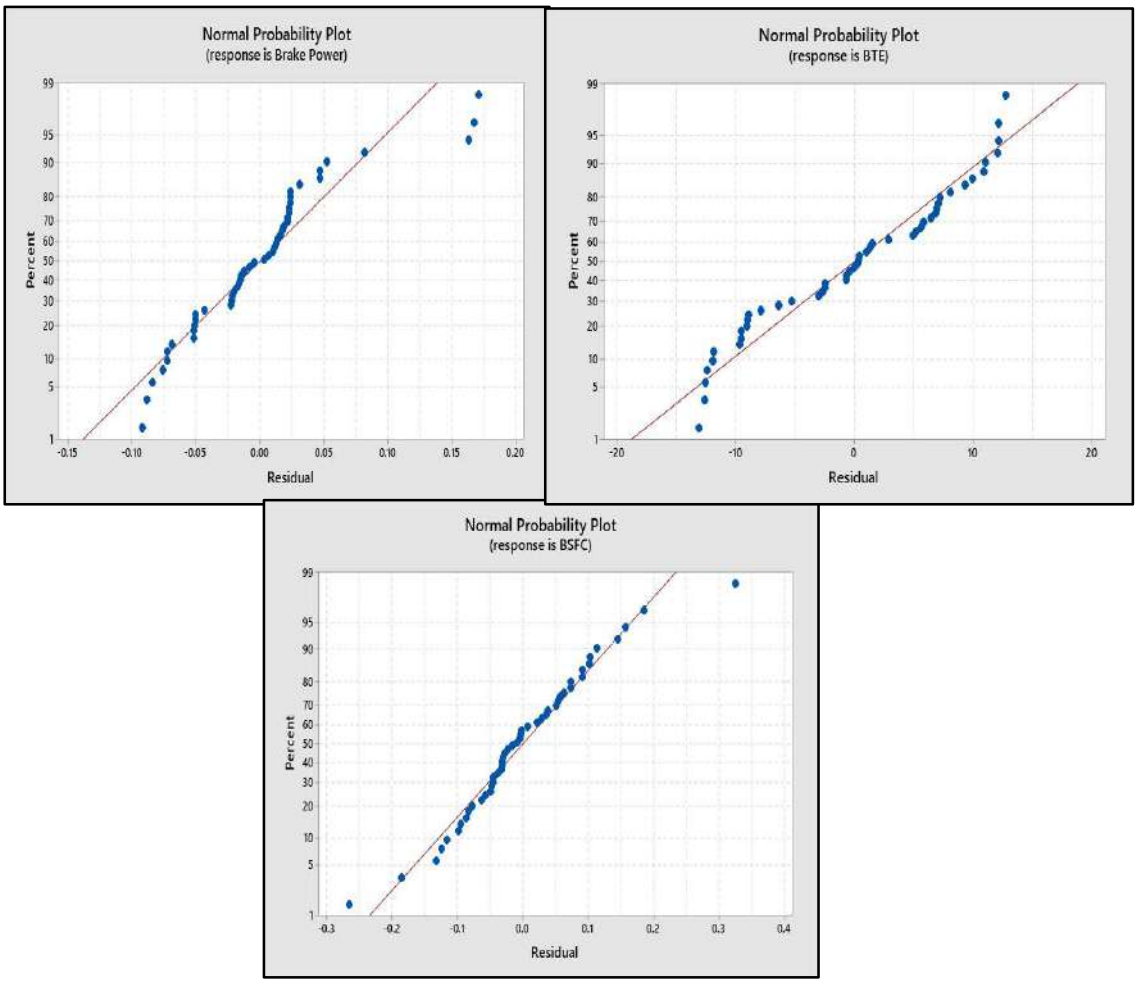

Fig.4.65. Normal probability plots for performance parameter

4.6.5 RSM regression analysis

The Response Surface Methodology (RSM) does a second-order multivariate polynomial regression. The result is a regression model, which is used to predict the target/output based on the input variables. These equations primarily feature a linear term, a square term, and a higher-order two-way interaction term of independent variables to predict output responses. RSM automatically generates the coefficient of all these equations by predicting the relationship between experimental data for independent and dependent responses. The term "non-significant model" refers to a regression model that was unable to effectively predict outputs

based on responses. The efficiency of these equations can be quantified by the magnitude of R^2 value and residuals values. Higher efficiency of the model means a higher magnitude of R^2 value and a lower magnitude of residuals. EL, CR, and the ER were selected as the study's decision variables among three independent characteristics. The seven dependent responses are BP, BTE, BSFC, HC, CO, CO_2 and NO_X. RSM created second-order equations based on independent parameters to estimate performance-dependent parameters, which are illustrated in Eqs. 2-8. Experimental design matrix of 48 trials is tabulated in **table 4.35**

BP = 0.36 - 0.029 ER - 0.032 CR + 0.03492 EL - 0.052 ER*ER + 0.00094 CR*CR - 0.000022 EL *EL + 0.0034 ER*CR - 0.000082 ER*EL - 0.000034 CR*EL (2)

BTE = -188 + 49.6 ER + 21.4 CR + 0.448 EL - 59.9 ER*ER - 0.613 CR*CR - 0.002885 EL *EL - 0.71 ER*CR + 0.0491 ER*EL + 0.00433 CR*EL (3)

BSFC = -22.6 + 5.97 ER + 2.57 CR + 0.0539 EL - 7.20 ER*ER - 0.0737 CR*CR - 0.000347 EL*EL - 0.085 ER*CR + 0.00590 ER*EL + 0.000520 CR*EL (4)

CO = -0.134 + 0.460 ER + 0.0441 CR - 0.006134 EL - 0.017 ER*ER - 0.00187 CR*CR + 0.000014 EL*EL - 0.0159 ER*CR - 0.001773 ER* EL + 0.000240 CR*EL (5)

HC = -92 + 216.8 ER + 16.0 CR - 1.167 EL - 105.0 ER*ER - 0.594 CR*CR + 0.001669 EL*EL - 6.48 ER*CR - 0.506 ER*EL + 0.0544 CR*EL (6)

CO_2 = -26.3 - 5.44 ER + 3.27 CR + 0.0011 EL - 0.34 ER*ER - 0.0969 CR*CR - 0.000206 EL*EL + 0.375 ER*CR + 0.00654 ER*EL + 0.000787 CR*EL (7)

NO_X = 1481 - 688 ER - 181 CR - 1.35 EL + 50 ER*ER + 5.69 CR*CR - 0.03531 EL*EL + 33.9 ER*CR + 2.628 ER*EL + 0.320 CR*EL (8)

Table 4.35. Experimental design matrix of 48 trials

ER	CR	LOAD (%)	BP (kW)	BTE (%)	BSFC (Kg/kWh)	CO (Vol.%)	HC (ppm)	CO_2 (Vol.%)	NO_X (ppm)
0.43	18	0	0.1	2.8163	0.33858	0.125	31.3	1.694	37
0.43	18	33.33	1.2	19.9866	2.40284	0.045	12.3	1.994	162
0.43	18	66.66	2.3	27.1955	3.26951	0.015	7.3	2.094	279
0.43	18	100	3.3	29.3769	3.53175	0.005	0.3	1.294	205
0.43	17	0	0.1	2.9788	0.35811	0.145	32.3	1.494	18
0.43	17	33.33	1.2	20.8849	2.51083	0.085	21.3	1.994	95
0.43	17	66.66	2.3	26.7866	3.22034	0.025	13.3	1.894	213
0.43	17	100	3.3	29.209	3.51157	0.015	6.3	1.294	170
0.43	16	0	0.1	2.9226	0.35136	0.175	42.3	1.294	9
0.43	16	33.33	1.2	18.4035	2.21251	0.085	21.3	1.894	83
0.43	16	66.66	2.3	24.9134	2.99514	0.025	11.3	1.494	159
0.43	16	100	3.3	27.3346	3.28623	0.015	5.3	0.794	99
0.32	18	0	0.1	3.3673	0.40483	0.105	21.3	1.594	44
0.32	18	33.33	1.2	20.4259	2.45564	0.045	13.3	1.894	151
0.32	18	66.66	2.3	26.3897	3.17263	0.015	12.3	1.894	280
0.32	18	100	3.3	29.209	3.51157	0.005	8.3	1.194	208
0.32	17	0	0.1	3.2957	0.39621	0.135	30.3	1.494	19
0.32	17	33.33	1.2	20.4259	2.45564	0.055	19.3	1.994	128
0.32	17	66.66	2.3	25.2668	3.03763	0.025	15.3	1.894	229
0.32	17	100	3.3	27.9321	3.35806	0.005	12.3	0.994	140
0.32	16	0	0.1	2.8684	0.34485	0.165	45.3	1.494	15
0.32	16	33.33	1.2	20.4259	2.45564	0.095	23.3	1.794	70
0.32	16	66.66	2.3	27.4047	3.29466	0.025	16.3	1.494	139
0.32	16	100	3.3	29.5467	3.55217	0.015	11.3	1.094	128
0.21	18	0	0.1	3.5204	0.42323	0.085	22.3	1.494	48
0.21	18	33.33	1.2	19.9866	2.40284	0.035	14.3	1.394	112
0.21	18	66.66	2.3	27.4047	3.29466	0.015	5.3	1.694	235
0.21	18	100	3.3	29.0431	3.49162	0.005	4.3	1.094	202

0.21	17	0	0.1	3.1611	0.38004	0.105	22.3	1.294	8
0.21	17	33.33	1.2	19.1624	2.30375	0.045	13.3	1.694	86
0.21	17	66.66	2.3	26.7866	3.22034	0.015	8.3	1.594	179
0.21	17	100	3.3	30.0681	3.61485	0.005	3.3	1.094	144
0.21	16	0	0.1	2.9788	0.35811	0.135	31.3	1.194	1
0.21	16	33.33	1.2	16.1631	1.94316	0.035	14.3	1.494	106
0.21	16	66.66	2.3	24.2355	2.91364	0.015	9.3	1.194	139
0.21	16	100	3.33	27.1476	3.26375	0.005	5.3	0.794	87
0.1	18	0	0.1	3.0372	0.36514	0.065	9.3	1.294	39
0.1	18	33.33	1.2	14.409	1.73228	0.015	9.3	1.694	223
0.1	18	66.66	2.3	22.9846	2.76326	0.005	7.3	1.394	215
0.1	18	100	3.3	26.2132	3.15141	0.005	1.3	0.794	124
0.1	17	0	0.1	2.383	0.28649	0.095	17.3	1.494	36
0.1	17	33.33	1.2	16.7455	2.01319	0.035	10.3	1.794	152
0.1	17	66.66	2.3	23.9102	2.87453	0.015	9.3	1.394	169
0.1	17	100	3.3	26.7622	3.21741	0.005	6.3	0.794	95
0.1	16	0	0.1	2.383	0.28649	0.125	22.3	1.394	19
0.1	16	33.33	1.2	13.8713	1.66764	0.025	12.3	1.494	123
0.1	16	66.66	2.3	21.5916	2.59579	0.015	7.3	1.094	127
0.1	16	100	3.3	24.3408	2.92631	0.015	4.3	0.794	76

4.6.6 ANOVA assessment

Tables 4.36 and 4.37 show the ANOVA results for engine efficiency and emissions, accordingly, F-value represents the statistical importance of the model, along with variables and their relationships, in the table. The stronger the F factor, the more the influence of the components on the output responses. The P-value is by far the most useful characteristic of the model; if its magnitude is more than 0.05, the P-value is typically regarded as insignificant [110]. According to an engine output ANOVA study, the intensity of F-value in the instance of Brake Power is largest for EL, specifying that the brake power of the engine is predominantly

impacted by fluctuating EL. Higher-order notions such as 2-way interaction and square have no bearing on BP. This is the case since the P-Value is greater than 0.05. The most essential control element for BrakeThermal Efficiency is variable EL, followed by the ER and CR. The size of the F-Value of EL is largest for BSFC and BTE, as shown in Table 4.36. This illustrates that the most essential aspect in increasing engine efficiency is engine load.

Table. 4.36. ANOVA regarding the performance of the engine.

		BP		**BTE**		**BSFC**	
Source	**DF**	**F-Value**	**P-Value**	**F-Value**	**P-Value**	**F-Value**	**P-Value**
Model	9	45113.74	0	338.12	0	68.99	0
Linear	3	135284.78	0	899.18	0	140.24	0
ER	1	0.02	0.003	32.78	0	0.05	0
CR	1	0.17	0.686	7.28	0	2.9	0.0001
EL	1	405854.15	0	2657.47	0	417.77	0
Square	3	56.52	0.741	114.42	0	64.95	0
ER*ER	1	0.11	0.851	16.55	0	0.02	0.009
CR*CR	1	0.06	0	2.63	0.113	0.3	0.006
EL*EL	1	169.38	0	324.09	0	194.51	0
Interaction	3	0.12	1	0.77	0.041	1.45	0.245
ER*CR	1	0.03	1	0.16	0.002	0.75	0.391
ER*EL	1	0.04	1	1.60	0.008	0.04	0.85
CR*EL	1	0.3	1	0.55	0.011	3.55	0.067
Error	38						
Total	47						

The impact of engine load on emissions is greater than the impact of CR, according to an ANOVA investigation of emission characteristics. Square terms for the emission of CO estimation are insignificant since the P-Value is larger than the required threshold of importance as shown in Table 4.37. According to the experiment, the proportion of Hydrocarbon in the emission rises as the ER rises. EL has a significant influence on UHC, accompanied by ER., as seen in the table. The most significant parameter for limiting CO_2 concentration in emissions is the compression ratio, according to the CO_2 F-value Emissions are the most important criterion in engine experimental study.

Table. 4.37. ANOVA regarding emissions from the engine

		CO		**HC**		**CO_2**		**NO_x**	
Source	**DF**	**F-Value**	**P-Value**	**F-Value**	**P-Value**	**F-Value**	**P-Value**	**F-Value**	**P-Value**
Model	9	162.01	0	48.24	0	32.09	0	37.25	0
Linear	3	409.24	0	123.13	0	46.30	0	71.03	0
ER	1	79.78	0	47.25	0	45.61	0.001	2.10	0.155
CR	1	59.02	0	32.71	0	23.23	0	62	0.027
EL	1	1088.91	0	289.44	0	70.08	0	149	0.006
Square	3	51.28	0	8.10	0	47.44	0.018	35.02	0.876
ER*ER	1	0.03	0	7.65	0	0.05	0.062	0.02	0.489
CR*CR	1	0.49	0.870	0.37	0.009	5.43	0.122	0.49	0.00
EL*EL	1	153.33	0.488	16.29	0.546	136.84	0.03	104.56	0.003
Interaction	3	25.51	0	13.49	0	2.51	0.032	5.70	0.381
ER*CR	1	1.60	0.008	2.00	0.165	3.70	0.053	0.79	0
ER*EL	1	41.45	0.096	25.51	0.001	2.34	0.077	9.86	0.03
CR*EL	1	33.48	0.1	12.97	0.001	1.50	0.121	6.45	0.015
Error	37								
Total	46								

4.6.7 Parametric impact using 3-D surface plot

As three independent characteristics, the ER, CR, and EL were selected as choice variables for the investigation. This is because these three variables have the biggest impact on improving engine efficiency and cutting emissions. The seven reactions are BP, BSFC, BTE, CO, CO_2, HC, and NO.

4.6.8 Brake Power

The engine braking power is primarily responsible for an engine's power. The power available at the crankshaft is referred to as brake power. The simultaneous influence of ER, CR, and EL on the engine's BP is depicted in **Fig.4.66.** The graphic shows that braking power grows linearly as engine load increases As the load increases, it might be as a result of a decrease in heat energy loss and an enhancement in power [139]. BP nearly remains constant as the CR rises. The chart also shows that the engine's BP is nearly independent of the gasifier's Equivalence ratio.

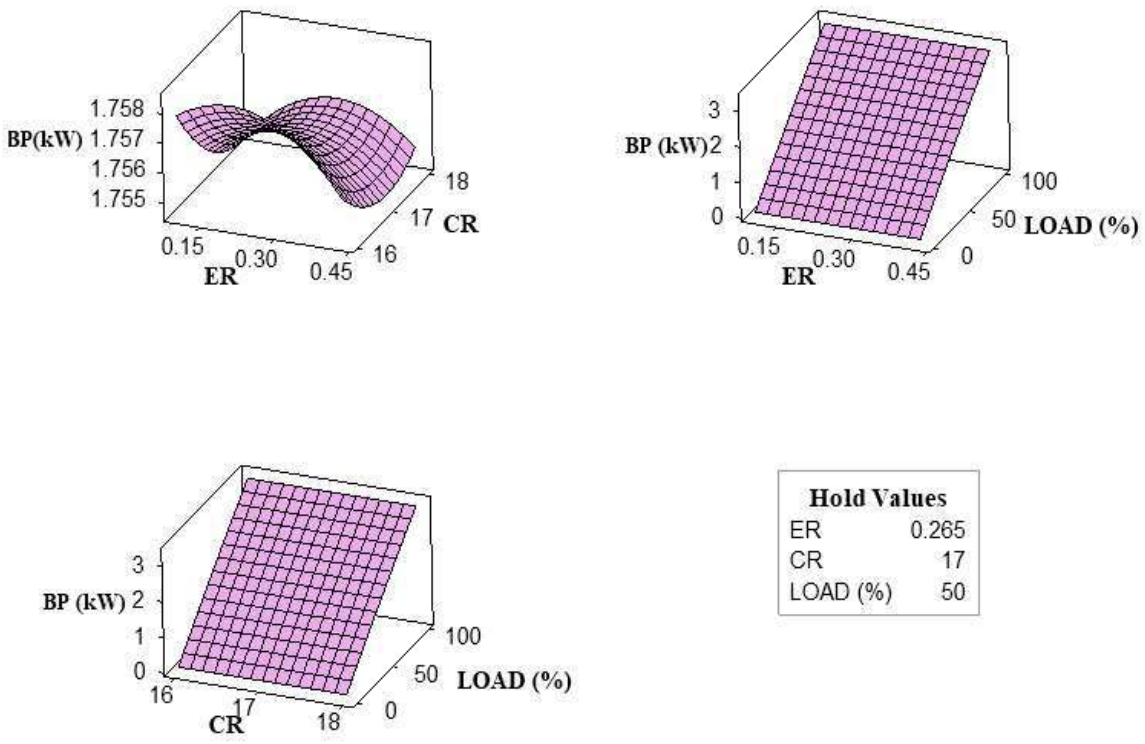

Fig.4.66. Surface plot of BP

4.6.9 Brake thermal efficiency

When evaluating and comparing an engine's power, among the most significant points to consider is brake thermal efficiency. The BTE allows some of the produced fuel energy to be used to propel the crankshaft [141]. **Fig.4.67** demonstrates the simultaneous effect of many independent factors on the BTE. The chart displays how increasing the EL while lowering the gasifier's Equivalence ratio increases the engine's braking thermal efficiency. It might be due to toa low ER improving the combustion efficiency of the engine. The second rationale is that when influential fuel is combined with biodiesel, the influenced fuel's overall lower heating value is reduced. Its because biodiesel has a lower heating value than normal fuel. The experimental data of Somboatwong et al. were used to support the results of this investigation [140], which reveals that the greatest BTE reached was 26.65% at pilot diesel, but the highest BTE obtained was 29.37% at dual fuel system, according to the current analysis. Dhole et al.

[158] investigated the effect on performance and emissions of a dual fuel diesel engine fuelled with hydrogen and PG as the secondary fuel. They found that maximum brake thermal efficiency was 20.7%. In comparison to the dual-fuel mode, brake thermal efficiency increases by approximately 29.51% concerning the triple mode obtained in the present investigation. On the other hand, the surface plot of BTE revealed a definite link between engine EL and BTE. This may be due to the engine's thermal performance being greater at higher ELs than at lesser ELs. The BTE, on the other hand, rose somewhat as the compression ratio was raised. Because of the reduced ignition delay, it's feasible that the greater CR increases efficiency. The efficiency of the engine rises as the generating gas is less volatile, leading to better combustion at high temperatures. Higher efficiency is further boosted by decreased heat loss and increased braking power when EL is used. The extra oxygen in the product gas promotes better burning, therefore improving efficiency. Due to decreased compression temperature and pressure, a lengthier combustion process, and higher dilution by residual gases, a drop in CR affects efficiency.

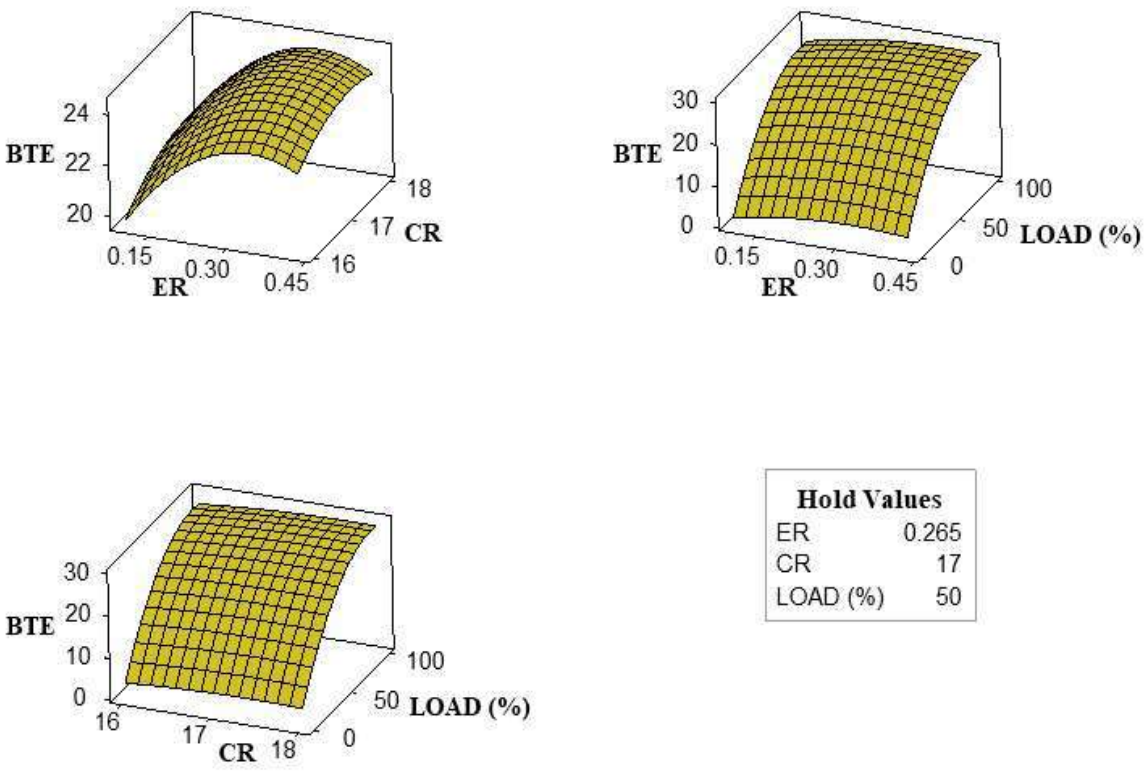

Fig.4.67. Surface plot of BTE

4.6.10 Brake specific fuel consumption.

When evaluating and comparing an engine's power, one of the most significant elements to consider is brake thermal efficiency. The BTE permits a portion of the energy created by the fuel to be utilized to propel the crankshaft [141]. **Fig.4.68** shows the simultaneous influence of multiple independent factors on the BTE. The chart indicates that increasing the load and decreasing the GER increases the BTE of the engine. This might be because a low Equivqlence Ratio improves the engine's combustion efficiency. BSFC demonstrated the same pattern of impacts when the CR of the E6 engine was adjusted[143]. The rise in BSFC can be concluded by raising the equivalency ratio. It might be because higher ER decreases the volatile element in the producer gas, lowering the HHV of the gas. As a result, the producing gas becomes less combustible, and BSFC rises. It's possible to extrapolate that biodiesel decreases BSFC more than diesel when the compression ratio rises. It may be due to a decrease in volatility. It is

found from the comparative analysis of triple mode with dual fuel mode that the magnitude of BSFC was higher in dual fuel mode as compared with triple mode. It may be due to the less amount of fuel consumption in triple mode as compared to dual-mode.

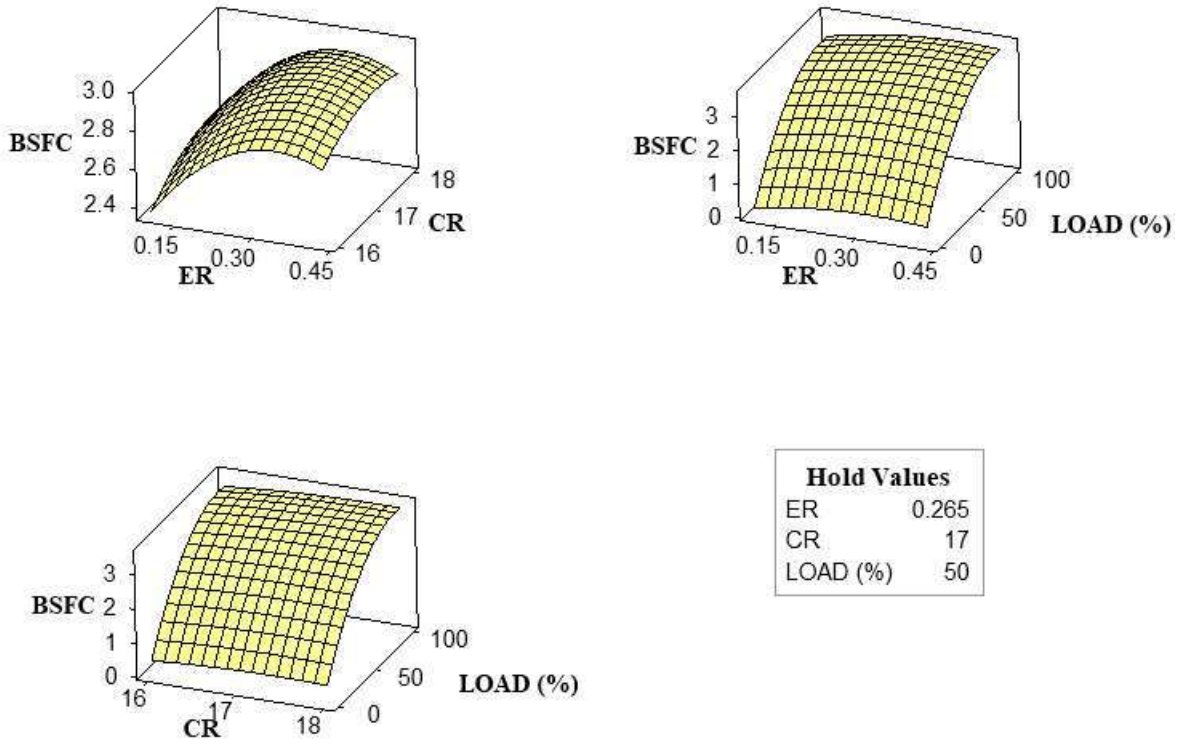

Fig.4.68. Surface plot of BSFC

4.6.11 Engine exhaust emissions

The simultaneous impacts of equivalency ratio, EL, and CR on NOx and CO_2 are shown in **Fig.4.69 and Fig.4.70**. Nitrogen is studied as an inert gas at normal temperature. It can only respond when the temperature exceeds 1100^0C [144]. It converts into nitrogen oxide after interacting with oxygen [145]. As the equivalency ratio grows over 0.2, As can be seen in the figure, the proportion of NOx content in the emission rises. It might be because the supply of oxygen in developing ER is rising, including the availability of oxygen at greater temperatures. As the load increases, so does the concentration of NOx. This is a result of the fact that when

the engine load grows, the temperature inside the engine rises. Samet et al., for example, found similar results [144]. The intensity of NOx levels increases when the CR is increased, according to the experiment. The temperature within the engine cylinder continues to rise due to greater combustion within the cylinder at a higher CR. CO_2 is the primary source of global warming and GHC emissions [146]. The combined effect of numerous choice factors on CO_2 emissions is depicted in Fig.4.69. Until 66.66% of the load, there is an increase in CO_2 emissions concentration. The maximum concentration of NO_x in the dual fuel mode was 300 ppm when producer gas was simply blended with air and diesel fuel [159]. Comparative analysis of the triple fuel mode with the dual-fuel mode on the concentration of NO_x depicts that magnitude of NO_x concentration was approximately 17% lower in triple mode as compared to dual fuel mode. The magnitude of CO_2 concentration was also found to be lower in triple fuel mode as compared to dual fuel mode. It may be due to the biodiesel blending with the diesel fuel.

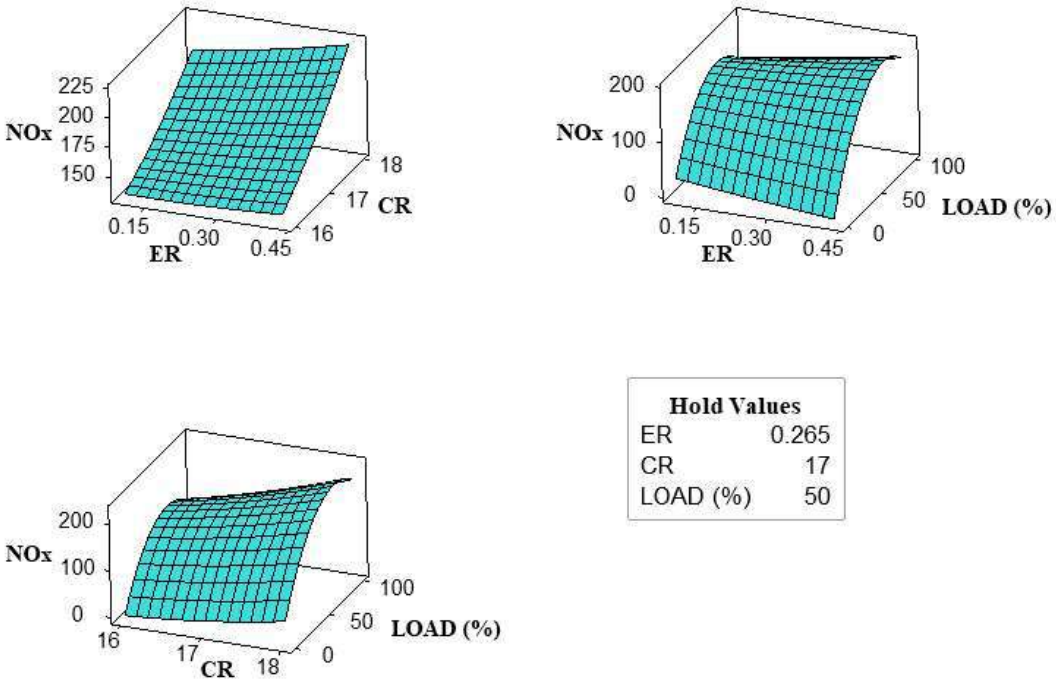

Fig.4.69. Surface plots of NO_x emission.

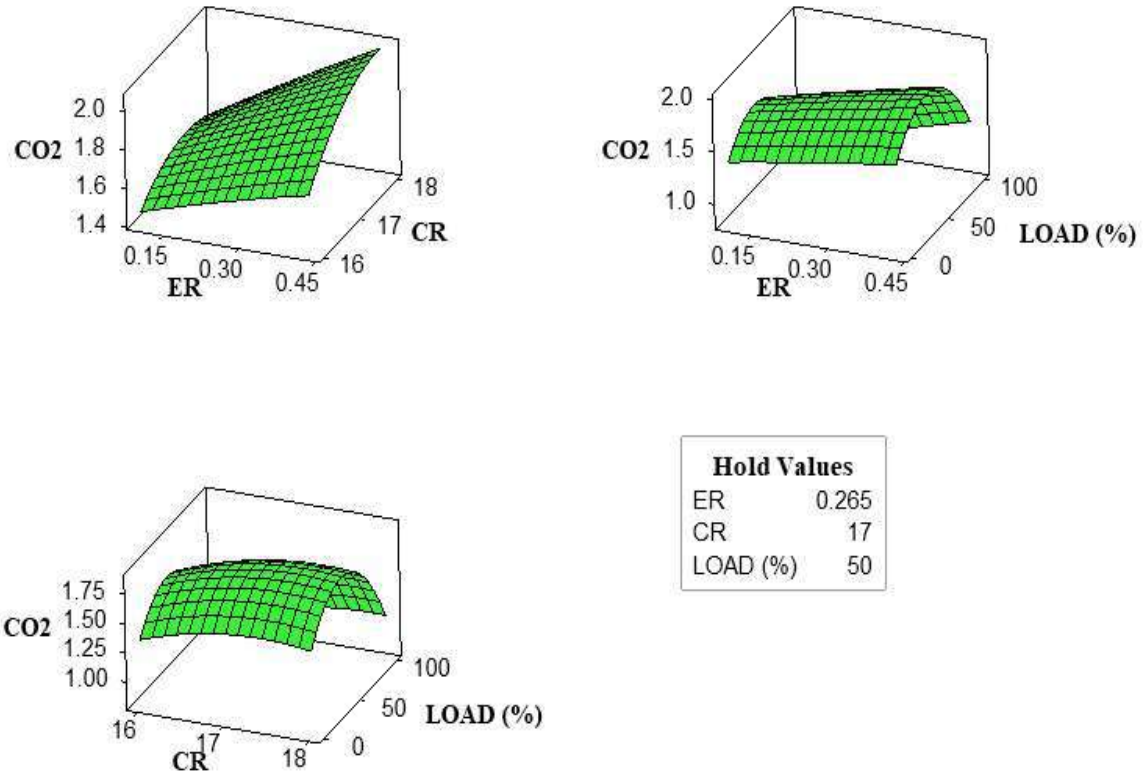

Fig.4.70. Surface plots of CO_2 emission

The impact of the ER and EL on the HC is seen in **Fig.4.71**. The unburned HC's minimal magnitude shows the combustion efficiency of the fuel. Growing the ER has been found to increase HC. Due to the high concentration of oxygen, the equivalency ratio has risen. The size of HydroCarbon decreases as the CR rises. As seen in the plot, the minimal magnitude of HC may be reached by using a greater CR, that is 18, and a lower ER and engine load %. The influence of the ER, EL, and CR on CO emissions as a whole is depicted in **Fig.4.72**. This illustrates that a greater CR, such as 18, and a larger engine load %, such as more than 85%, reduce Carbon monoxide emissions in the exhaust.

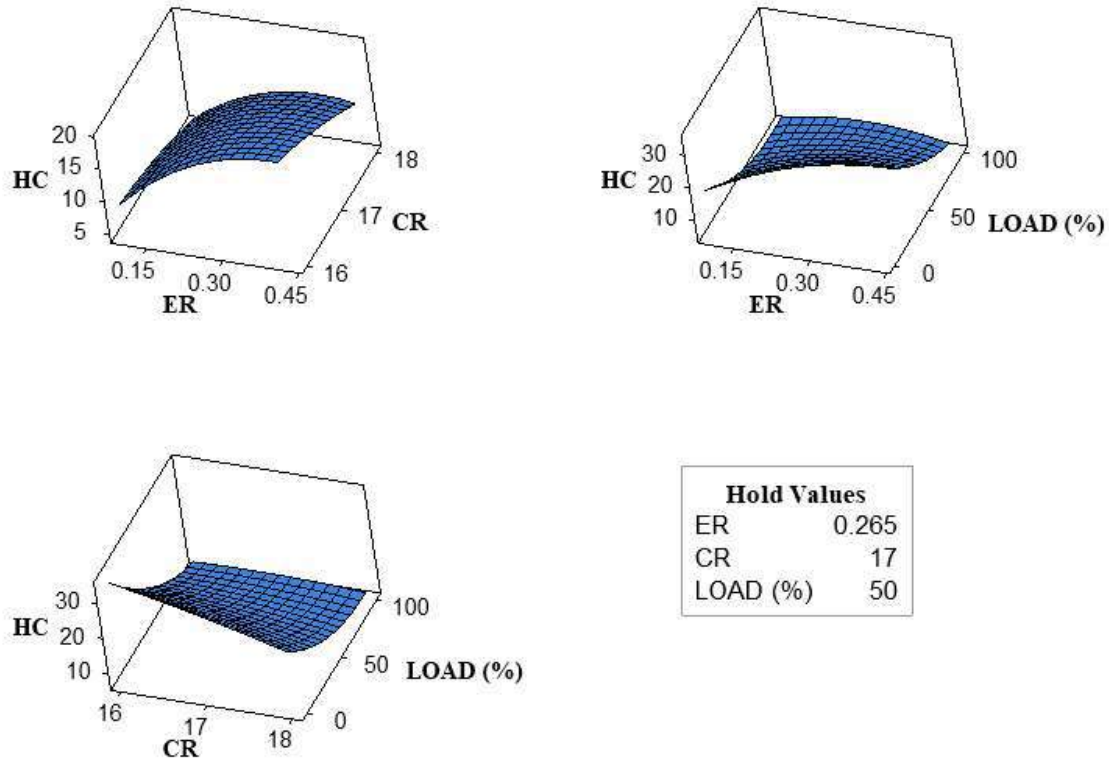

Fig.4.71. Surface plots of UHC emission.

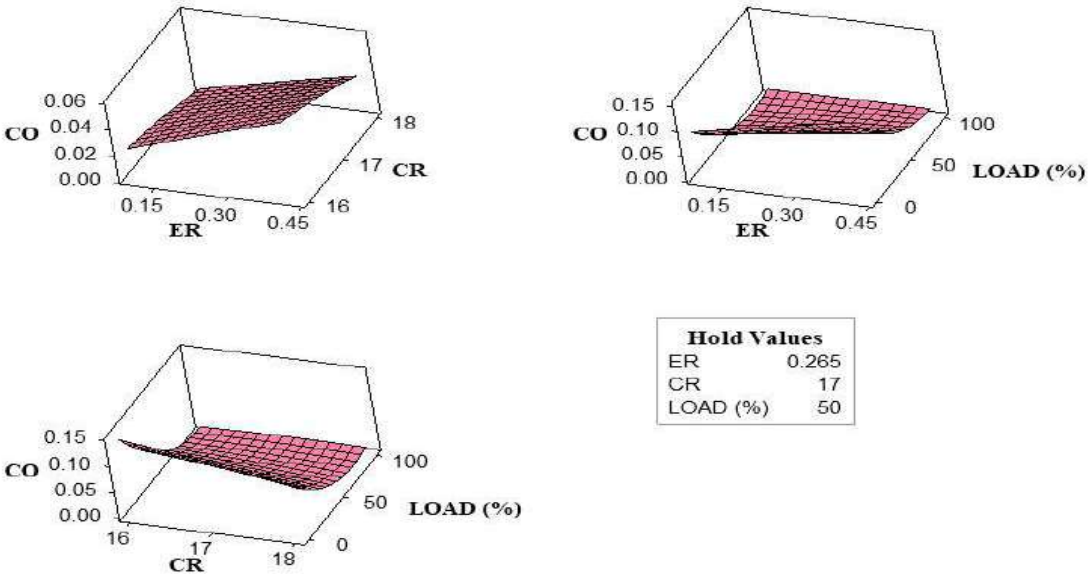

Fig.4.72. Surface plots of CO emission.

4.6.12 Response optimizer

The optimal output and emission parameters were discovered by executing concurrent optimizations of the decision variables. It was generated using the Minitabs RSM optimizer module, which describes each response using unitless desirability values (d) and magnitude counts ranging from 0 to 1. An answer with a minimum value of 0 is considered unsatisfactory, whereas a response with a maximum value of 1 is considered ideal. The solution to the desirability equation has been characterized as "smaller-the-better" (SB) or "larger-the-better" (LB). **Fig.4.73** depicts the RSM optimizer, where the optimizer software provides results. The cumulative composite desirability was discovered to be around 0.4951. The best values for Brake thermal Efficiency, Brake Power, Brake Specific Fuel Consumption, Carbon monoxide, Unburned Hydrocarbon, carbon dioxide, and NO, respectively, are 27.57%, 2.49 kW, 3.31 kg/kWh, 0.0081 (% volume), 8.60 (ppm), 1.53 (% volume), and 182.32 (ppm). The magnitude that was optimized for the independent factors ER 0.2, CR 17.2, and EL 73.4%. According to the current research, waste Mahua biomass might be a suitable feedstock for power generation for the remote population via the biomass gasification method.

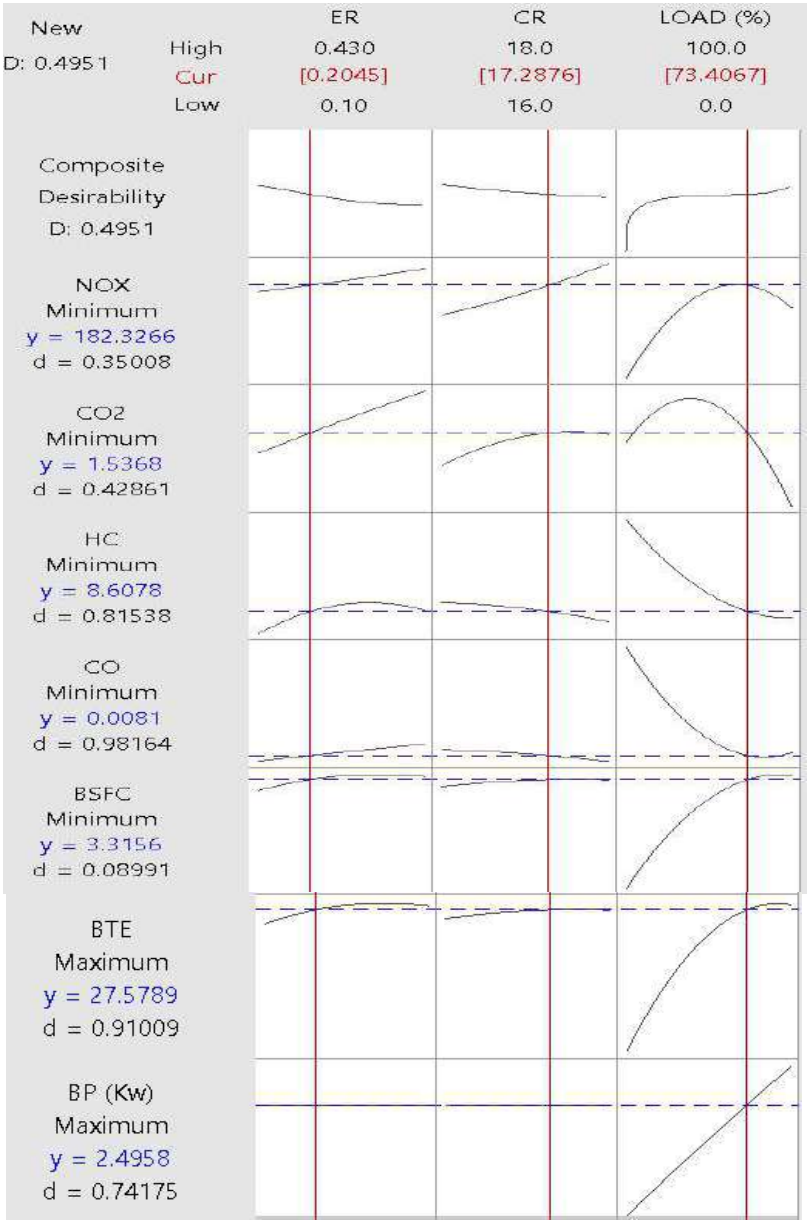

Fig.4.73. RSM optimizer plot

4.6.13 Summary of the present work

The experimental investigation has been successfully conducted to run a triple fulled mode CI engine with producer gas generated from Mahua tree waste and blended with safflower-based biodiesel and diesel. To obtain the best response of performance, optimization has been conducted for input variables such as compression ratio, equivalence ratio, and engine load

using the RSM optimizer tool. The seven responses to the output were BTE, BP, BSFC, CO, CO_2, NOx, and UHC. A total of 48 experiments have been conducted on the VCR CI dual-fuel engine. The biodiesel was blended with diesel at a ratio of B20. The major goal of this analysis is to conduct a parametric experiment and optimization of operating variables to maximize engine power while decreasing exhaust pollution. With a high level of assurance of 95%, regression models generated using ANOVA data have been demonstrated to be quite reliable in predicting performance response variables. According to ANOVA regression analyses' F-Value, Engine load is by far the most essential element for engine performance parameters. The gasifier's Equivalence ratio, on the other hand, controls a large percentage of the engine's emission characteristics. According to the response optimizer, the optimal values of the independent factors like compression ratio, equivalence ratio, and engine load are 17.2, 0.2, and 73.4 % respectively. 27.57%, 3.31 kg/kWh, 2.49 kW, 0.0081 % (vol percent), 1.53 (vol percent), 8.60 (ppm) and 182.91 (ppm) are the best amounts for BTE, BSFC, BP, CO, CO_2, UHC, and NOx, correspondingly. The cumulative composite longing was discovered to be approximately 0.49. RSM model is a valuable tool for identifying the engine operating settings that work well for increasing engine performance and emissions responses. Thus, this study concludes that the CI engine can run effectively and efficiently with triple fuel mode (PG+Biodiesel+Diesel) with optimized operating conditions. Further, this study will provide a base for the end-users and researchers to adopt gasification and integration with IC engines to save conventional fuel and the environment.

4.7 Experimental Investigation on the coal gasification

The efficient and optimum utilization of energy resources could bring an encouraging effect on our well-being, atmosphere, and economy. The purpose of the present study is to determine the optimum engine operating condition of dual fuelled engines using low grade coal-based producer gas (PG) and diesel. To do this, variation of gasifier equivalence ratio, engine compression ratio, and engine load has been considered as Gasifier-IC engine input variables to optimize the response of engine performance and emissions using response surface methodology (RSM). The optimization of input variables is mainly attributed to maximize brake power (BP), brake thermal efficiency (BTE), and minimize the brake specific fuel consumption (BSFC) and exhaust emission (CO, UHC, CO_2, and NO_x). In the experiment, a total of 48 number of the experimental matrix were executed to perform RSM optimization and ANOVA sensitivity test. RSM result reveals that the optimal values of independent parameters of equivalence ratio, compression ratio, and engine load are 0.12, 17.01, and 12 kg respectively. The corresponding optimal repose values of BP, BTE, BSFC, CO, UHC, CO_2, and NO were observed to the value of 3.54 kW, 28.23 %, 0.38 kg/kWh, 0.0231 (% vol), 4.2539 (ppm), 0.9569 (vol %), and 9.6958 ppm respectively. Maximum diesel saving at compression ratio (CR) 16, 17, and 18 observed was 14.38%, 22.48%, and 49.05% respectively using Dual fuel mode.

4.7.1 Test fuels

Low-grade coal was obtained for the experiment from the local market of Varanasi, Uttar Pradesh, India, and belonged to the open cast mines of Madhya Pradesh and Bihar state mines. In this study, hard coke, a low-grade coal, was employed for the experimental research; table 4.38 lists the coal characteristics in detail.

Downdraft gasification system with thermocouple integrated, blower, air control valve,

scrubber, cyclone separator, test flare, water pump, three-chamber for fine filtering system, and combined with compression ignition (CI) engine make up the gasifier-ICE experimental configuration. Variable compression ratio (VCR) engine with direct injection, water-cooled, naturally aspirated engine, eddy current dynamometer, and governor regulated 1500 engine rpm. Engine combustion and performance parameters were recorded on a computer using the Engine Soft integration software. The air and gas flow rates were measured independently using an orifice and a manometer. Add Gasifier operating procedure—A total of 48 trials were carried out to conclude the experimental research.

Table. 4.38. Basic property of hard coke-low grade coal [160]

Particular	**Value**
Proximate analysis	
Fixed carbon (%)	57.5
Ash (%)	39.52
Volatile matter (%)	1.31
Moisture (%)	1.67
Ultimate analysis	
Carbon (%)	58.999
Hydrogen (%)	0.215
Nitrogen (%)	0.546
Sulphur (%)	0.304
Gross Calorific Value (MJ/kg)	17.371

4.7.2 RSM Normal Probability Plots

Using normal probability plots, the normality hypothesis for the computed data was particularly verified [137]. It's also known as inquiry plots, and it's a type of plot used to examine residual distributions. Responses are dispersed throughout a theoretical normal distribution, with the point forming a roughly straight line and variations from this line indicating residual magnitude. The Y-axis denotes % worth, whereas the X-axis represents residual. This narrative was created using Minitab software. A supplemental file with a normal distribution, which is one of the prerequisites for ANOVA's validity, contains normal probability graphs of BP, BTE, BSFC, CO, CO2, HC, and NOX. These mathematical models were created using least-square methods, which are multiple regression procedures that adapt a model to set the experimental results with less problems.

4.7.3 RSM regression analysis

Equivalence ratio (ER), Compression ratio (CR), and Engine Load were chosen as the study's decision variables among three independent characteristics. The seven production responses are BP (kW), BTE (percent), BSFC (kg/kWh), HC (ppm), CO (vol. percent), CO2 (vol. percent), and NOX (vol. percent) (ppm). RSM created second-order equations based on independent parameters to estimate performance-dependent parameters, which are illustrated in Eqs. 2-8.

Brake Power = -4.50 + 0.47 ER + 0.57 CR + 0.2034 Load + 0.96 ER·ER - 0.0174 CR·CR + 0.001550 Load·Load - 0.063 ER·CR + 0.0094 ER·Load + 0.00386 CR·Load (2)

BTE = 126 - 56.7 ER - 13.6 CR + 2.26 Load - 15.8 ER·ER + 0.363 CR·CR - 0.1749 Load·Load+ 3.83 ER·CR + 0.849 ER·Load + 0.1170 CR·Load (3)

BSFC = 12.9 + 1.7 ER - 0.99 CR - 1.114 Load - 1.38 ER·ER + 0.027 CR·CR + 0.05408 Load·Load- 0.091 ER·CR + 0.056 ER·Load + 0.0093 CR·Load (4)

$$CO = 3.50 - 3.79\ ER - 0.347\ CR + 0.0277\ Load - 0.930\ ER \cdot ER + 0.0091\ CR \cdot CR + 0.001048\ Load \cdot Load + 0.2739\ ER \cdot CR - 0.0320\ ER \cdot Load - 0.00359\ CR \cdot Load \quad (5)$$

$$HC\ (ppm) = 1389 - 805\ ER - 146\ CR + 1.48\ Load - 493\ ER \cdot ER + 3.95\ CR \cdot CR + 0.488\ Load \cdot Load + 66.0\ ER \cdot CR - 7.04\ ER \cdot Load - 0.718\ CR \cdot Load \quad (6)$$

$$CO_2\ (\%vol) = 10.8 - 16.16\ ER - 0.83\ CR + 0.084\ Load - 1.14\ ER \cdot ER + 0.0207\ CR \cdot CR - 0.01751\ Load \cdot Load + 0.916\ ER \cdot CR + 0.1680\ ER \cdot Load - 0.00194\ CR \cdot Load \quad (7)$$

$$NOx\ (ppm) = 706 - 551\ ER - 70\ CR - 18.04\ Load + 498\ ER \cdot ER + 1.81\ CR \cdot CR - 0.1384\ Load \cdot Load + 16.1\ ER \cdot CR + 12.91\ ER \cdot Load + 1.067\ CR \cdot Load \quad (8)$$

4.7.4 Gasifier performance and diesel saving

The quality of the produced gas in terms of heating value can be used to measure gasification performance. Cold gas efficiency, lower heating value, and energy distribution are the key performance criteria of the gasifier [161]. It may be defined as the ratio of producer gas heating value to biomass heating value. The coal gasification experiment yielded 33.06 percent cold gas efficiency and a lower heating value of 2.08 MJ/Nm3, respectively. The energy distribution in the gasifier is depicted in Fig.4.74 using a Sankey diagram. From the Sankey diagram, it can be deduced that about 33% of the energy was transferred from coal to producing gas. Total energy losses, including tar residues, account for around 49% of total energy losses. This energy loss might be caused by small gas leakage caused by the perimeter of temperature sensors, the gasifier lid, and other pipe connections. The composition of the producer gas generated from coal gasification at 0.2 equivalency ratio H_2, CO, CO_2, CH_4, and N_2 is around 7-10%, 5-8%, 10-15%, 1-3%, and 70-85 percent, respectively. Table 4.39 shows the experimental data matrix for independent and dependent parameters.

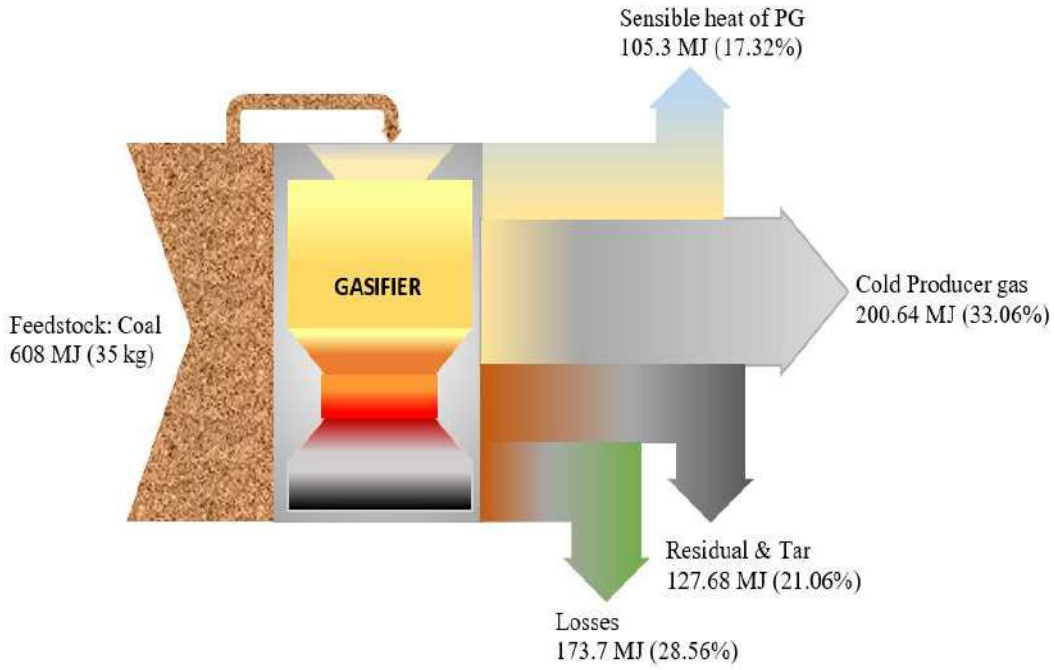

Fig. 4.74. Sankey diagram for energy balance in gasifier.

Table 4.40 shows that at greater compression ratios, diesel savings are the largest for all compression ratios at all load conditions. The information that greater compression ratios enhance the engine's thermal efficiency may be ascribed to. Table 4.40 shows the consumption of diesel and producer gas, as well as the mass flow rate of air and gas. When producer gas is used in conjunction with diesel, the amount of diesel consumed is reduced. It was also discovered that when the CR increases, the consumption of producing gas as gaseous fuels increases, resulting in proper gaseous fuel combustion. The greatest diesel savings recorded were 49.05 percent with CR 18 at an 8 kilogram load, 22.3 percent with CR 17 at no load, and 10.09 percent with CR 16 at a 4 kg load. Table 4.40 shows that blending producing gas with diesel is cost-effective, as diesel savings increase to 49.05 percent

Table. 4.40. Comparative analysis of diesel and producer gas diesel saving

CR	Load (kg)	Brake power (kW)	Diesel mode		Dual-mode			Diesel saving (%)
			Diesel (kg/h)	Air (kg/h)	Diesel (kg/h)	Air (kg/h)	Producer gas (kg/h)	
16	0	0	0.318	26.34	0.278	21.59	4.75	14.38
	4	1.3	0.542	25.92	0.488	21.33	4.59	9.96
	8	2.4	0.742	25.29	0.677	20.82	4.47	8.76
	12	3.4	0.926	24.63	0.871	20.29	4.34	5.93
17	0	0	0.378	27.15	0.293	21.59	5.56	22.48
	4	1.3	0.607	26.54	0.488	21.33	5.21	19.6
	8	2.4	0.761	25.92	0.687	20.82	5.1	9.72
	12	3.4	0.931	25.29	0.891	20.29	5	4.29
18	0	0	0.388	27.15	0.303	21.84	5.31	21.90
	4	1.3	0.577	26.54	0.363	20.82	5.72	37.08
	8	2.4	0.791	25.71	0.403	20.56	5.15	49.05
	12	3.4	0.926	25.68	0.602	20.02	5.66	34.98

Table. 4.39. Experimental design matrix for 48 trials

ER	CR	Load (kg)	BP (kW)	BTE (%)	BSFC (kg/kWh)	CO (%vol)	HC (ppm)	CO_2 (%Vol)	NO_x (ppm)
0.43	18	0	0.1	2.49	3.3294	0.67	137	2.7	5
0.43	18	4	1.1	20.04	0.41495	0.37	56	2.7	15
0.43	18	8	2.4	30.97	0.2685	0.14	12	2.5	58
0.43	18	12	3.5	33.67	0.24702	0.04	5	1.8	108
0.43	17	0	0.1	2.03	4.0812	0.33	66	2.1	9
0.43	17	4	1.1	16.22	0.51259	0.21	30	2.4	29
0.43	17	8	2.4	25.46	0.32667	0.1	9	1.9	58

0.43	17	12	3.5	29.14	0.28537	0.04	2	1.1	52
0.43	16	0	0.1	1.98	4.1886	0.28	52	1.9	9
0.43	16	4	1.1	15.63	0.53211	0.2	30	2.2	20
0.43	16	8	2.4	26.37	0.31548	0.1	13	1.9	45
0.43	16	12	3.5	28.69	0.28998	0.04	2	1	32
0.32	18	2	0.1	2.247	3.7053	0.36	88	2.5	6
0.32	18	4	1.1	17.22	0.4833	0.25	49	2.8	11
0.32	18	8	2.4	28.38	0.29311	0.14	18	2.5	24
0.32	18	12	3.5	31.52	0.26390	0.03	3	0.9	14
0.32	17	0	0.1	2.093	3.9738	0.46	109	2.6	9
0.32	17	4	1.1	16.54	0.50283	0.29	52	2.7	15
0.32	17	8	2.4	26.94	0.30878	0.13	20	2.1	23
0.32	17	12	3.5	30.27	0.27464	0.05	8	1.2	18
0.32	16	0	0.1	1.986	4.1886	0.41	93	2.3	9
0.32	16	4	1.1	15.78	0.52724	0.25	44	2.4	16
0.32	16	8	2.4	27.54	0.30206	0.13	21	2	28
0.32	16	12	3.5	31.70	0.262363	0.05	5	1.1	24
0.21	18	0	0.1	2.213	3.759	0.34	86	2.4	6
0.21	18	4	1.1	17.21	0.4833	0.25	51	2.7	10
0.21	18	8	2.4	27.95	0.2976	0.1	19	1.8	13
0.21	18	12	3.5	32.46	0.25623	0.04	9	1.3	21
0.21	17	0	0.1	2.151	3.8664	0.39	99	2.7	5
0.21	17	4	1.1	16.71	0.49795	0.25	56	2.6	8
0.21	17	8	2.4	26.94	0.30878	0.09	4	1.8	10
0.21	17	12	3.5	29.79	0.27924	0.03	2	1	8
0.21	16	0	0.1	1.912	4.3497	0.4	105	2.8	13
0.21	16	4	1.1	15.35	0.54188	0.21	51	2.4	12
0.21	16	8	2.4	25.64	0.32444	0.13	31	2.4	18
0.21	16	12	3.5	28.69	0.28998	0.03	13	1	13
0.1	18	0	0.1	2.011	4.1349	0.25	48	2.6	9
0.1	18	4	1.1	15.21	0.54676	0.18	27	2.7	15

0.1	18	8	2.4	24.95	0.33339	0.07	12	2.2	32
0.1	18	12	3.5	26.84	0.30993	0.02	6	0.9	18
0.1	17	0	0.1	1.912	4.3497	0.29	57	2.7	8
0.1	17	4	1.1	14.95	0.55653	0.2	35	2.8	12
0.1	17	8	2.4	24.95	0.33339	0.1	16	2.2	20
0.1	17	12	3.5	27.38	0.30379	0.03	5	0.9	9
0.1	16	0	0.1	1.912	4.3497	0.32	75	2.3	9
0.1	16	4	1.1	15.21	0.54676	0.24	47	2.7	12
0.1	16	8	2.4	26.18	0.31773	0.11	23	2	18
0.1	16	12	3.5	27.24	0.30532	0.03	10	1	11

4.7.5 ANOVA analysis

Tables 4.41 and 4.42 show the results of the ANOVA for engine efficiency and emission, respectively. The F-value in the table depicts the statistical significance of the model, as well as variables and their interactions. The larger the size of the F factor, the greater the influence of the factors on the response variables. The P-value is the most important parameter in the model; if its magnitude is larger than 0.05, the P-value is typically regarded as insignificant [110]. According to an engine output ANOVA study, the magnitude of F-value in the case of BP is largest for engine load, indicating that the engine's BP is largely impacted by variable engine load. Higher-order concepts like 2-way interaction and square have no bearing on BP. Because the P-Value is larger than 0.05, this is the case. The major control factor for BTE is variable engine load, followed by the Equivalence ratio and compression ratio. The size of the F-Value of engine load is largest for BSFC and BTE, as shown in Table 4.41. This indicates that the most significant element in increasing engine efficiency is engine load

Table. 4.41. ANOVA for engine performance parameters.

Source	DF	BP		BTE		BSFC	
		F-Value	P-Value	F-Value	P-Value	F-Value	P-Value
Model	9	892.18	0	200.29	0	53.37	0
Linear	3	2667.8	0	568.19	0	114.35	0
ER	1	0.13	0.009	6.26	0.017	0.19	0.001
CR	1	0.99	0.007	2.25	0.142	0.1	0
Load	1	8003.37	0	1693.12	0	342.44	0
Square	3	1.34	0.276	39.63	0	49.7	0
ER·ER	1	0.66	0.423	0.56	0.46	0.06	0.812
CR·CR	1	0.33	0.57	0.45	0.507	0.03	0.854
Load·Load	1	2.92	0.096	117.04	0	149.07	0
2-Way Interaction	3	0.41	0.744	2.76	0.056	0.14	0.933
ER·CR	1	0.2	0.659	2.27	0.14	0.02	0.897
ER·Load	1	0.13	0.722	3.33	0.076	0.19	0.662
CR·Load	1	0.93	0.34	2.7	0.108	0.23	0.638
Error	38						
Total	47						

Load has a higher influence on emissions than compression ratio, according to an ANOVA analysis of emission characteristics. Because the size of the P-Value is larger than the necessary threshold of significance, square terms for CO emission prediction are inconsequential, as shown in Table 4.42. According to the experiment, increasing the equivalency ratio increases the concentration of HC in the emission. The engine load has the largest influence on unburned hydrocarbon, followed by the equivalency ratio, as seen in the table. CR is the most significant parameter for managing CO_2 composition in emissions, according to the CO_2 F-value. The most important parameter in the experimental examination of engines is emissions. The load

has the largest impact on NOx concentration, followed by the equivalency ratio, and lastly the compression ratio, according to the emission table. This is because when the load increases, the fuel supply of a diesel engine increases, the combustion temperature in the cylinder improves, and the working fluid's residence time in the cylinder at high temperature increases, resulting in an increase in NOx emissions.

Table. 4.42. ANOVA for engine emission

Source	DF	CO		HC		CO_2		NO	
		F-Value	P-Value	F-Value	P-Value	F-Value	P-Value	F-Value	P-Value
Model	9	47.28	0	40.16	0	52.45	0	11.19	0
Linear	3	132.29	0	105.16	0	111.94	0	18.99	0
ER	1	11.65	0.002	0.87	0.003	0.61	0.441	26.62	0
CR	1	2.51	0.002	0.31	0.002	9.99	0.003	1.2	0.001
Load	1	384.09	0	314.66	0	326.52	0	28.74	0
Square	3	3.1	0.038	11.3	0	32.95	0	5.81	0.002
ER·ER	1	2.9	0.097	12.63	0.001	0.24	0.624	15.35	0
C ·CR	1	0.42	0.521	1.23	0.274	0.12	0.728	0.31	0.582
Load.Load	1	6.27	0.017	21.1	0	97.97	0	2.02	0.163
2-Way Interaction	3	9.3	0	7.67	0	7.29	0.001	9.46	0
ER·CR	1	17.33	0	15.56	0	10.85	0.002	1.11	0.298
ER·Load	1	7.05	0.012	5.3	0.027	10.89	0.002	21.27	0
CR·Load	1	3.81	0.058	2.36	0.133	0.06	0.804	6.21	0.017
Error	38								
Total	47								

4.7.6 Parametric impact using 3D Surface plot

As three independent factors, the equivalence ratio, compression ratio, and engine load were chosen as choice variables for the investigation. This is because these three variables have the biggest impact on improving engine efficiency and decreasing emissions. The seven production reactions are BP, BTE, BSFC, CO, HC, CO2, and NO.3.5.1 Common impact of the independent parameters on Brake Power

The engine braking power is primarily responsible for an engine's power. The power available at the crankshaft is referred to as brake power. The simultaneous influence of Equivalence ratio, CR, and EL on the engine's brake power is depicted in Fig.4.76a. The graphic shows that braking power grows linearly as engine load increases. It might be owing to a decrease in heat loss and an increase in power as the load increases [139]. Brake power nearly remains constant as the compression ratio rises. The picture also shows that the engine's braking power is nearly independent of the gasifier's Equivalence ratio.

4.7.7 Common impact of the independent parameters on Brake thermal efficiency

When calculating and comparing an engine's power, one of the most significant things to consider is brake thermal efficiency. The BTE allows a part of the fuel energy produced to power the crankshaft to be used [141]. Fig.4.76b shows the simultaneous influence of many independent factors on the BTE. The graphic illustrates that increasing the load and decreasing the gasifier's Equivalence ratio increases the engine's braking thermal efficiency. This might be because a low ER improves the combustion efficiency of the engine. On the other hand, the surface plot of BTE revealed a clear connection between engine load and BTE. It's possible that this is due to the engine's thermal performance being better at greater loads than it is at lower loads. The BTE, on the other hand, rose just slightly as the compression ratio was raised.

4.7.8 Common impact of the independent parameters on Brake specific fuel consumption.

The fuel economy of an engine is affected by its thermal efficiency over time. Brake-specific fuel consumption is the rate of fuel consumption required to produce a unit of BP (BSFC). The typical effect of several choice factors on the BSFC is seen in Fig.4.76c. The chart demonstrates that by utilising a higher Equivalence ratio and a lower compression ratio, BSFC may be decreased. BSFC is directly related to engine load. This is because when engine load increases, so does engine power, necessitating the usage of additional fuel to meet the higher load. When the compression ratio of the E6 engine was adjusted, BSFC exhibited a similar pattern of effects [143]. It is clear that increasing the equivalency ratio lowers BSFC.

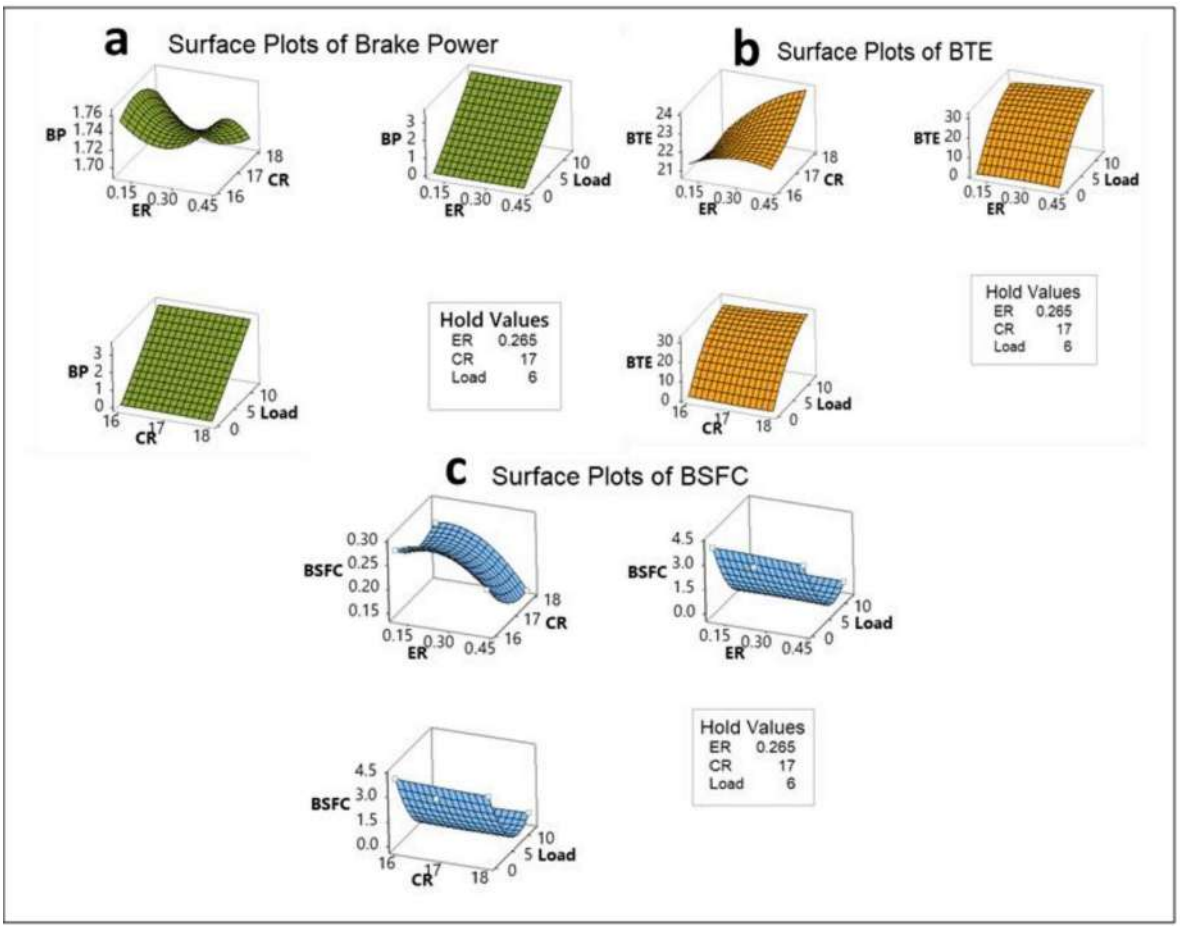

Fig. 4.76. Simultaneous impact of independent operating parameters on (a) BP, (b) BTE, (c) BSFC

4.7.9 Common impact of the independent parameters on engine exhaust emission

The simultaneous impacts of equivalency ratio, engine load, and compression ratio on NOx and CO2 are shown in Figures 4.77(a,b). Nitrogen is considered an inert gas at normal temperature. It can only react at extremely high temperatures, exceeding 1100 ^{0}C [144]. It turns into nitrogen oxide after interacting with oxygen [145]. As the equivalency ratio climbs over 0.2, the magnitude of NOx concentration in the emission increases, as seen in the graph. It might be due to the increasing amount of oxygen present in growing equivalency ratios, as well as the availability of oxygen at higher temperatures. As the load increases, so does the concentration of NOx. This is because the temperature within the engine rises as the load on the engine increases. Samet et al. [144] for example, found similar results. Increasing the compression ratio also increases the magnitude of NOx levels, according to the experiment. The temperature inside the engine cylinder steadily rises due to greater combustion inside the cylinder at a higher compression ratio. CO_2 is the primary source of greenhouse gas emissions and global warming [146]. The combined effect of several choice factors on CO_2 emissions is depicted in Fig.4.77b. Until 66.66 percent of the load, there is an increase in CO_2 emissions concentration.

The impact of the equivalency ratio and engine load on the unburned hydrocarbon is seen in Fig.4.77c (UHC). The unburned UHC's minimal magnitude shows the fuel's combustion efficiency. Growing the ER has been found to increase UHC. Due to the high concentration of oxygen, the equivalency ratio has risen. As the compression ratio increases, the magnitude of HC diminishes. As seen in the plot, the smallest magnitude of HC may be reached by using a greater compression ratio, i.e. 18, and a lower Equivalence ratio and load %. The influence of the Equivalence Ratio, Engine Load, and Compression Ratio on CO emissions as a whole is depicted in Fig.4.77d. Fig.4.77d demonstrates that a greater compression ratio, such as 18, and a larger load percentage, such as more than 85%, reduce CO emissions in the exhaust.

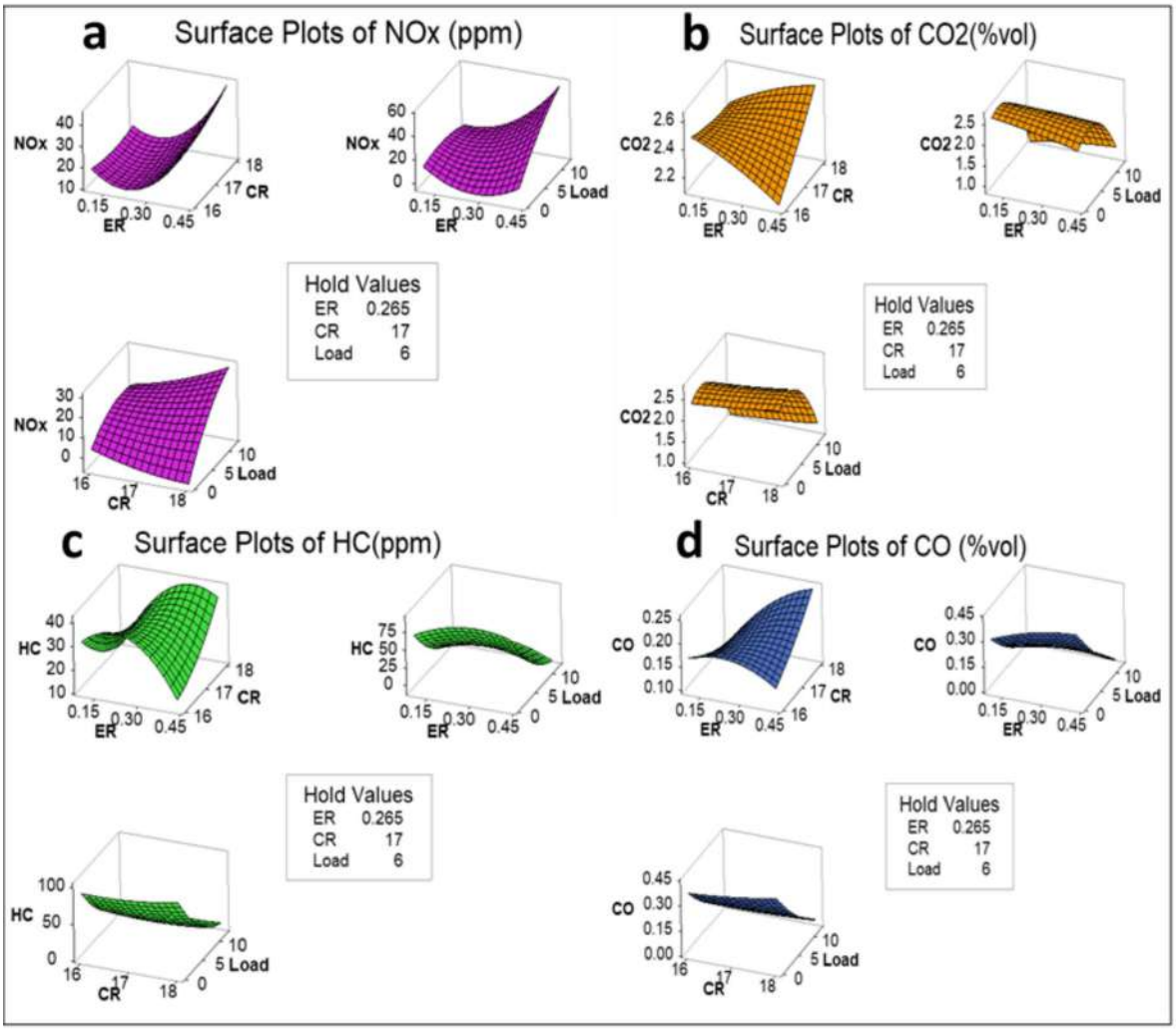

Fig. 4.77. Simultaneous impact of independent operating parameters on (a) NO_X (b) CO_2 (C) HC and (d) CO

4.7.10 Response optimizer

The optimal output and emission parameters were discovered by conducting simultaneous optimizations of the decision variables. It was generated using the Minitabs RSM optimizer module, which uses unit less desirability values (d) and magnitude counts ranging from 0 to 1 to characterise each response. A answer with a minimum value of 0 is unsatisfactory, whereas a response with a maximum value of 1 is desired. The solution to the desirability equation has been categorised as either "smaller-the-better" (SB) or "larger-the-better" (LB) (LB). Fig.4.79

shows the RSM optimizer in action, with the optimizer software producing results. The cumulative composite desirability was determined to be around 0.9520. Fig.4.78 shows the RSM optimization setup with the restrictions in place. The optimal values for BP, BTE, BSFC, CO, UHC, CO2, and NO are 3.54 kW, 28.23 percent, 0.38 kg/kWh, 0.0231 percent (percent vol), 4.2539 (ppm), 0.9569 (vol percent), and 9.6958 ppm, respectively. The magnitude of the independent parameters that were optimised: Equivalence ratio 0.12, compression ratio 17.01, and engine load 12 kg. Low grade coal may be a feasible feedstock for generating power for the rural sector utilising the biomass gasification technology, according to the present research.

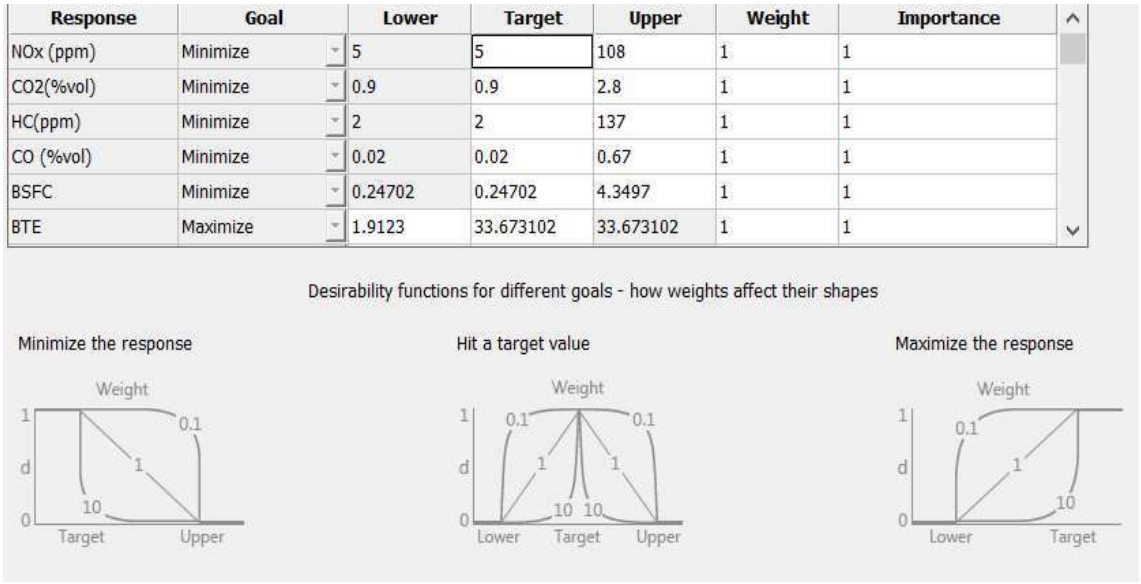

Response	Goal	Lower	Target	Upper	Weight	Importance
NOx (ppm)	Minimize	5	5	108	1	1
CO2(%vol)	Minimize	0.9	0.9	2.8	1	1
HC(ppm)	Minimize	2	2	137	1	1
CO (%vol)	Minimize	0.02	0.02	0.67	1	1
BSFC	Minimize	0.24702	0.24702	4.3497	1	1
BTE	Maximize	1.9123	33.673102	33.673102	1	1

Fig. 4.78. RSM optimization setup

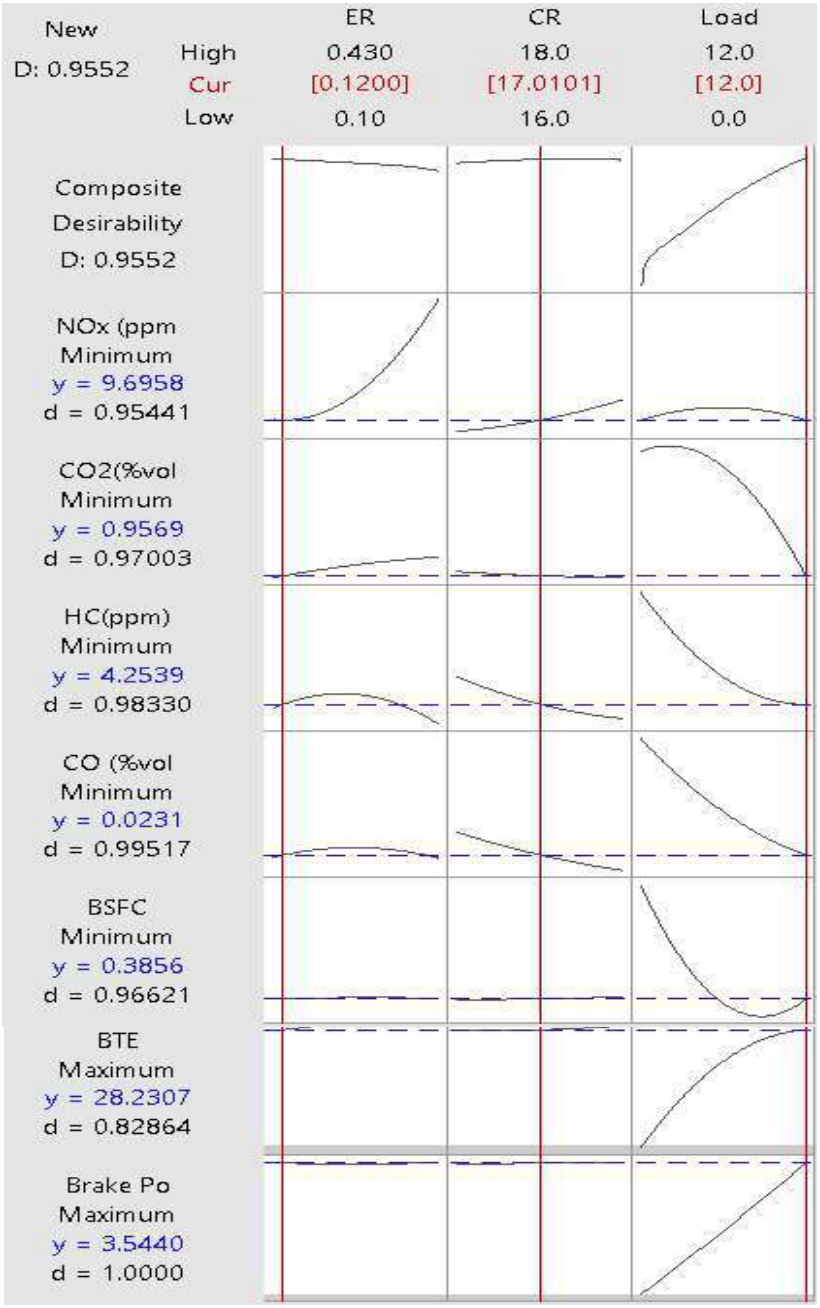

Fig. 4.79. RSM optimizer plot

4.7.11 Summary of the present work

Three operational parameters will be optimised in this study: equivalency ratio, compression ratio, and engine load. Seven output responses, including efficiency and emission parameters, are optimised using the RSM optimization technique: BP, BTE, BSFC, CO, UHC, CO2, and NOx. Low-grade coal was utilised for the production of producer gas. A total of 48 experimental trials were done on the dual-fuel VCR CI engine. Regression models developed from ANOVA data are shown to be very reliable in predicting performance response variables, with a confidence range of 95%. Engine load, according to the F-Value from ANOVA regression analysis, is the most significant parameter for engine performance characteristics. The Equivalence ratio of the gasifier, on the other hand, determines a major portion of the engine's emission characteristics. The ideal values of independent parameters such as equivalence ratio, compression ratio, and engine load, as determined by the response optimizer, are 0.12, 17.01, and 12 kg, respectively. The optimal values for BP, BTE, BSFC, CO, UHC, CO2, and NO are 3.54 kW, 28.23 percent, 0.38 kg/kWh, 0.0231 percent (percent vol), 4.2539 (ppm), 0.9569 (vol percent), and 9.6958 ppm, respectively. Around 0.9520 was found to be the cumulative composite desirability. The RSM model is a valuable approach for determining the optimal engine operating settings for improving engine performance and emissions responses. Because biomass has a low density, it necessitates a considerable amount of space for storage, processing, and feeding. Co-gasification of high-ash coal and various forms of biomass has the potential to become a future technique for valuing LGC and biomass. Transporting such a huge amount of inert material over long distances is not cost-effective due to the poor quality of coal in India, which contains a high proportion of ash (40–50 wt%). As a result, our research suggests that waste biomass and low-grade coal be valorized in a cost-effective manner.

4.8 Experimental investigation- Gasification of Syzygium cumini biomass

The performance of the Gasifier-IC engine significantly depends upon gasification efficiency in terms of quality of producer gas, feedstock, air-fuel ratio, gasification temperature, and outlet temperature of the gas. The present research aims to investigate the experimental and simulation-based studies for different gasifier equivalence ratios (ER) using Syzygium cumini biomass. Four altered nozzle opening positions were selected conforming to 4 different ER (0.12 to 0.48) to investigate the performance of the downdraft gasifier. Fuel consumption and Diesel saving at different engine loads, equivalence ratio, and compression ratio using a 14-kW fixed bed downdraft gasifier coupled with variable compression ratio (VCR) compressed ignition (CI) engine were investigated. The temperature was recorded at different zone of gasifier through K type thermocouple. The optimum equivalence ratio observed was 0.36 corresponding to a 75% nozzle quarterly closed position. The maximum diesel saving was found out to be 53.52% with dual-fuel (DF) mode at 2.4 kW brake power (BP) at ER 0.36. Maximum diesel saving at compression ratio (CR) 15, 16, 17, and 18 observed was 9.73%, 14.38%, 22.48%, and 49.05% respectively using DF mode. Thus, results proved that producer gas derived from Jamun (Syzygium cumini) biomass and its application in CI engine is viable alternate fuel for power generation.

4.8.1 Biomass characteristics

Syzygium cumini is one of the most widely distributed trees of India, occurring in the major forest groups except in the very arid regions. It may grows in both moist and dry areas, occurring in the tropical wet evergreen, tropical semi evergreen, tropical moist deciduous, littoral and swamp, tropical dry deciduous, tropical dry evergreen, subtropical broadleaved hills, and subtropical pine forests. It is a fast-growing tree, which provides excellent firewood and charcoal. It possesses a specific gravity of 0.77, and calorific value 4800-5310 kcal/kg

[162, 163]. . that's why Jamun wood or black plum (Syzygium cumini) biomass was used for the gasification experiment to produce a PG. Initially, the bigger size of Jamun wood was cut into a smaller piece and then sun-dried to remove any traces of moisture. Size of biomass used for the present study is 3.3-5.5 cm in the form of wood block.The proximate and ultimate analysis (Sutar, Kohli et al. 2017) of Jamun (Syzygium cumini)biomass fuel is given in table 4.43.

Table. 4.43. Proximate and Ultimate analysis of Syzygium cumini.

Proximate analysis on % dry ash-free basis	
Volatile matters	78.98
Fixed carbon	21.02
Ultimate analysis in % dry ash-free basis	
Carbon	44.5
Nitrogen	0.77
Hydrogen	4.98
Oxygen	49.54
Sulfur	0.22
Higher Calorific value of dry biomass (MJ/kg)	18.1

4.8.2 Effect of Gasifier equivalence ratio (ER) on gasification temperature

Fig. 4.80 demonstrates the variation of the average temperature of drying (T1 and T2), pyrolysis (T3), oxidation (T4), and core (T5) reduction zone of the downdraft biomass gasifier with the variable ER ranging between (0.12-0.48). The temperature inside the gasifier was ranging from 1300C to 5000C. As the ER decreases from 0.48 to 0.36 (which decreases airflow rate), the temperature inside the reactor was amplified along with the core temperature. It may be attributed to the fact that when airflow rate enhanced, it will result in more amount of oxygen to oxidize but it will also bring inert gas N2 along with themselves, which behaves like a heat carrier, and eventually, it will lead to reducing the temperature of pyrolysis as well as oxidation zone(Ratnadhariya and Channiwala 2009) The optimum value of the equivalence ratio was determined by the maximum value of temperature in the oxidation and pyrolysis zone. In addition to all this, we found that thermal stability was achieved after 10-30 min of the gasification process. The comparable temperature profile was publicized by Wei et al.(Wei, Pordesimo et al. 2011) where drying zone temperature was at 80oC, pyrolysis (600oC), and oxidation (800oC). The analogous temperature profile was obtained may be due to the amassing of char content on the grate system. The other factor may be due to the diminution of pyrolysis gases when the gasification process was continued for a longer amount of time and cools the oxidation zone. The gases present in the pyrolysis zone could be reduced as the quantity of pyrolysis gas shrank, it is attributed to the fact that approximately all the reactions that happened between pyrolysis gases and the char are endothermic (Köse and Ciniviz 2013).

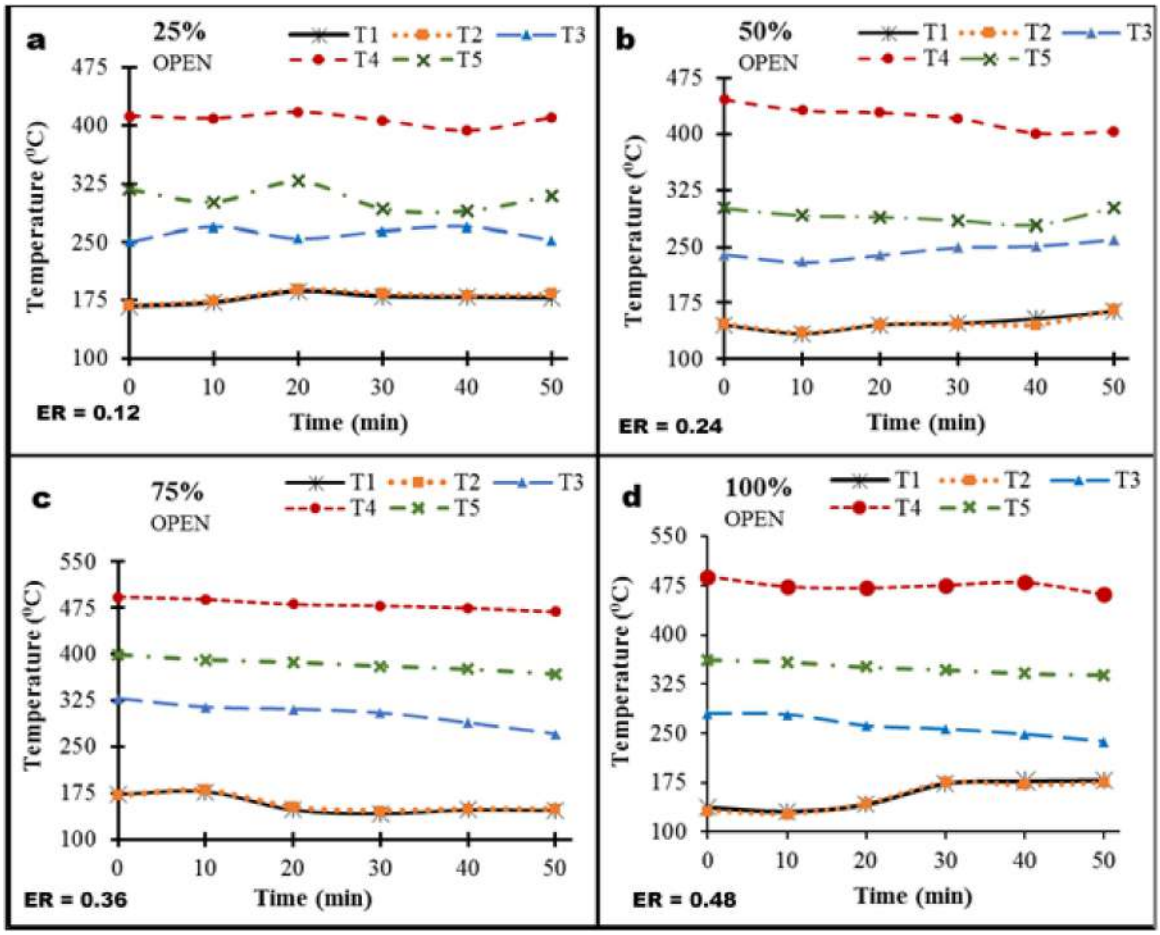

Fig. 4.80. Temperature profile inside the reactor at different ER.

4.8.3 *Effect of Gasifier ER on fuel consumption with and without PG at different BP.*

The effects of ER on the fuel consumption with and without producer gas (PG) means (purely diesel) at variable brake power (BP) and time is depicted in fig 4.81. ER directly controls the volume flow rate of air as well as air velocity simultaneously, and therefore, it takes some time for stability. The ER was varied from 0.12 to 0.48. It can be analyzed from the graph that when thermal stability was achieved which is in the range of (20-30 min).

The rated power of the engine is 3.5 kW at 1500 rpm but the maximum power achieved during the experiment is 3.4 kW corresponding to maximum load 12 kg as shown in fig 4.81. Engine

derating was observed during experiment [164]. It may be due to the reason that experimental engine is designed to operate at 30°C, and the ambient temperature reaches approximately 40°C during the experiment due to which engines experiences a reduction in power at full load. At ER 0.48, saving in fuel consumption at 2.4 kW was 19.04%. It might be attributed to the information that when the nozzle was fully opened, the overall conversion was reduced, combustion was enhanced due to highest airflow but there was very little time remaining for increased reduction and also fuel gas gets diluted due to increased flow of N2 and CO2 whereas at ER 0.36, it gets increased to 53.52%. it might be due to a decrease in airflow rate which leads to the conversion of carbon to combustible gas like CO as due to insufficient amount of air, the mixture becomes rich which eventually increases the calorific values of producer gas whereas, at ER 0.24 and 0.12, consumption reduces to 31.9% and 27.81% respectively. This might be because decreasing ER will decrease the conversion of hydrogen to H2 and the conversion of carbon to CO decreases while conversion of CO2 will increase due to alteration in the equilibrium situations of the water gas shift reactions at these conditions (Nisamaneenate, Atong et al. 2015). Due to the excess air present in the oxidation zones, combustible species and carbonaceous residue will oxidize via methanation reaction, Boudouard reactions, and water-gas reactions. In addition to this, extra heat will be required during the gasification processes and product quality should be improved through tar destruction. Awais et al. (Awais, Li et al. 2020) investigated an experimental investigation on downdraft gasifier using coconut shell and sugar bagasse and reported that heating value of PG was enhanced from 4.40 to 5.40 MJ/Nm3 and increment in the ER from 0.17 to 0.22 increases the quality of syngas and thus diesel saving also increases.

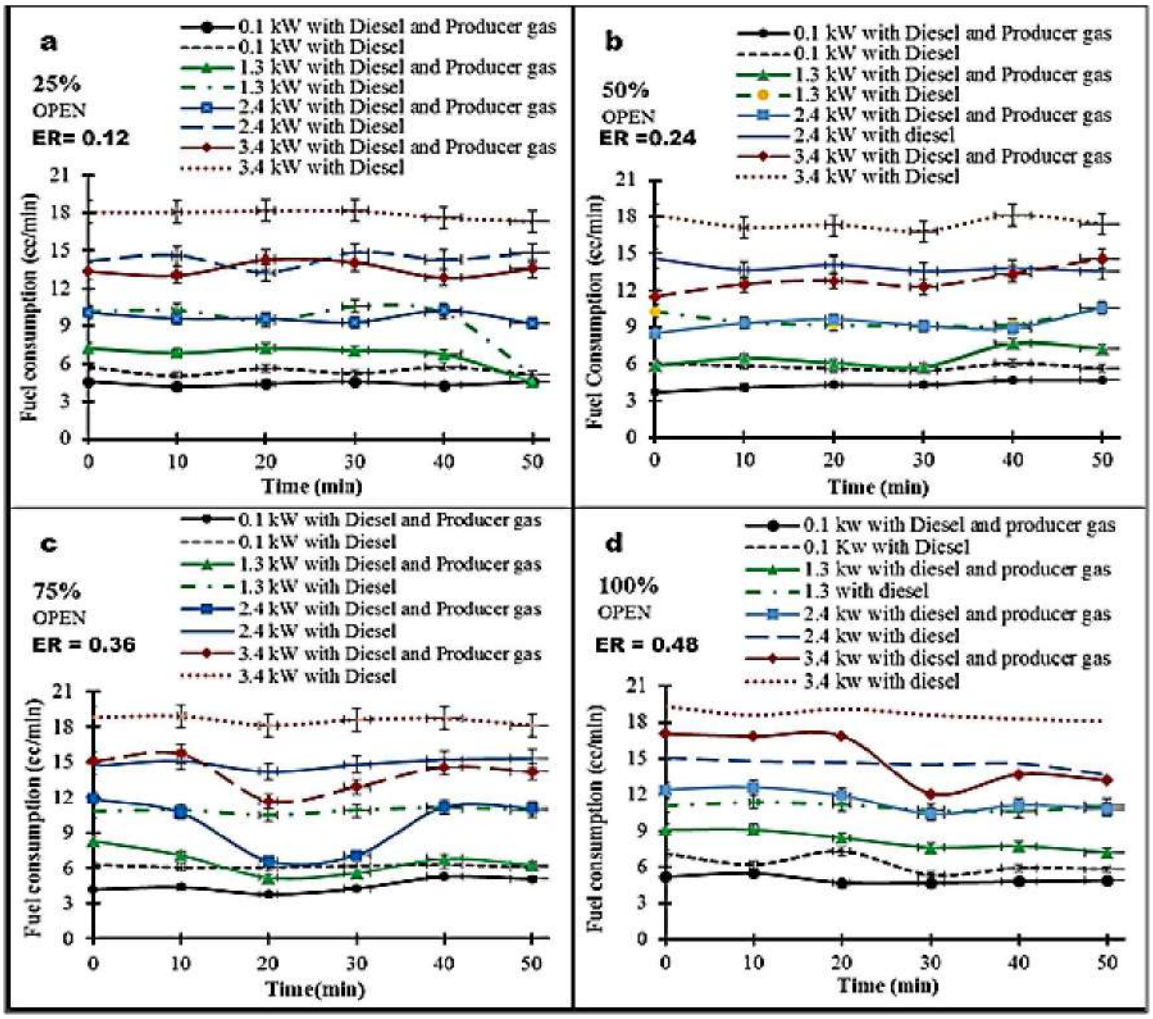

Fig. 4.81. Effect of variable ER on fuel consumption with and without PG at different BP.

4.8.4 Diesel saving at different Gasifier ER and Engine load

It can be inferred from the bar chart in fig.4.82 that 75% throttle opening position corresponding to ER 0.36 is the most optimized equivalence ratio followed by ER 0.24, 0.48, and 0.12 as the amount of diesel saving is highest at ER 0.36 approximately at all load condition. This may be due to decrease in air flow rate which leads to the conversion of carbon to CO as due to inadequate amount of air, mixture become rich which eventually increases the calorific value of producer gas.

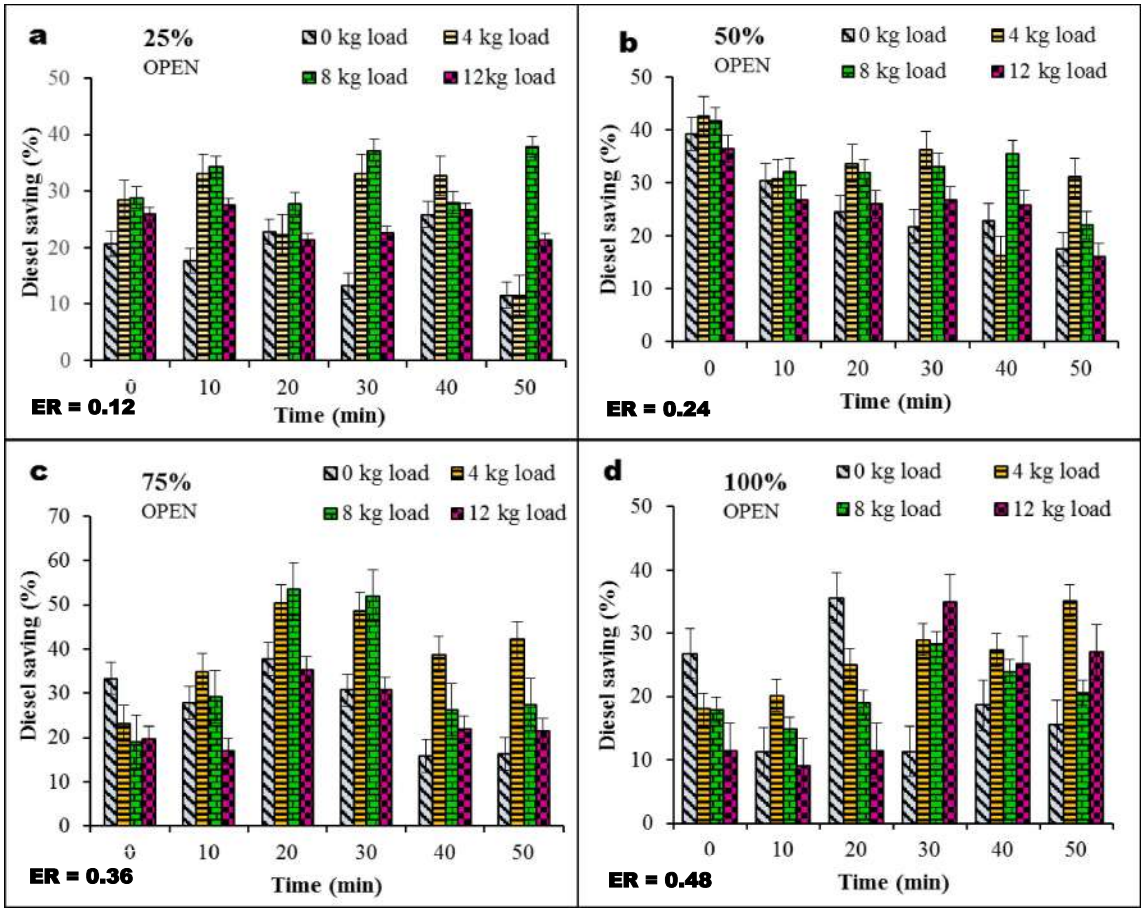

Fig. 4.82. Variation of Diesel saving at variable ER and BP

4.8.5 Effect of CR on fuel consumption with and without PG at different Engine load

Compression ratio and load variation in an engine significantly controls the efficiency and fuel consumption. After the production of clean syngas, PG is blended with the air and discharged to the VCR (variable compression ration) engine. The performance parameter of the engine has been acquired at a variable compression ratio (15,16,17,18). The volume of fuel consumption with diesel and dual-fuel mode at ER 0.48 has been investigated at different loads ranging from 0 to 12.

4.8.6 Diesel saving at different CR.

It can be observed from Fig.4.83 that at a higher compression ratio diesel saving is highest among the entire compression ratio at all the load condition. It can be accredited to the information that at higher compression ratios, the thermal efficiency of the engine increases. The use of producer gas along with diesel reduces the consumption of diesel fuel. it was also observed that consumption of producer gas as gaseous fuels enhances with the the higher CR which ultimately led to proper combustion of gaseous fuel. The maximum saving in diesel observed was 49.05% with CR 18 at the load of 6 kg, 22.3% with CR 17 at no load condition, 10.09% with CR 16 at the load of 4 kg, and 9.69% with CR 15 at the load of 12 kg. The comparative Diesel fuel saving at different loads with a variable compression ratio has been shown in fig.4.84. The Fig.depicts that at maximum load conditions, the saving of diesel fuel is reduced. It may be because at higher load condition richer mixture was required to maintain the constant rpm 1500.

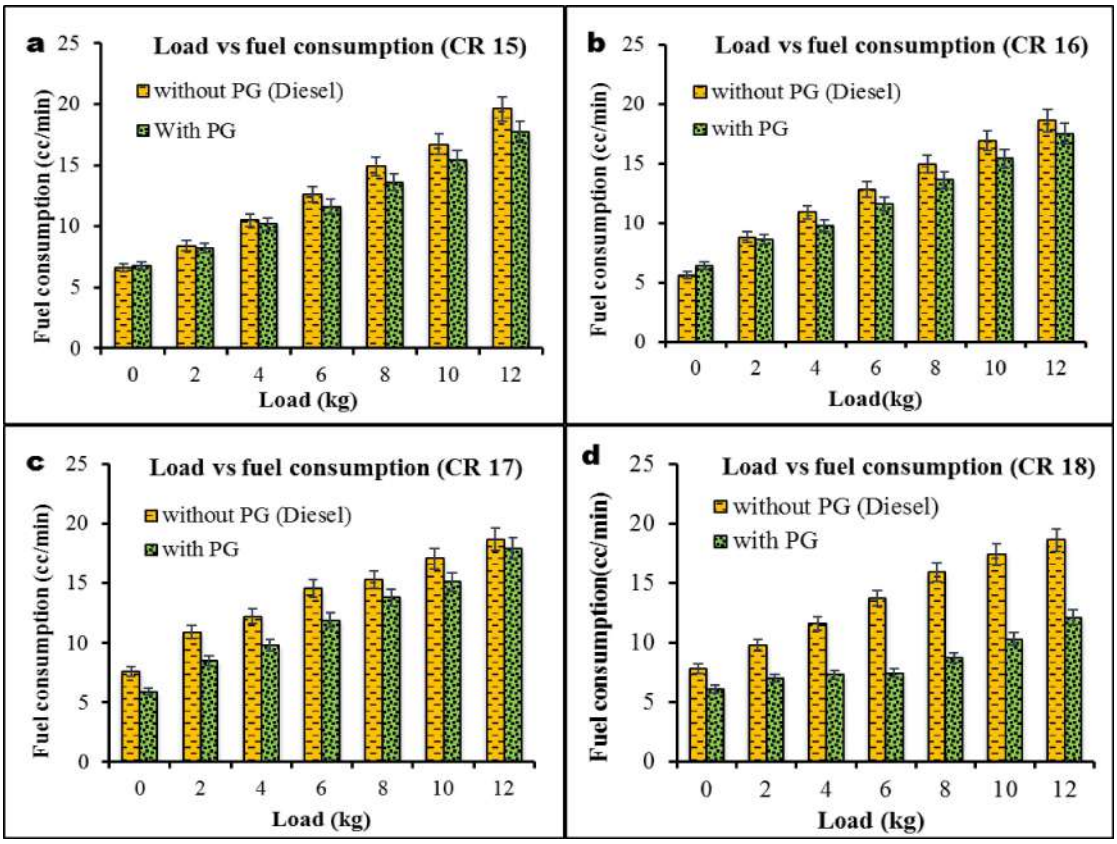

Fig. 4.83 Variation of fuel consumption at load with a variable CR (15, 16, 17, and 18)

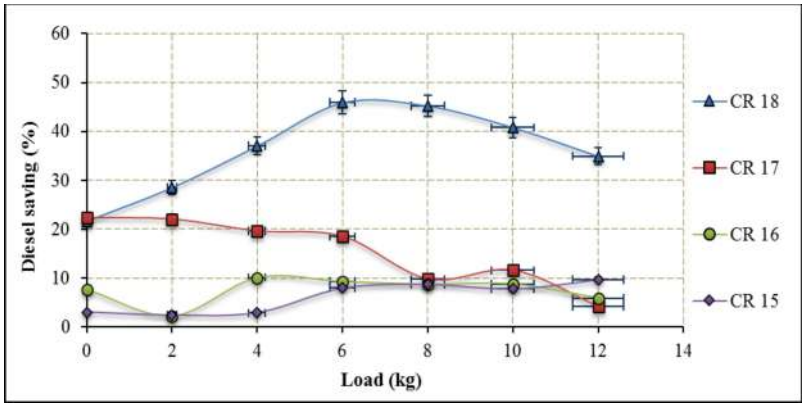

Fig. 4.84. Variation of diesel saving with load at a different compression ratio

4.8.7 *Effect of CR on Brake specific fuel consumption (BSFC) with and without PG.*

Brake-specific fuel consumption (BSFC) is the measure of fuel efficiency. The calculation of BSDFC with and without PG was done with the help of the density of diesel and volumetric fuel consumption at the variable compression ratio. From fig 4.85 it can be observed that BSDFC at 3.5 kW for the dual fuel mode remained 0.33 kg/kWh which was 21.21% higher than diesel mode at compression ratio 18. It can also be acquired after the graphical analysis that the magnitude of BSDFC for the part-load condition was of higher value than at a higher load. It can be clinched that BSDFC attains its minimum value at 3.5 kW for the compression ratio 18 and the value was 0.332 kg/kWh. It might be due to the maximum efficiency which was observed at this load condition. It had been investigated that BSDFC can be improved at 75- 85% load condition for compression ratio 18. Ramadhas et al. (Ramadhas, Jayaraj et al. 2008) stated maximum BSFC of 0.34 kg/kWh and 0.282 kg/kWh in dual and diesel fuel mode respectively using rubber seed oil and coir pitch biomass in his paper. Maximum BSDFC of

0.335 kg/kWh and 0.265 kg/kWh except at 3.5 kW brake power condition were observed in dual fuel mode and diesel fuel mode in this present research work. It may be because the volume of fuel consumption with PG condition is lower than without PG condition as the use of gaseous fuel along with diesel reduces the consumption of diesel fuel. Shrivastava et al. (Shrivastava, Jha et al. 2013). reported supreme BSDFC of 0.49 in dual fuel mode whereas 0.30 kg/kWh in diesel mode using wood chip and mustard oil cake. Maximum BSDFC of 0.282 kg/kWh and 0.4 kg/kWh in diesel and dual fuels mode using charcoal were reported by Sombatwong et al.(Sombatwong, Thaiyasuit et al. 2013). It can be concluded that BSDFC in dual fuel mode was higher than diesel because dual fuels mode depends on the calorific value of gaseous fuel as well as the percentage of magnitude of gaseous fuel.

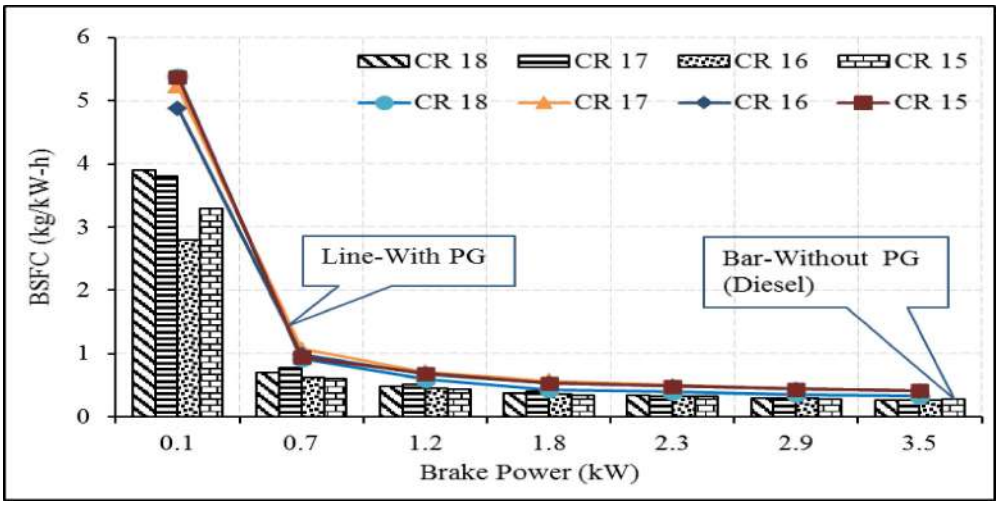

Fig. 4.85 Brake specific fuel consumption of the engine with PG without PG at a different compression ratio

4.8.8 Mass balance

The by-product of the gasification process is char, ash, and unburnt wood. All these by-products are considered in the analysis of mass balance along with the feedstock. The calculation of material balance incorporates the weight of biomass feedstock which acts as an input source whereas output includes gas, unburnt wood, ash, charcoal, tar, etc. The image of unburnt wood, charcoal, feedstock, and ash is depicted in fig 4.86.

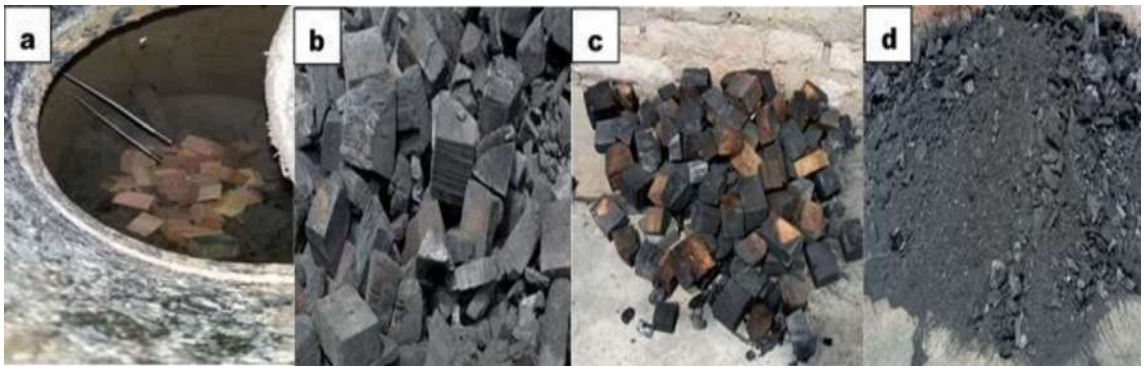

Fig. 4.86 Photographs of **(a)** Feedstock **(b)** Charcoal **(c)** Unburnt wood **(d)** Ash collected after the experiment.

According to mass balance, a total of 35 kg of woodblock are used for the gasification experiment out of which 17.4% of wood remains unburnt because they are extreme downside or at the extreme points where the proper amount of heat does not reach intensively. 21.4% converted into charcoal whereas 6.01% transformed into ash and 26.86% of the total weight of wood lost their energy to surrounding during the gasification experiment. It may be due to conduction, convection, and radiation heat transfer. According to energy balance, a total of

633.5 MJ of energy content was available as input source out of which 57.43% of cumulative energy comes out as unburnt wood, charcoal, ash whereas 61.31% of useful energy was utilized for the gasification reaction and the remaining 38.68% of energy is lost to the surroundings. This loss of energy is may be due to minor gas leakage which can be due to the circumference of temperature sensors, gasifier lid, and from the several joints in piping.

4.8.9 Summary of the present work

This study investigated the experimental and simulation-based studies for different gasifier equivalence ratios (ER) using Syzygium cumini biomass. Fuel consumption and Diesel saving at different engine loads, equivalence ratio, and compression ratio using fixed bed downdraft gasifier integrated with VCR CI engine were also quantified. The following conclusions can be drawn out from the present investigation.

- Thermal stability was found out to be in the range of (10-30 min) after the start of the gasification experiment as the temperature profile was somewhat linear in this time range.
- The optimum equivalence ratio (ER) observed was 0.36 corresponding to a 75% nozzle opening position. The diesel saving at this ER increased to 53.52% at the 2.4 kW Brake power (BP) with DF mode.

- The maximum amount of diesel that was saved at ER 0.48, 0.36, 0.24, and 0.12 throttle opening position was 19.04%, 53.52%, 31.91%, and 27.81% respectively with DF mode
- The maximum amount of fuel saved was 9.69%, 10.09%, 19.6%, and 45.9% at the compression ratio 15, 16, 17, and 18 respectively with DF mode.

Conclusively, it could be suggested that integration of gasifier-engine system offers better peformance parameter for engine power. Co-gasification of different biomass can be one of the future recommendation for the present study. Further, this study will provide a base for academician to extend research and development, and supportive for the small scale industries to adopt this system to save conventional fuel and the environment. It can be recommended from the present study that waste Syzygium cumini biomass can be valorized efficiently using the gasification technique in a cost-effective manner